An Examination of the Cardiothoracic Tissue Biophysical Response to Electroporation
Therapies

A Thesis
SUBMITTED TO THE FACULTY OF
UNIVERSITY OF MINNESOTA
BY

Lars M. Mattison

IN PARTIAL FULFILLMENT OF THE REQUIREMENTS
FOR THE DEGREE OF
DOCTOR OF PHILOSOPHY

Advisor:
Paul A. Iaizzo

February 2019

Acknowledgements

There is a long list of people who have helped me along the way to complete my degree, and I would like to take this opportunity to thank them.

First and foremost, Paul. His passion and relentlessness have helped to create a world-renowned lab that is any biomedical engineer's playground. His ability to encourage you to dream bigger allows you to achieve more than you ever thought possible. Because of this, the opportunities afforded to me through Paul's work have been a huge benefit to my education, learning, and experience. The number of times I have had to ask myself if this was real life during my time in lab are too many to count.

I also must thank the many graduate students (due to my extended VHL tenure) that I have had the opportunity to work with along the way. The late nights, early mornings, and long days were made tolerable by your fellowship. A journey taken with friends is much more enjoyable.

There are also many important members of the staff in the Visible Heart Lab as well. Mike and Tinen, who were able to help and provide advice along the way, Monica who was always willing to put down anything she was working on to help in any way possible, Gary who provided programming expertise, Rita helping to organize

everything, and Charles, Arpan, and Weston who made managing such a large workload much easier.

The support of my family has also been important along the way. My parents, who both pursued advanced degrees of their own, were extremely supportive and offered plenty of advice along the way (including asking when I would ever get a "real job"). My sister, who is also working to complete her PhD (and way smarter than I am, but don't tell her I said that) not only worked in the lab but was willing to provide a scientific sounding board.

Last and not least, I must thank Andrea. While I was playing in lab during the many late nights and early mornings, she was forced to spend extended periods of time without me. Many plans were cancelled, and events missed or delayed. She put up with me on the good days and the bad days and was supportive the entire way. Safe to say that I would not have made it here without her.

Dedication

To those who could one day benefit from the understanding of this work. It is important to remember that the impact of science resides in its adoption and use. Many small steps add up to make giant leaps.

Table of Contents

List of Tables

List of Figures

Thesis Summary

Atrial fibrillation (AF) is a disease that affects the normal function of the cardiac conduction system and is exemplified by the uncoordinated contraction of the heart's atrial chambers. This chaotic atrial contraction causes inefficient filling of the ventricles, reducing cardiac output and critically causing decreased quality of life. Additionally, the lack of contraction can allow for stasis of the blood, thus potentially forming thrombi which in turn can lead to stroke.

This disease currently affects between 2.1 to 6.7 million people in the United States alone, a number which is expected to double in the next 25 years. It typically effects an older population (99% of cases are in patients 65 or older) and costs the US health care system approximately $9,000 per patient. AF causes an estimated 467,000 hospitalizations per year and contributes to more than 99,000 deaths annually[1]. In the clinical setting the disease is typically defined as either paroxysmal, persistent, or long-standing persistent AF in the order of increasing severity.

Currently, there are multiple treatment options available for AF patients. A regimen of anti-arrhythmic drugs is typically the first step. However, for some patients, drugs are not effective in correcting cardiac conduction and may cause undesired systemic side-effects. In these cases, tissue ablation is considered as an alternative therapy. Ablation involves the selective termination of abnormally functioning cardiac tissue in an attempt to restore normal conduction. Currently, the primary technologies for performing cardiac ablative procedures

are radio frequency (RF) and cryoablation therapies. These are both thermal technologies that burn or freeze the target tissue respectively and both have been reported to be effective in treating AF, however, neither technology is without its limitations. Successful treatment of the diseased tissue relies on the need to create transmural cardiac lesions. Creating these lesions with thermal technologies increases the risk of damage to collateral anatomic structures nearby the heart. Typical complications include induced atrioesophageal fistulas and/or phrenic nerve injury. Due to the potential minimization of these collateral traumas, irreversible electroporation (IRE) is being considered as a novel means for applying cardiac ablations[2].

The primary purpose of my thesis was to examine the functional responses of various cardiothoracic tissue types typically susceptible to complications during cardiac ablation procedures. Additionally, the effect of an applied therapy on the biomechanical properties of these tissues was assessed. Throughout the project IRE was compared to currently utilized ablation modalities allowing for a thorough understanding of the risks and benefits of each with respect to the various tissue types surrounding the heart. The inclusion of a broad sampling of cardiothoracic tissue types including skeletal muscle, smooth muscle, cardiac muscle, and nerves will provide a unique understanding regarding how these technologies could be best applied. The information presented in this project will not only be of value to practicing clinicians, but also to medical device designers developing novel ways to deliver these therapies could be best applied to each tissue type. Such information will not only be of value to clinicians, but medical device developers as well.

Chapter 1: Atrial Fibrillation, Ablation, and Electroporation

The heart is a pump that circulates blood through the body, beating an estimated 2 billion times in one's lifetime. Any man-made pump with this type of efficiency and reliability would be highly sought after. However, several different diseases can affect the heart and cause it to not function as originally intended. According to the CDC 1 in 4 deaths are due to some sort of cardiac disease. Due to this, investigations into curative and preventative medicine have become more important. Here we will explore a disease state known and atrial fibrillation (one of many applications) and a potential new way to treat the disease that could result in less complications for patients, electroporation.

Atrial Fibrillation

Atrial fibrillation (AF) is a disease in which there is a disturbance of the conduction system in the top chambers of the heart. Instead of the signals propagating through the heart as they typically would, a second area of activation causes the chambers to contract in an uncoordinated manner. Since the atria are responsible for approximately 20% of the cardiac output, this reduced filling can cause discomfort to patients. Additionally, patients have an elevated stroke risk as the blood moves slowly through the atria. If the blood ends up being static for prolonged periods it can form thrombi which can break apart and cause a stroke or heart attack.

Atrial fibrillation is affects an estimated 2.1 to 6.7 million patients in the United States

alone. As it also has a higher prevalence in an older population, the number of cases is

expected to rise with the aging population of the United States. There are three different

classifications of the disease: paroxysmal, persistent, and long-standing persistent AF.

This is based on how often a person's heart is experiencing the arrhythmia. To treat the

disease, physicians first attempt to treat using anti-arrhythmic drugs. In the case where

patients don't respond well to or cannot tolerate the drugs, treatment by ablation is the

next step.

Ablation Technologies
When a patient needs a cardiac ablation, there are currently two primary different types

of ablations performed via a catheter. In both cases a small incision is made in either the

left or right leg and transvenous access is obtained. Once the source of the arrhythmia is

identified, the energy can be applied killing the problematic tissue allowing for the heart

to return to a normal rhythm. The two primary energies that are used in cardiac ablation

are radiofrequency (RF) and Cryoablation (cryo). RF ablation is the application of

alternating current (AC) energy to the tissue that causes cell death by heating the tissue

above 55° C. This is the most commonly used ablation technology that has been used

since the 1980s. It is relatively quick and fast acting, allowing physicians to immediately

understand if they have targeted the correct spot. In contrast to RF ablation, is

cryoablation. This is the application of extreme cold (-80°C) to the cardiac tissue to

cause cell death. Currently the benefit of cryoablation is that it is easy to use with

balloon-based application allowing for a continuous lesion. This is important for the efficacy of the lesion.

However, no technology is perfect. Both technologies are thermal based applications. To target cardiac tissue and ensure transmurality (essential for an efficacious treatment), physicians can end up providing too much energy. If this is the case, it is possible to reach to damage structures beyond the intended treatment zone. Common sights for damage include phrenic nerves and esophageal tissue, particularly with pulmonary vein isolation. Phrenic nerve injury can result in decreased respiratory function and a damage to the esophagus can result in an atrial-esophageal (AE) fistula. An AE fistula is almost always fatal for patients. Prevention is key for these injuries.

The investigation of this thesis is building an understanding of the different thresholds of damage of cardiothoracic tissues including cardiac, skeletal muscle, smooth muscle, and phrenic nerve. More information on this novel energy source is provided in the next section.

Electroporation ablative therapy as a clinical tool: An old technology revisited

Abbreviated Title: Electroporation as clinical tool

Lars M Mattison, BS, Brian T. Howard, PhD, Paul A. Iaizzo, PhD

Preface

This book chapter was published in <u>Engineering in Medicine: Advances and Challenges</u>.

It serves a summary of the work that has been done in the field across several different

disciplines.

For a field that has origins dating back to 1754, there is still a lot that is not understood.

This includes the exact mechanism of electroporation (once thought to be understood),

but recently has become a topic for debate.

The content has been modified for use in my thesis, including the addition of more recent

developments as well as the removal of content that is presented in other parts of this

thesis.

Synopsis

Electroporation is considered a novel means for treating tissue using high voltage, short

duration, direct current pulses to elicit different cellular responses. Varying the

parameters of the therapeutic pulses allows for either temporary or permanent cellular

damage. It is believed that applied direct current (DC) pulses disrupt cell membranes;

with larger electric fields causing more damage. A wide variety of input parameters

allows for the potential of tuning this technology to target various tissue types. Since the

delivery of energy is based on an electric field compared to a thermal field, there is also

potential to better target specific areas while minimizing collateral tissue damage. The

ability to apply electroporation therapy in its latest technological forms is currently being

explored to understand all of its potential clinical applications.

Key Words: electroporation, irreversible electroporation, electrochemotherapy, ablation

technology, catheter ablation, surgical ablation

As the fields of catheter and surgical interventions mature, electroporation is being

investigated as a revitalized alternative to traditional approaches. Even though DC

ablation has been around for nearly 40 years (and was used for the first transcatheter

ablations), it hasn't been until the last decade that widespread research has been

performed on its therapeutic effects. There are many proposed applications in the

medical field ranging from supplementing/targeting chemotherapy treatments to the

regeneration of skin from chronic wounds. This "new" or revisited technology, likely has

many useful applications, but first let's examine how this technology is considered to

function therapeutically.

With respect to current ablation (purposefully killing or removing body tissue)

technologies with widespread uses, the predominant ones are radiofrequency (RF) and

cryoablations. These technologies are applications of thermal energy using either

extreme heating (RF) or cooling (cryo) of the tissues to induce cell death. RF is the

application of alternating current (AC) energy to tissues which caused resistive (Joule)

heating while cryo is done thru the application of refrigerant either to the tip of a catheter,

or through the use of an inflatable balloon, causing focal freezing of the water molecules

in the nearby cells, leading to their death. Electroporation uses high voltage DC energy

delivered in short pulses, on the order of micro to nano seconds, to the target tissue(s).

This results in damage to the associated cell membranes, which can be controlled to

cause different therapeutic effects.

Historic Overview

It is widely believed that the first reported instance of irreversible electroporation dates back to 1754, when lesions were noted after the discharge of static electricity onto skin.[3] The first focused research relating to electroporation wasn't reported until 1898, when G. W. Fuller described the use of electric fields to purify water from the Ohio River.[4] This early research into water purification also exemplifies the uniqueness of the field of DC energy application that has greatly benefited from investigations in both the food industry as well as for medical applications. Electroporation research really began to take off in the 1950s and by 1960 a basic understanding of the underlying mechanisms of action were discovered. Over the next 40 years, further investigation took place setting the groundwork for the development of clinical applications for electroporation, including electrochemotherapy as described by L. M. Mir.[5] The field further broadened to the focal ablation of tissues, with the move to clinical soft tissue ablations reported in 2003 by Boris Rubinsky and Rafael Davalos.[6,7]

Mechanism of cell death

When describing this therapy's underlying mechanisms for inducing cell death, electropermeabilization might be a more correct description versus "electroporation". The exact mechanism is still debated within the community, but it is understood that there is a disruption of the lipid bilayer. One theory is that pores form in the cell membrane when the electric field is applied that cause either temporary or permanent destabilization of the cell membrane. This was the previously accepted theory, but more recent examinations have shown that the period of permeabilization is extended beyond

when the electric field is applied. Additionally, despite many efforts, no one has been

able to show images of pore formation actually happening.

Reversible vs Irreversible Electroporation Therapies

Being able to alter the intensity of the electric field applied to cell membranes, causing

differing amounts of damage to cells, is the genesis of reversible versus irreversible

electroporation. Using less intense electric fields, less damage is done to the cells, which

allows for them to quickly recover from the application of energy: this is known as

reversible electroporation. Importantly, this temporary pore generation affect still allows

for larger molecules to cross the treated cell membranes. Irreversible electroporation

induces an ion imbalance within the treated cell, thus it can no longer maintain proper

concentrations of sodium, potassium, and calcium. Over the course of approximately 20

minutes, apoptosis will ultimately occur. Being able to fine tune the applied electric

fields allows for different therapeutic effects to be applied to a given tissue.
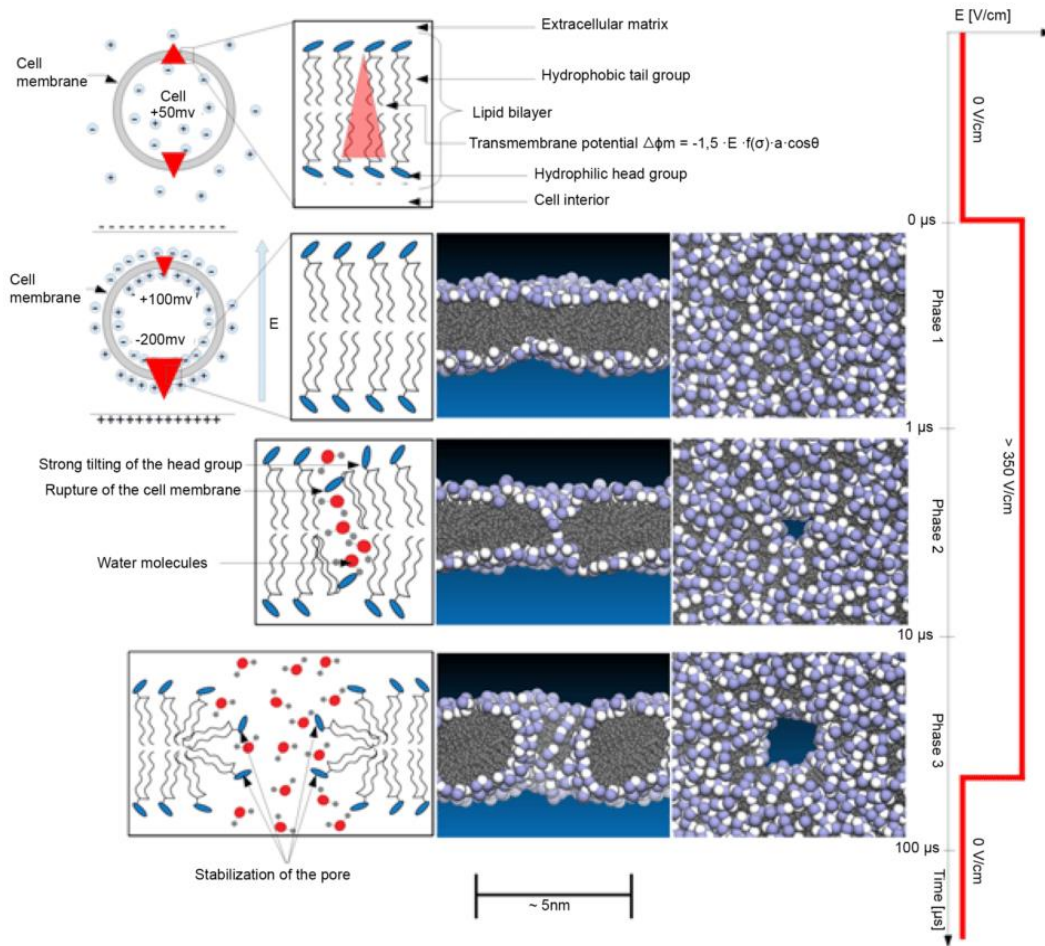
Figure 1: A. Example of a molecular dynamic simulation suggesting that pores are created in the cell membrane when an electric field is applied to the cell. (Adapted from https://vitusprostate.com/en/science/treatment/ire-technology-in-detail/)
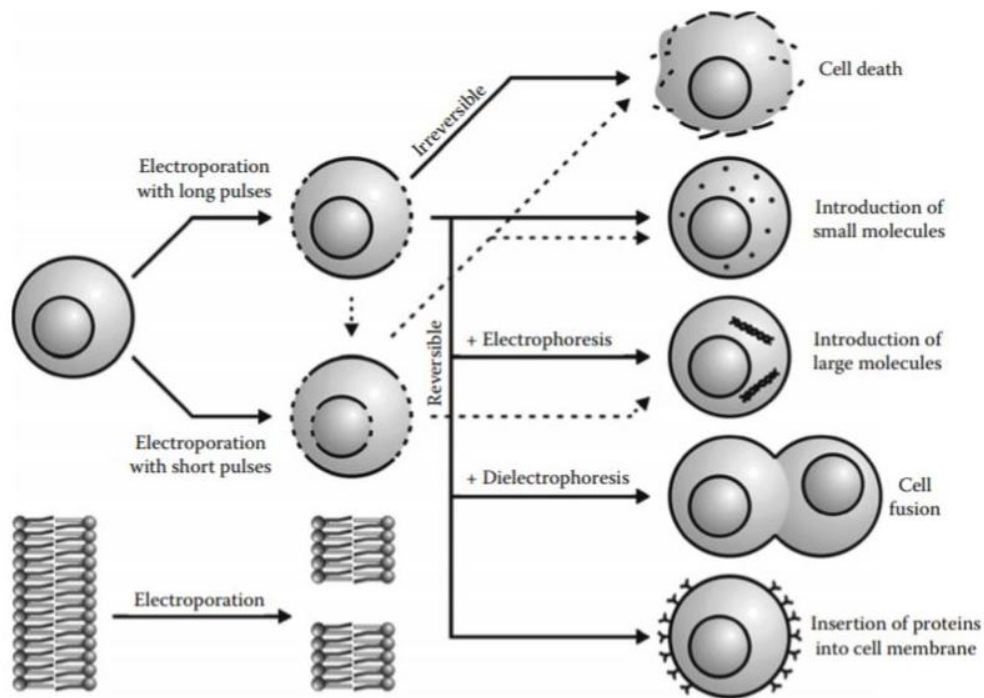
Figure 2: Possible outcomes of electroporation demonstrated showing how when using the proper parameters, different outcomes can occur.

Electroporation Generator Parameters and Waveforms

As previously mentioned, there are many different parameters that go into the

development and production of the various waveforms used in the applied fields for

electroporative therapies. Many different groups of investigators have pursued various

methodologies to discover optimal waveforms for their application. The most basic and

common of these is a square wave pulse field. For discussion purposes, the following

section will use square waves to help demonstrate the key points of a generalized

electroporation therapy.
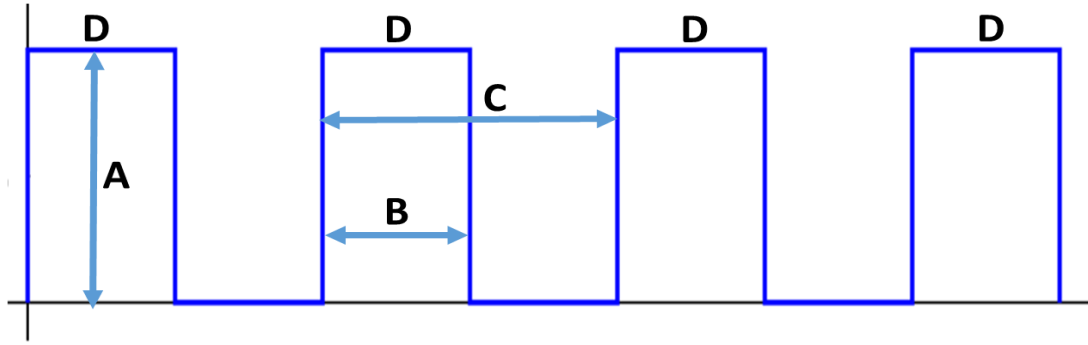
Figure 3 A standard square wave that represents various parameters of electroporation. A. Amplitude, B, Pulse Width, C. Frequency, D. Number of Pulses

Amplitude

Of the many different parameters one can control to regulate electroporation therapies, the most important one relative to inducing damage to the tissue, is the amplitude of the applied electric field: the larger the field, the more damage.[8]   The range of applied therapies that are currently utilized range from anywhere between 300 to 3000V/cm. While larger voltages are possible, there are other limitations such as tissue arcing as well as the ability of a given hospital's power supply to accommodate such large voltages. It is typical for employed clinical therapies utilized today, that the actual amplitude that is delivered to be controlled by the physician during the treatment (see Clinical section below).

Pulse Width

The applied field pulse width is also a commonly controlled aspect of electroporative therapy. One shortcoming of many of the employed clinical electroporation technologies, is that they can also induce unwanted, intense muscle stimulation and contractions. While it is possible to give various drugs to minimize the impact of

stimulation (i.e., neuromuscular blockers), a shorter pulse width often will induce lower amounts of muscular stimulations; even with the larger amplitude energies. A typical electroporative pulse width ranges on the order of micro- to nano- seconds. Longer ablation pulses have been used, but it is generally believed that this causes cell death due to thermal effects. Thus the shorter pulses are important to create less heating while still exposing the tissue of interest to the desired electric fields.

Number of pulses

The number of pulses employed for a given therapeutic application varies widely. This can range from a single pulse to hundreds of pulses. Typically, the more pulses that are delivered in a given treatment, the larger and more complete the resultant lesion is. Commonly, the total number of pulses delivered can also be determined by the physician at the time of clinical therapeutic delivery. It is typical that multiple applications of multiple short pulsed energy fields will be required for an effective treatment. However, this also comes with the possibility of creating longer procedural times.

Frequency

The frequency within a given pulse train is also important: the faster the frequency the pulses are delivered, the higher the likelihood there is for additional resistive heating of the tissue. The current system with FDA approval, the NanoKnife (Angiodynamics, Latham, NY), has two preset configurations of 90 and 240 pulses per minute (Figure 3). Other frequencies investigated using other systems have utilized much faster pulses, in the range of 6 to 10 Hz.[8] It is important to note that the pulse frequency component

becomes highly important when one considers utilizing therapies around the heart; especially using longer pulse widths. In cases near the heart, it is important to synchronize pulse delivery to the ECG to avoid inducing fibrillation by delivering a shock while the heart is mid-repolarization. This means that the energy delivery is determined in part by the patient's heart rate. In summary, the frequency of the energy delivery mostly impacts procedural times, so should be as fast as possible, while not too fast to cause focal heating.

Figure 4: The NanoKnife system, which is the only FDA approved device for the ablation of soft tissue in the US (adopted from http://www.angiodynamics.com/products/nanoknife)

Waveform characteristics

Up until this point, the discussion has centered around unipolar square waves therapeutic pulses. While the number of possible waveforms are limited to one's imagination, there has been increased interest in bipolar waveforms which as it turns out has some unique use properties.

16

Bipolar

Using a bipolar waveform has some unique properties over those of unipolar. Specifically, a bipolar waveform affords one the ability to create bipolar cancelation paradigms; minimizing the effects of the pulses on surrounding tissues.[9] This is not to say that bipolar pulses are not capable of causing damage to the cells, but just to a lesser degree then a cumulative unipolar pulse would.

High Frequency irreversible electroporation (H-FIRE) waveforms

Recently, Dr. Rafael Davalos at Virginia Polytechnic Institute and State University has also examined the effectiveness of a waveform called high frequency irreversible electroporation (H-FIRE). While electroporation therapies have been proven to be effective at causing cell death, one of their largest drawbacks has been the inductions of broad muscle stimulations. Their research team has developed and investigated H-FIRE which has shown that using a bipolar waveform it is possible to not cause muscle stimulation while still creating effective, well defined treatments i.e. providing similar outcomes to unipolar ablations.[10]
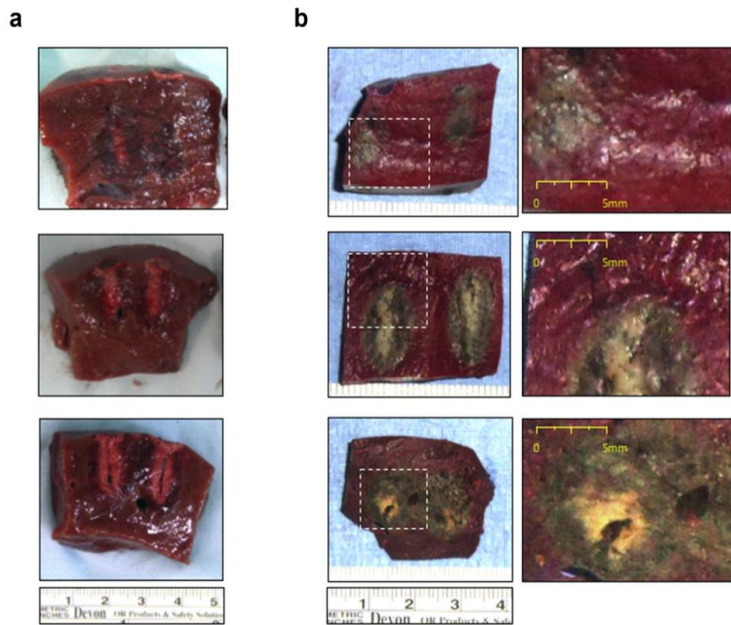
Figure 5: Example liver lesions following the application of IRE of 100- 200- or 300-pulses (2 250 V, 2-5-2us pulse configuration, 1.5 cm spacing) (A), and HFIRE energies of the same amount to liver tissue (B). On the far right (C) the volume of the lesion can be observed.[10]

Electrode Probe shapes and sizes

The sizes and relative shapes of the generated electric fields are also dependent on the electrode probe designs. For most clinical procedures, the primary probe design is a needle based. While a needle allows for the easiest application, it also can require several of them to effectively deliver the focal therapy. In the case of utilizing the NanoKnife system for electroporative therapy, this requires the physical insertions of several needles. Other clinically employed systems also utilize several needles on a single catheter that can then be placed onto a lesion (more common with electrochemotherapy). Nevertheless, these types of therapies require advanced procedural planning, or intraprocedural imaging so to ensure proper placements of the probes; commonly done today with computed tomography scan (CT.)   Another commonly employed electrode

18

design that is used is plates. Such plate electrodes allow for the creation of more uniform

electric fields to be generated across larger treatment areas. A lot of predictive modeling

has been performed to determine exact output and how probe design, placement, and

orientation can be optimized for maximum procedural efficacy.
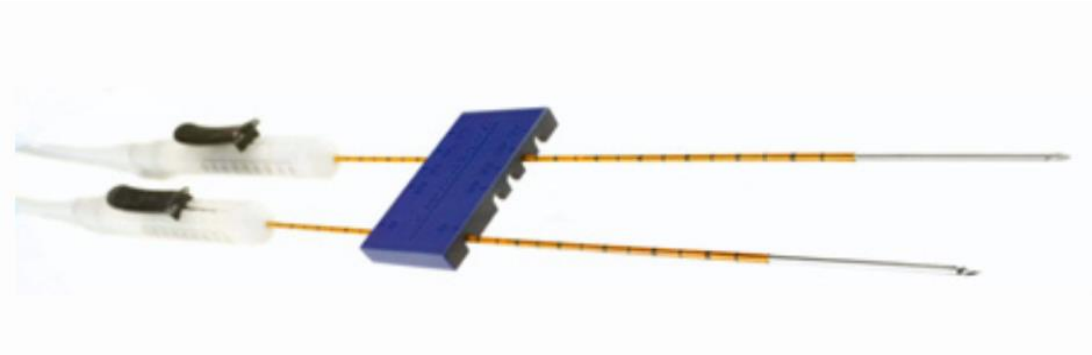
Figure 6: Needle type probes used for clinical irreversible electroporation. These probes are designed for use with the NanoKnife system and have an adjustable sheath to allow for different exposed probe lengths (Image adopted from http://www.angiodynamics.com/products/nanoknife)
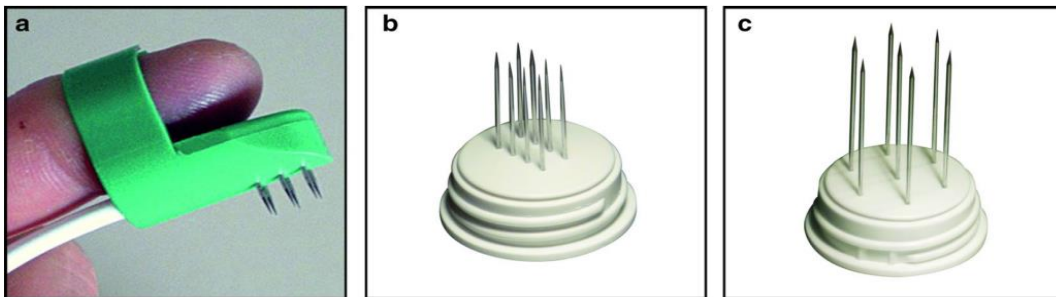
Figure 7: A pin array electrode type that is commonly used in the application of reversible electroporation for skin lesions.[11]

Applications of Electroporation

In the medical field, there are many different applications of various forms of

electroporative therapy. The primary areas of application are electrochemotherapy,

wound healing, and ablations. The variety of applications speaks to the potential

19

versatility of this energy form and how changing the electroporation application

parameters can allow for many different outcomes.

Clinical Use of Electrochemotherapy

Figure 8: The Cliniporator (shown here) is a clinical unit used in Europe for electrochemotherapy. (Image adapted from http://www.igeamedical.com/)

Today, electrochemotherapy is one of the most widely practiced applications of

electroporative therapeutic technologies. In principle, it utilizes a reversible

electroporation dose to create temporary pores in the cell membrane. In practice, this can

allow for larger chemotherapy agents to be delivered in a targeted manner to tumors. It

has been known for some time that the combination of electroporation and drugs can be a

more effective treatment than either drugs or the electric shock therapies alone. Several

different agents have been and continue to be investigated, but the one primarily in use

today, is bleomycin. More specifically, investigations have shown that electroporative

therapy of a 5kV/cm, 2ms pulses, applied with the treatment of bleomycin was more

effective than either treatment individually for reducing tumor sizes.[12] It should be noted

that this is often performed with needle probes using a system like the NonoKnife for

treating larger/internal organ tumors, located within abdomen such as the liver, kidneys, prostate, etc. Topical treatments for skin cancer are also a popular application.

Wound Healing using Electroporative Technologies

The etiologies of chronic wounds have long puzzled physicians; and for such are only afforded limited treatment options. With regards to treating ulcers, high voltage stimulation has been shown to help heal what were otherwise characterized as chronic wounds.[13] It has also been reported that patients elicited harder scars, which also formed faster in response to the application of focal DC current.[14] This has been considered then to help an otherwise untreatable patient population receive an effective treatment and thus greatly improve their quality of life. The field continues to evolve, with more recent studies focusing on utilizing gene electrotransfer of various agents to facilitate the treatments of chronic wounds.[15-17]

Ablations with Irreversible Electroporation

The previous sections have focused mostly on non-lethal doses of electroporation, or the clinical uses of reversible electroporation. While employing the principles of irreversible electroporation (IRE), the primary goal is to cause cell death, or induce an ablation of the tissue. This is where the application of focused larger electric fields to tissues, are employed to create large pores in the associated cell membranes, ultimately resulting in cellular death. While in clinical uses today, there are currently well-established ablations protocols such as RF, Microwave, and Cryoablations, these all rely on generating thermal

fields which then causes cell death by induced thermal injuries. IRE has the advantage of

causing non-thermal death.
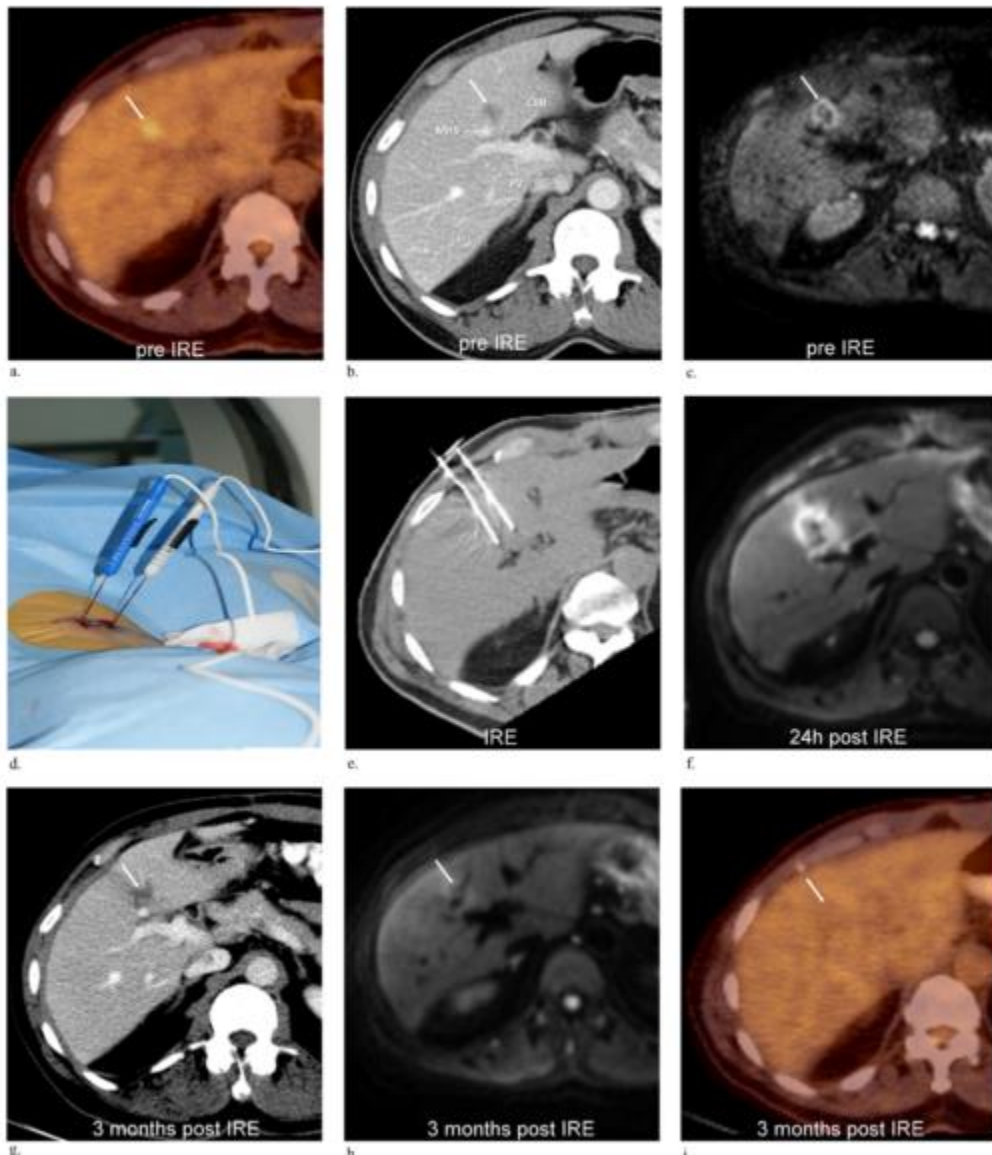
Figure 9: This series of images shows the delivery of an IRE lesion in the liver that is located close to sensitive structures including the hepatic vein and bile duct. A-C show pre-procedural imaging using Fluorodeoxyglucose positron emission tomography, contrast enhanced CT, and MRI. D and E show intraprocedural imaging both external and CT. F shows 24-hour follow up with MRI imaging that shows where the ablation took place. G-H show 3-month follow up.[18]

Non-thermal electroporation and its potential clinical benefits

Such approaches utilize short applications of electroporative energies, i.e. pulse width, so to minimize associated heating of the target tissues. In other words, this induces a non-thermal death of treated cells. Due to this nature of IRE it has been dubbed "NTIRE" for non-thermal irreversible electroporation. Other technologies, such as RF, microwave, and cryo rely on extreme temperatures to induce cell death. One important part of any successful ablation procedure, is that cell death within the entirety of the target tissue is induced: e.g., in the heart one wants to generate a transmural lesion. As one might imagine for a thermal ablation, this requires generating a large thermal gradient that can propagate further often beyond the desired targeted tissues. Predicting the actual heat transfer from the ablation probe to the tissue, becomes an even more complex problem when one considers the variable heat sinks due to blood flow and other surrounding anatomies. In certain clinical cases, it is possible to damage sensitive surrounding structures as well. Since electroporation is a non-thermal way to induce targeted cell death that relies on the appropriately applied electric fields, the targeted tissue will be affected by their tissue conductivities. While creating a perfectly uniform electroporative field is difficult, it is thought that this could be more easily controlled compared to thermal approaches. This potential upside of this technology may make to more likely to limit collateral damage to surrounding structures and thus could be therapeutically very enticing.

Additional Benefits of Electroporative Technologies

NTIRE provides additional upsides compared to more traditional technologies, which may importantly include minimized damage to nearby blood vessels and nerves, as well as preserved biomechanical integrities of the treated tissues. In other words, a common problem that can be observed following a thermal ablative therapy, is the development of stenosis of sensitive structures such as arteries and veins particularly when treating the liver and heart.[19] To date, these negative therapeutic side-effects have not been observed while employing electroporation; allowing treated tissue to remain pliable. Another advantage to NTIRE is that it better preserves the extracellular matrix. Whether it is the denaturing of proteins due to RF ablation or damaging ice crystals from cryoablation, the tissue integrity can be affected by these applications of energy.[20]   When performed around nervous tissue, limited damage has been observed compared to the surrounding tissues.[21-24]   While nerves are not immune to NTIRE treatments, they do seem to have a higher threshold which could be beneficial when performing ablations in areas where damaging the nerve could cause negative side effects. However, IRE is not a perfect ablation modality and has shortcomings (see below).

Potential Shortcomings of IRE Therapies

To date, a noted problem associated with relying on IRE alone for purposes of tumor ablations, has been with the precise control of the applied electric fields. More specifically, as the induced electric fields between electrodes induce a continuum of effects and can, in some cases, be highly non-uniform, (e.g., being higher near and between the electrodes and lower the further away from the targeted region), there are

substantial risks for not completely ablating the target tumor. The subsequent clinical

risks for incomplete ablations using IRE alone, would be akin to a surgeon resecting all

but a portion of a tumor: hence allowing for regrowth. Furthermore, when treating

patients with complex tumor geometries, clinical efforts are now being made to model the

effective region of the ablations prior to therapeutic applications.[25] Such advances have

and will allow for computer guidance during such procedures: as well as

recommendations for therapeutic applications, so to better ensure the areas of concern

receive the necessary dosage for the desired results.[26]   The alternative method to

ensuring complete coverage of a tumor is the aggressiveness of applying multiple

treatments: similar to where a surgeon removes generous portions of surrounding tissues

to ensure that all the tumor cells have been removed. The tradeoff or potential risks onto

the non-targeted (non-tumor) region, is something that has and will require intense

investigations: i.e., studies showing positive safety signs for efficacious IRE levels with

respect to neighboring nerves[27] and vasculature.[28, 29]

That being said, there is a wide body of literature looking into the many different tissue

types that IRE can be applied to. These include liver (with the largest body of literature,

due to its largely uniform nature), prostate, pancreas, kidney, lung, lymph node,

bronchus, esophagus, diaphragm and cardiac tissues.[18]   Many of these applications have

shown favorable outcomes with minimal complications.

Table 1: *A review of various papers that have been published on the efficacy of IRE showing 67-100% success in the application of IRE in tumors [Adopted from 16]*

Reference	# Patients	# Lesions	Size (cm) median (range)	Primary Efficacy
Cannon et al	44	48	2.5 (1.1-5.0)	97
Cheung et al	11	18	1.9 (1-6.1)	67
Kasivisvanathan et al	1	1	2.8	100
Kingham et al	28	54	1.0 (0.5-5.0)	96
Silk et al	9	19	3.0 (1.0-4.7)	NS
Thomson et al	13	45	2.8 (1.0-8.8)	67
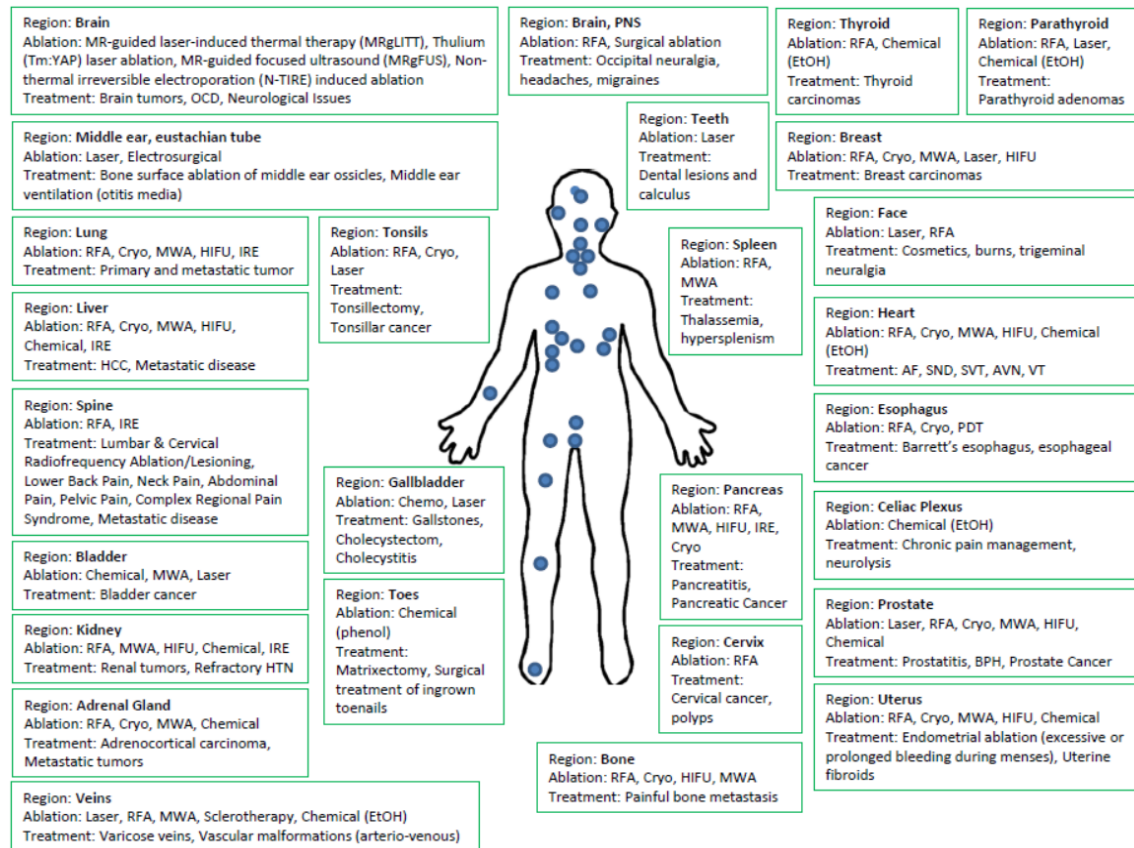
Figure 10: There are many different potential ablation sites within the body that are typically treated with thermal or chemical ablation.

Current Clinical Ablation Practice

Tumors

Irreversible electroporation is progressively making its way into routine clinical use. To

date, the only device approved for use in the United States is the NanoKnife produced by

Angiodynamics. (Figure 3). It has been approved for soft tissue ablation and is typically

used clinically for liver and prostate ablations. For example, the Nanoknife

Electroporation Ablation Trial (NEAT) examined the use of this system for prostate

ablations and showed feasibility of using IRE for such with minimal complications and

was able to successfully treat 67% of patients. This is not quite as good other studies, but

the results are promising for an early trial.[30] More recent studies have reported positive

clinical results for liver ablations; i.e., the effective use of electroporation for the

treatments of various sized liver tumors.[18, 31]

Irreversible Electroporation for Cardiac Ablations

It is important to note, that recently there has been a renewed push into the utilizations of

IRE in the cardiovascular ablation space. For example, three companies have currently

published their recent findings: Abbott Medical, AtriaCure, and Boston Scientific.

Abbott has fostered a research collaboration with Kars Neven at the University Medical

Center of Utrecht (Netherlands). They have developed a novel catheter design that

utilizes the waveform from a Lifepak 9 defibrillation unit. This group has reported the

abilities to create lesions both endo- and epicardially. Their benchtop and preclinical

results have allowed the group to do first in man studies in the fall of 2017. AtriaCure,

with a focus on surgical ablations (opposed to trans-catheter delivered therapies) has

presented preclinical research showing that they were able to create transmural lesions in the atria of swine; both through a single and two layers of tissue. They have also demonstrated the ability to create transmural lesions in the ventricle, at tissue thicknesses of up to 6 mm.   Their pulse protocol parameters have shown promise in applied surgical cardiac interventions. Boston Scientific has been involved with the development of a balloon catheter for the administration of IRE, with collaborators at the Mayo clinic; the goal being to target pulmonary veins. These advancements suggest that in the field of cardiac ablations, IRE treatment will have many future applications.

Non-medical applications

Outside of the medical community, there are other significant applications for electroporation technologies. One of the primary area of interest, is in the food processing industry, where the applied electroporation treatments are known as *pulsed electric fields.* Application of pulsed electric fields prior to juicing fruits and vegetables has been reported to increase the yield of juice, while preserving nutritional contents and importantly the flavor from fruits and vegetables compared to traditional methods.[32, 33] In these applications, the pulsed electric fields are used to generate permeable membrane which leads to the increase yield of juice. There are also important sterilization effects/benefits that have been shown in a process similar to pasteurization; ie., using pulsed electric fields to kill bacteria in juices. Yet, it should be noted that the industrial application of pulsed electric fields in juice production, in one case in the United States was not successful, due primarily to the large amounts of energy consumption needed to

generate large electric fields across a fluid; which has to a point made the technology fall

out of favor, yet future advancements may reverse such.

Summary
While the principles of electroporation have been around for a long time, one should

consider that it is still just entering into its infancy stage as a clinical technology. There

are many critical investigations associated with these technologies that are still needed;

from confirming the basic underlying mechanisms of action on various cell populations

to determining how to safely create larger lesions required for many clinical therapies.

Nevertheless, the use of high voltage DC energies and the many parameters that go into

generating optimal waveforms allow for the unique abilities to customize the use of these

technologies to many different applications. Electroporation will continue to be an

exciting field to watch as it rapidly grows and matures. It is likely that many new

applications remain to be discovered and will provide important therapeutic interventions

for large populations of individuals globally.

Chapter 2: Skeletal Muscle Response to Ablative Therapies

The biophysical response of skeletal muscle to irreversible electroporation therapies compared to other therapies including RF, Cryo, HIFU, microwave, and chemical ablation modalities. The methodologies that will be applied across all muscle types will be discussed here. While not a common target for most ablations, skeletal muscles is present over the entire body making it a candidate for collateral damage.

Assessment of Ablative Therapies in Swine: Response of Respiratory Diaphragm to Varying Doses

Ashish Singal, Lars M. Mattison, Charles L. Soule, John R. Ballard, Eric N. Rudie,

Erik N.K. Cressman, Paul A. Iaizzo

Abbreviated title: Assessment of Ablative therapies in swine

Preface

Synopsis

Ablation is a common procedure for treating patients with cancer, cardiac arrhythmia, and other conditions, yet it can cause collateral injury to the respiratory diaphragm. Collateral injury can alter the diaphragm's properties and/or lead to respiratory dysfunction. Thus, it is important to understand the diaphragm's physiologic and biomechanical properties in response to ablative therapies, in order to better understand ablative modalities, minimize complications, and maximize the safety and efficacy of ablative procedures. In this study, we analyzed physiologic and biomechanical properties of swine respiratory diaphragm muscle bundles when exposed to 5 ablative modalities. To assess physiologic properties, we performed in vitro tissue bath studies, measuring changes in peak force and in baseline force. To assess biomechanical properties, we performed uniaxial stress tests, measuring force-displacement responses, stress-strain characteristics, and avulsion forces. After treating the muscle bundles with all 5 ablative modalities, we observed dose-dependent sustained reductions in peak force and transient increases in baseline force—but no consistent dose-dependent biomechanical responses. These data provide novel insights into the effects of various ablative modalities on the respiratory diaphragm, insights that could enable improvements in ablative techniques and therapies.

Key Terms: Radiofrequency ablation; cryoablation; microwave ablation; high-intensity focused ultrasound ablation; chemical ablation

Abbreviations

BF = baseline force

CHA = chemical ablation

CRA = cryoablation

HCC = hepatocellular carcinoma

HIFU = high-intensity focused ultrasound

MWA = microwave ablation

PF = peak force

RFA = radiofrequency ablation

Introduction

The respiratory diaphragm, a skeletal muscle separating the thoracic and abdominal cavity, plays an important function in respiration.[8] Any injury to it can significantly alter its function, compromising respiration. Injury can occur in many ways, but in this swine study, we focused on collateral damage from ablative therapies. Because of the diaphragm's susceptibility to collateral injury, it is essential to understand both its physiologic and biomechanical properties in response to various ablative modalities, in order to minimize or prevent collateral damage.

For our in vitro analyses of isolated swine diaphragm skeletal muscle bundles, we tested 5 ablative modalities: radiofrequency ablation (RFA), cryoablation (CRA), high-intensity focused ultrasound (HIFU) ablation, microwave ablation (MWA), and chemical ablation (CHA). Our in vitro physiologic assessments included measuring peak force (PF, i.e., strength of contractions) and baseline force (BF, i.e., resting muscle tension) of isolated diaphragm muscle bundles stimulated in tissue baths.[16] Our biomechanical assessments included measuring uniaxial stress-strain characteristics of the same tissue samples.

Our study is particularly relevant to minimizing complications in these 3 conditions in human patients:

Hepatocellular Carcinoma

Surgical resection remains the first-line curative treatment for hepatocellular carcinoma (HCC), but many patients are unable to undergo resection because of their advanced

disease stage, severe liver dysfunction, poor clinical status, and/or comorbidities.

Therefore, less invasive techniques have been adopted, such as image-guided

percutaneous tumor ablation.[30] For ablation of liver tumors, the selected methods must be

safe and therapeutic, especially if administered near vital structures and near structures

that are difficult to visualize and approach by percutaneous techniques. Collateral injury

of the diaphragm from ablative procedures for HCC has been documented. In one study,

of 29 patients who underwent percutaneous RFA of hepatic tumors adjacent to the

diaphragm, 5 (17%) suffered diaphragm injury that was apparent with referred right

shoulder pain.[13] In addition, pneumothorax has been reportedly caused by RFA, under

real-time imaging guidance, of hepatic tumors beneath the diaphragm.[18]

Lung Cancer

The diaphragm has been shown to be susceptible to damage from RFA in patients with

lung cancer.[14] Common complications—such as pneumothorax, pleural effusion, and

parenchymal hemorrhage—can be treated conservatively. However, potentially fatal

complications—such as massive hemorrhage, pulmonary artery pseudoaneurysm, and

diaphragm injury—require extensive medical management. A case of intestinal

obstruction due to left diaphragm hernia was reported after RFA of pulmonary

metastasis.[25] Another group described a patient with lung metastasis whose diaphragm

suffered collateral damage after RFA of the laterobasal segment of the lower lobe of the

right lung.[22]

Cardiac Arrhythmia

The diaphragm is susceptible to collateral injury from epicardial or endocardial ablation performed in the ventricles to treat ventricular arrhythmia. This is because the right ventricle rests on the diaphragm. For a successful cardiac ablation, it must be transmural meaning that the cardiac tissue very near the diaphragm must be ablated as well.

Materials and Methods

Tissue Preparation

Our study was approved by the University of Minnesota Institutional Animal Care and Use Committee. We obtained fresh diaphragm biopsy specimens from swine (n = 56) that were euthanized as part of another unrelated protocol. From each biopsy specimen, we prepared multiple samples (>26 muscle bundles).

After resection, each biopsy specimen was pinned in a dissection dish and dissected in oxygenated, modified Krebs buffer solution. Each bundle was prepared in a cylindrical shape, oriented parallel to the long axis of the muscle fibers; bundles were 15 to 25 mm long and 2 to 4 mm in diameter. The bundles were then tied on each end with silk sutures, with a free loop on either end, so that they could be mounted either in the tissue baths for physiologic assessment or on the uniaxial machine for biomechanical assessment.

Ablative Modalities

The 5 ablative modalities we investigated can be divided into 2 categories: thermal (RFA, CRA, MWA, and HIFU) and chemical (CHA, using 4 different agents: acetic acid,

ethanol, hypertonic sodium chloride, and urea). We had already identified effective

doses from our pilot data for the following 5 experimental groups:

- *RFA* (484 KHz sinusoidal waveform) for 60 seconds at 5 doses: 50°, 55°, 60°, 65°,

  and 70°C (corresponding to 348, 580, 812, 1043, and 1275 J); 20 bundles (n = 4 at

  each dose)

- *CRA* (operated in the clinical mode, about -75°C) at 4 doses: 15, 30, 60, and 120

  seconds; 16 bundles (n = 4 at each dose)

- *MWA* (1.3 GHz continuous sinusoidal waveform) at 6 doses: 168, 289, 410, 821,

  1231, and 1642 J; 24 bundles (n = 4 at each dose)

- *HIFU* (2.5 MHz sinusoidal waveform, 80% duty cycle) at 6 doses: 98, 116, 132, 232,

  464, and 696 J; 24 bundles (n = 4 at each dose)

- *CHA* (performed independently, injecting each of the 4 agents individually at 6 doses

  representing clinical equivalents: 10, 25, 40, 50, 75, and 100 µl; 24 bundles (n = 4 at

  each dose for each agent)

In addition, our study included the following 3 control groups: ***control–in bath*** (bundles

left in the tissue bath throughout the physiologic assessment; n = 4), ***control–unmounted***

(bundles unmounted from the tissue bath and subjected to the same thermal conditions,

except for ablation, as the 4 thermal study groups; n = 4), and ***control–Krebs injected***

(bundles injected with Krebs-Ringer buffer solution, instead of chemical agents, at 6

different volumes: 10, 25, 40, 50, 75, and 100 µl; total of 24 bundles, n = 4 at each dose).

Physiologic Assessment

The tissue bath system that we used is an adaptation of one previously described.[15,16] It contained Krebs buffer solution, maintained at 37°C with 95% O_2 and 5% CO_2 to ensure tissue viability. The lower end of the muscle bundle was secured to a fixed hook; the upper end, to a force transducer. For data acquisition, we used custom software (Laboratory Virtual Instrument Engineering Workbench [LabVIEW], National Instruments, Austin, TX, USA).

After the bundles were mounted, they were allowed to stabilize, during which time the stimulation voltage and length-tension relationship were optimized for each bundle.[16] The bundles were stimulated once every 10 seconds with a square-wave pulse (1.0 ms wide). The bundle length that resulted in maximal PF (isometric twitch force) was used for the remainder of our study. If reproducible mechanical twitches could not be elicited with stimulation, or if the PF was <1.0 g after stabilization, the bundle was discarded.

Each bundle was randomly assigned to a group. As illustrated in Fig. 11, we measured PF and BF before and after each ablative procedure for every bundle. After a given ablative procedure, tissues were allowed to recover for 3 hours, so that we could assess the relative tissue damage (necrosis) and recovery as a result of exposure to different ablative modalities of varying doses.
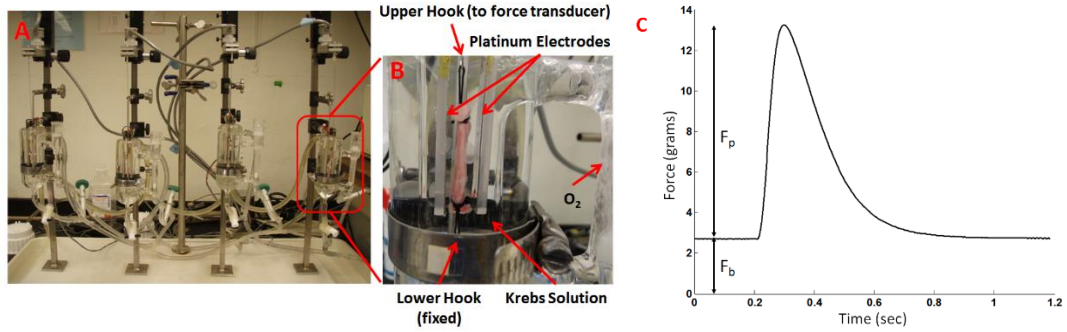
Figure 11: A. Tissue bath system setup for performing physiologic assessment. Data from 16 muscle bundles (4 shown) were acquired simultaneously. B. One tissue bath showing the respiratory diaphragm muscle bundle in the bath. C. Representative example of electromechanical stimulation response (raw data) from respiratory diaphragm muscle bundle showing the PF (F_p, strength of contraction = 13.0 – 2.8 = 10.2 g), and BF (F_b, resting muscle tension = 2.8 g).

Thermal Modalities

Each thermal ablative modality (RFA, CRA, MWA, and HIFU) had a custom fixture that

allowed the bundles to be submerged in a 37°C oxygenated Krebs buffer solution during

energy delivery. The bundle was unmounted from the tissue bath and stretched to the

same length as in the tissue bath. Each procedure was performed near the center of the

bundle. For the 3 contact ablative modalities (RFA, CRA, and MWA), a constant force of

0.1 N was applied to the bundle. All procedures were performed in a manner that

minimized the amount of time the bundle was not in the original muscle bath.

Chemical Modalities

For the chemical modalities, the tissue bath was lowered from around the bundle without

altering it in any way; the chemical agent was injected near the center of the bundle.

During injections, we exercised extreme care, especially to localize the entire volume of

the agent within the bundle, thereby preventing the agent from oozing out and maximizing efficiency and repeatability.

Biomechanical Assessment

The biomechanical properties of any tissue indicate how that tissue will react to internal and/or external physical forces. After we completed the physiologic assessment protocol, we subjected the bundles to a uniaxial stress test protocol, in order to assess changes in biomechanical properties as a result of ablative therapies. We tested the bundles until they failed, which is why biomechanical assessment was the last step done in the protocol. To perform the uniaxial stress tests, we used a digital uniaxial force measurement system (Chatillon TCD 110 Series, Largo, FL, USA). This system was equipped with a 10-N force transducer with an accuracy of 0.01 N and resolution of 0.001 N.

The biomechanical properties of respiratory diaphragm tissue do not change as quickly as the physiologic properties, because the tissue is not as critically dependent on temperature, oxygen, and nutrients. Therefore, we relaxed the criterion for tissue viability to $22.5 \pm 2°C$ and completed this step within 2 hours. We used a controlled stretch of bundle samples of 10 mm/min until avulsion. With soft biologic tissue sample alignment has been considered to be less of a concern, but the problems of firmly gripping the tissue on the test machine are much more severe. The gripping technique must be capable of securely holding soft tissue without damaging it. For added support, enhanced grip, and

increased bonding strength, we applied liquid super glue (Loctite Liquid, Henkel Corp.,

Rocky Hill, CT, USA) on either end of the bundle at the suture-tissue interface.

Force-Displacement Measurement

Once the glue dried, tissue samples were mounted. One suture loop was secured to the

immobile hook; the other suture loop was fixed to the uniaxial machine's force

transducer (**Fig. 12**). All tissue samples were stretched along the longitudinal axis of the

sample until it failed. We collected data at a sampling rate of 100 Hz. Before starting the

test protocol, we recorded the length and diameter of each sample; we used a caliper with

a resolution of 0.01 mm, in order to allow determination of the elastic modulus.
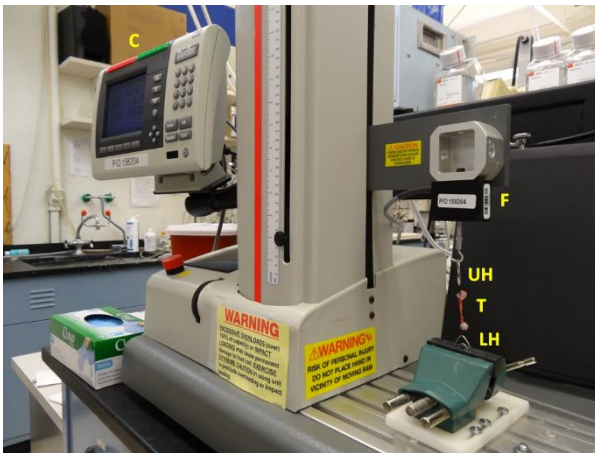
Figure 12: Uniaxial force measurement system for performing uniaxial biomechanical testing of respiratory diaphragm tissue, including of tensile strength. C = system console to control the operation of the uniaxial system; T = a diaphragm muscle bundle undergoing a uniaxial tensile stress test; F = a force transducer (load cell) connected to the movable arm of the uniaxial machine; UH = custom-designed upper tissue holder hook, connected to the force transducer; LH = custom-designed lower tissue holder hook, held firmly to the vise as a diaphragm sample is stretched.

Avulsion Location

Numerous factors determine where a given muscle bundle might avulse along its

longitudinal axis. For example, it could avulse at or near the center, or at the sutures.

Although our goal was to have every tissue sample avulse in the center, we knew that would not always be the case. So, to determine the exact location of avulsion for each bundle, we established a guideline for marking each bundle's avulsion location (**Fig. 13**); we determined 5 different locations and assigned a number to every sample based on its avulsion location (**Table 1**).
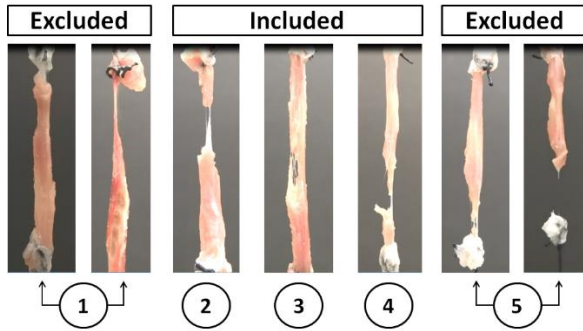
Figure 13: Representative examples of avulsion location of diaphragm muscle bundles.

***Table 1**:Description of Avulsion location and inclusion in data analysis*

Determination	Avulsion Location	Sample Data Included in Analysis?
1	Sample slipped out of the top suture, or avulsed at or near the top suture	No
2	Sample avulsed in between the center and top region of the muscle bundle	Yes
3	Sample avulsed near the center of the muscle bundle	Yes

4	Sample avulsed in between the center and bottom region of the muscle bundle	Yes
5	Sample slipped out of the bottom suture, or avulsed at or near the bottom suture	No

Stress-Strain Characteristics

Using our force-displacement data, we calculated nominal stress-strain characteristics for each tissue sample. The reduction in the cross-sectional area could be significant as the bundle is stretched along its longitudinal axis, so we assumed a constant volume model. We calculated the reduction in the cross-sectional area and then the Cauchy stress relationship (load/deformed area), which accounts for the reduced cross-sectional area as the bundle is stretched.[6] To calculate the elastic modulus of each sample and the averages for each experimental and control group, we developed a custom-designed software program and applied the following equation:

$$\text{Elastic Modulus (EM)} = (F/A) / (\Delta l/L) = (F/\Delta l) \times (L/A) \ (N/m^2)$$

The force data (F) and change in length (Δl) were acquired from the uniaxial machine. Before we initiated each test protocol, we measured the original length (L) and cross-sectional area (A).

42

Bundle Mass

After completing the uniaxial stress tests, we cut and discarded the sutures on both ends of each of the bundles. Using a weighing scale with a resolution of 10 mg, we measured the wet mass of each bundle.

Sample Size

On any given bundle, we used only 1 ablative modality. A random set of 4 bundles was subjected to each dose of any given ablative modality. A total of 212 bundles underwent physiologic assessment followed by biomechanical assessment. In addition, 327 bundles underwent only biomechanical assessment.

Data Analysis

To identify differences in PF and BF for all ablative modalities, we used analysis of variance (ANOVA) and the Tukey test; $P < 0.05$ was considered statistically significant. All data are presented as the mean ± standard deviation.

Results

Physiologic Assessment

A total of 212 muscle bundles underwent physiologic assessment in tissue baths (**Table 2**). The bundles' characteristics and allocations to different ablative modalities were similar across our experimental groups. Variation was not significant because we normalized our physiologic and biomechanical data to the bundles' physical characteristics.

43

We calculated the percent change in PF and BF in response to all ablative modalities. The response to RFA and CRA is shown in Fig. 4; data on all other ablative modalities are accessible in electronic supplementary material (Fig. S1-S6). We analyzed the data as the percent change in PF and BF with respect to the preprocedure value. We found dose-dependent sustained reductions in PF as well as transient increases in BF after treatment with all ablative modalities. Our functional assessment provided insight into what clinical observations might be. For example, a decrease in diaphragm force could translate to a patient having difficulty breathing. Note that, with RFA and hypertonic sodium chloride, PF initially decreased, but then improved over the 3-hour recovery period. This phenomenon of partial improvement in PF was more pronounced at lower doses. The largest decreases occurred with CRA and acetic acid, across all doses.

Table 2: *Characteristics of Diaphragm Muscle Bundles in Tissue baths (n=212)*

Ablative Modality	# of Doses	# of Bundles	Length (mm, mean ± SD)	Diameter (mm, mean ± SD)	Mass (mg, mean ± SD)	Preprocedure Peak Force (grams, mean ± SD)	Preprocedure Baseline Force (grams, mean ± SD)
RFA	5	20	23.2 ± 3.1	3.4 ± 0.6	277.0 ± 48.5	2.9 ± 1.2	2.1 ± 0.3
CRA	4	16	36.3 ± 5.7	3.3 ± 0.7	332.5 ± 137.9	3.4 ± 1.4	2.2 ± 0.5
MWA	6	24	36.6 ± 4.9	2.8 ± 0.4	235.8 ± 52.9	5.8 ± 2.2	2.5 ± 0.2
HIFU	6	24	27.3 ± 8.1	3.1 ± 0.5	264.0 ± 68.8	4.3 ± 2.6	2.2 ± 0.8
Acetic Acid	6	24	27.9 ± 4.6	2.9 ± 0.5	242.7 ± 55.5	4.4 ± 1.2	2.3 ± 0.2
EtOH	6	24	26.8 ± 5.5	2.9 ± 0.5	260.5 ± 85.8	4.1 ± 2.0	2.0 ± 0.2
NaCl	6	24	26.6 ± 3.7	2.9 ± 0.4	283.8 ± 60.1	4.0 ± 1.6	2.2 ± 0.2
Urea	6	24	26.9 ± 6.4	2.9 ± 0.6	296.2 ± 129.9	3.5 ± 1.6	2.2 ± 0.2
Krebs Injected	6	24	31.2 ± 4.0	3.1 ± 0.4	302.8 ± 50.5	4.7 ± 1.5	2.6 ± 0.2
Experimental Controls	NA	8	39.1 ± 3.7	3.2 ± 0.5	381.3 ± 40.9	3.2 ± 1.2	1.9 ± 0.3

A set of 4 bundles was exposed to every dose.

CRA = cryoablation; EtOH = ethanol; HIFU = high-intensity focused ultrasound; MWA = microwave ablation; NA = not applicable; NaCl = hypertonic sodium chloride; RFA = radiofrequency ablation; SD = standard deviation
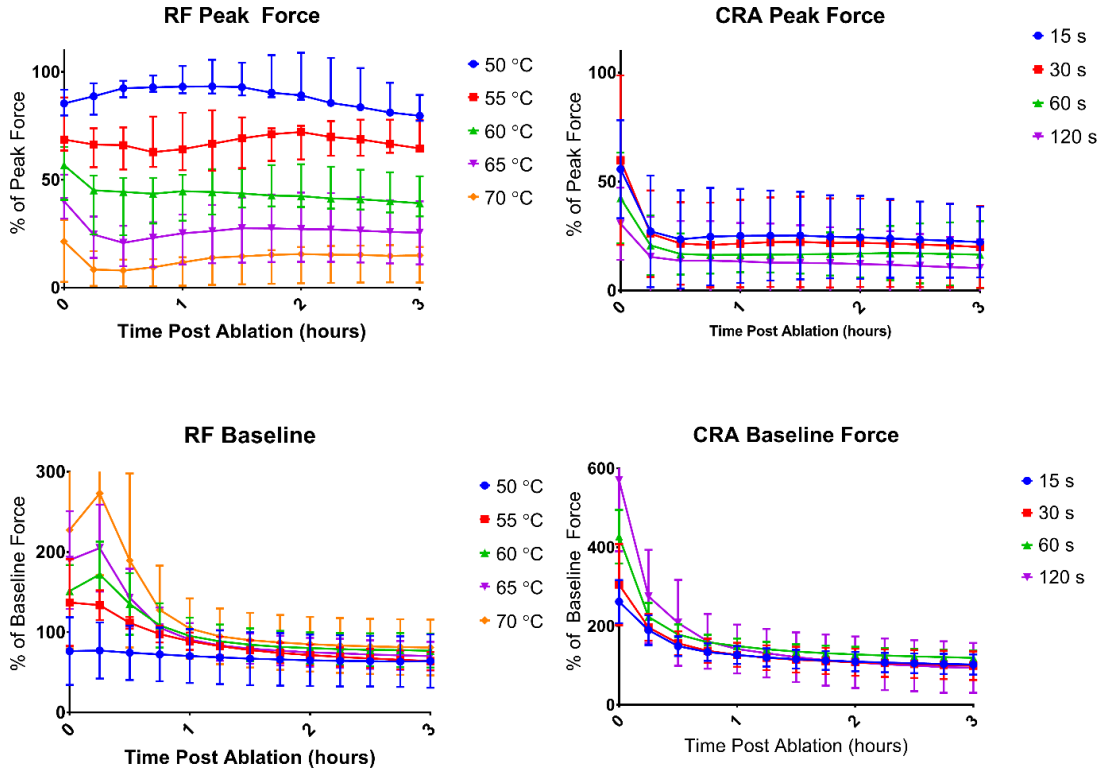
Figure 14: Dose effects of percent change in peak force (top) and baseline force (bottom) of swine diaphragm muscle bundles after RFA and CRA. CRA = cryoablation; RFA = radiofrequency ablation; s = seconds

For all ablative modalities (except for acetic acid, because of sustained contracture), we observed dose-dependent transient increases in BF; it consistently recovered to below the preprocedural value over the 3-hour recovery period. Interestingly, with the 100-µl dose of hypertonic sodium chloride, BF did not exhibit the dose-dependent response and significantly decreased (because of osmotic imbalance, intracellular dehydration, and damage to extracellular matrix and binding proteins). Typically, the transient elevation in BF was maintained for about 1-hour post procedure, but *not* with acetic acid (BF

remained elevated) or with hypertonic sodium chloride and urea (BF decreased to the preprocedure value within about 15 minutes).

For all chemical modalities, except acetic acid, the percent reductions in PF were similar at every dose. Acetic acid was the most potent agent: it caused the maximum reduction in PF at every dose. The percent changes in BF with ethanol were consistently the highest, at every dose; with hypertonic sodium chloride, consistently the lowest, at every dose.

For the control–in bath and the control–unmounted bundles, we observed similar changes in PF and BF (Fig. S7, electronic supplementary material), suggesting that unmounting the bundles from the tissue baths for application of ablative therapies had little or no impact on the subsequent physiologic response. For the control–Krebs injected group, PF and BF were similar at every dose, with no significant dose-dependent effects (Fig. S8, electronic supplementary material). Moreover, the response of bundles the control–Krebs injected group were similar to those of the control–in bath and control–unmounted groups, suggesting minimal damage to the bundles from the injection itself. A comparative representative example of acute tissue injury and lesion formation after each ablative modality is shown in Fig.15.
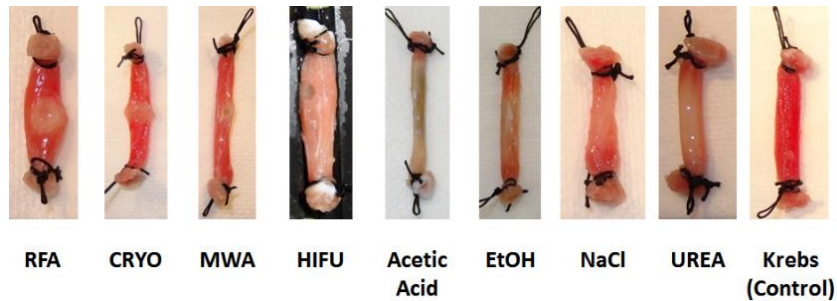
Figure 15:A representative example of acute tissue injury and lesion formation caused by each ablative modality. Thermal modalities resulted in focused tissue lesions; chemical modalities, in more diffuse tissue lesions. The shape and size of electrodes govern the dissipation of thermal energy within the tissue, whereas diffusion of chemical agents governs the damage within the tissue. CRYO = cryoablation; EtOH = ethanol, HIFU = high-intensity focused ultrasound; MWA = microwave ablation; NaCl = hypertonic sodium chloride; RFA = radiofrequency ablation

For all thermal modalities, we observed statistically significant differences ($P < 0.05$) both dose and time variables, as calculated using the Tukey test. For all chemical agents, we observed statistically significant differences ($P < 0.05$) for dose, time, and agent (Krebs-Ringer solution versus chemical agent) variables, as calculated using the Tukey test.

Biomechanical Assessment

A total of 539 muscle bundles underwent biomechanical assessment (212 that also underwent physiological assessment, plus 327 that underwent only biomechanical assessment and were not treated or ablated). Fig. 16 shows the graphical distribution of avulsion locations for each ablative modality. In our subsequent analyses, we included only the bundles with avulsion locations at or near the center. We calculated key biomechanical parameters of all samples in each experimental group (Table 3).
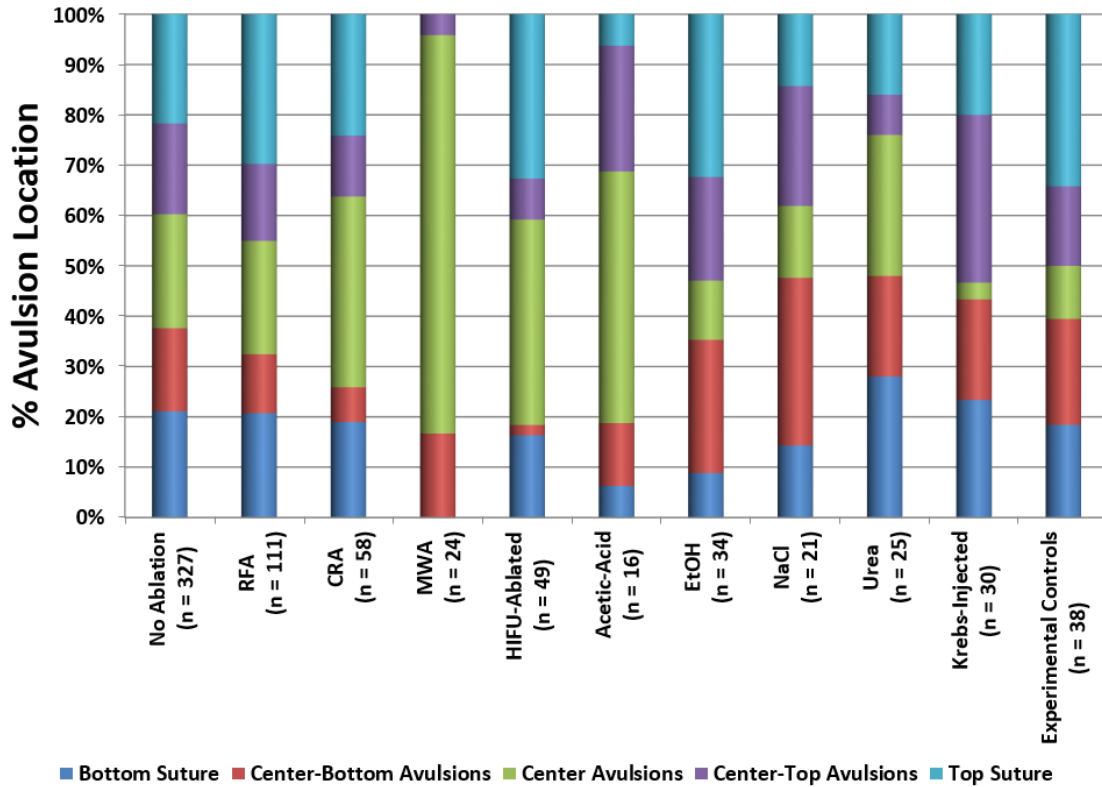
Figure 16: Avulsion location for each ablative modality (percent, for all swine diaphragm muscle bundles tested. CRA = cryoablation; EtOH = ethanol; HIFU = high-intensity focused ultrasound; MWA = microwave ablation; NaCl = hypertonic sodium chloride; RFA = radiofrequency ablation

Table 3: *Characteristics and Biomechanical Parameters of Swine Diaphragm Muscle Bundles that Avulsed at or near the Center (n=187)*

	Initial Cross-Sectional Area (mm², mean ± SD)	Initial Volume (mm³, mean ± SD)	Avulsion Force (N/mm², mean ± SD)	Elastic Modulus (N/mm², mean ± SD)	Avulsion Strain (Δl/L, mean ± SD)	Total Strain (Δl/L, mean ± SD)	Avulsion Energy (mJ/mm³, mean ± SD)	Total Energy (mJ/mm³, mean ± SD)
Biomechanical Assessment (n = 187)	8.9 ± 3.1	170.2 ± 60.3	0.2 ± 0.1	0.4 ± 0.2	1.1 ± 0.4	1.7 ± 0.7	48.1 ± 32.8	74.7 ± 56.0
RFA (n = 10)	8.9 ± 2.6	195.1 ± 68.7	0.2 ± 0.1	0.3 ± 0.2	1.0 ± 0.3	1.4 ± 0.4	42.0 ± 18.9	58.9 ± 27.4
CRA (n = 9)	7.5 ± 3.1	216.4 ± 81.2	0.2 ± 0.1	0.7 ± 0.5	0.7 ± 0.3	0.9 ± 0.4	27.4 ± 15.9	36.0 ± 17.6
MWA (n = 24)	10.6 ± 3.7	201.6 ± 48.9	0.1 ± 0.0	0.2 ± 0.1	1.3 ± 0.5	2.1 ± 0.8	37.8 ± 14.6	58.6 ± 24.1
HIFU (n = 13)	7.6 ± 2.5	212.3 ± 124.0	0.2 ± 0.1	0.4 ± 0.2	0.9 ± 0.3	1.4 ± 0.5	39.2 ± 23.3	59.1 ± 30.5
Acetic Acid (n = 20)	7.3 ± 1.9	190.9 ± 43.4	0.2 ± 0.1	0.5 ± 0.2	0.6 ± 0.2	0.9 ± 0.2	49.1 ± 20.1	69.9 ± 27.6
EtOH (n = 14)	7.4 ± 2.6	182.7 ± 65.8	0.2 ± 0.1	0.4 ± 0.2	0.8 ± 0.2	1.1 ± 0.4	46.0 ± 27.0	66.1 ± 45.1

NaCl (n = 17)	9.4 ± 2.4	241.1 ± 89.5	0.2 ± 0.1	0.4 ± 0.1	0.9 ± 0.2	1.2 ± 0.3	53.0 ± 25.5	70.9 ± 32.2
Urea (n = 14)	6.9 ± 1.9	149.3 ± 47.2	0.2 ± 0.1	0.4 ± 0.1	0.9 ± 0.2	1.4 ± 0.4	49.6 ± 15.3	73.4 ± 29.5
Krebs Injected (n = 14)	8.1 ± 1.8	202.4 ± 57.1	0.2 ± 0.1	0.4 ± 0.1	0.9 ± 0.2	1.3 ± 0.2	48.3 ± 14.2	68.2 ± 18.9
Experimental Controls (n = 4)	7.7 ± 3.9	249.1 ± 138.7	0.2 ± 0.1	0.7 ± 0.5	0.8 ± 0.4	1.1 ± 0.6	36.9 ± 25.6	51.1 ± 38.4

CRA = cryoablation; EtOH = ethanol; HIFU = high-intensity focused ultrasound; MWA = microwave ablation; NaCl = hypertonic sodium chloride; RFA = radiofrequency ablation; SD = standard deviation

All bundles were similar in size and shape. We normalized the avulsion forces to the cross-sectional area of the respective bundle, reporting our results in units of N/mm^2. We used the following definitions: *avulsion strain*, the ratio of stretch to the point of avulsion and the original length of the bundle; *total strain*, the ratio of stretch to the point where force returned to zero after avulsion and the original length of the bundle; *avulsion energy*, the integral of area under a given force-displacement curve until the point of avulsion; and *total energy*, the integral of area under a given entire force-displacement curve. Since the energy required to avulse the tissue depended on the avulsion force and stretch distance, we normalized it to the volume of the bundle, reporting our results in units of mJ/mm^3. Cross-sectional area normalization of avulsion forces and volume normalization of energies allowed for comparative assessment among our different experimental groups.

We also calculated the elastic modulus, avulsion and total strains, and avulsion and total energies of samples. To calculate the Cauchy stress, we took into account the reduction in the cross-sectional area of the samples during the stretch. The average avulsion stress was 0.11 MPa; the average Cauchy avulsion stress was 0.24 MPa (2.18 times higher). The avulsion strain was 1.35. The average elastic modulus was 0.36 ± 0.17 MPa, in the range of what has been reported in the literature.[23] In a similar manner, we calculated the stress-strain characteristics of all bundles in every experimental group (graphs not shown).

We calculated the percent change in each of the 6 biomechanical parameters (avulsion force, elastic modulus, avulsion strain, total strain, avulsion energy, and total energy) in every experimental group, but only for the 187 samples that underwent only biomechanical assessment and tore in the center. (Table S1, electronic supplementary material). A positive value indicated an increase, and a negative value a decrease, with respect to control samples.

The avulsion force increased for every modality, except RFA and MWA. It increased by 31% after treatment with acetic acid and decreased by 38% after treatment with MWA.

The elastic modulus also increased for every ablative modality, except RFA and MWA. It increased by 90% after treatment with CRA and decreased by 58% after treatment with MWA.

51

The avulsion and total strains decreased after treatment with every modality, except MWA. They significant decreased after treatment with CRA.

Using ANOVA, we did not observe any statistically significant dose effects in biomechanical parameters after any ablative modality. The dose effects after treatment with RFA are shown in Fig. 17; with CRA, in Fig. 18. and with all other ablative modalities, in Fig. S9-S15, electronic supplementary material.
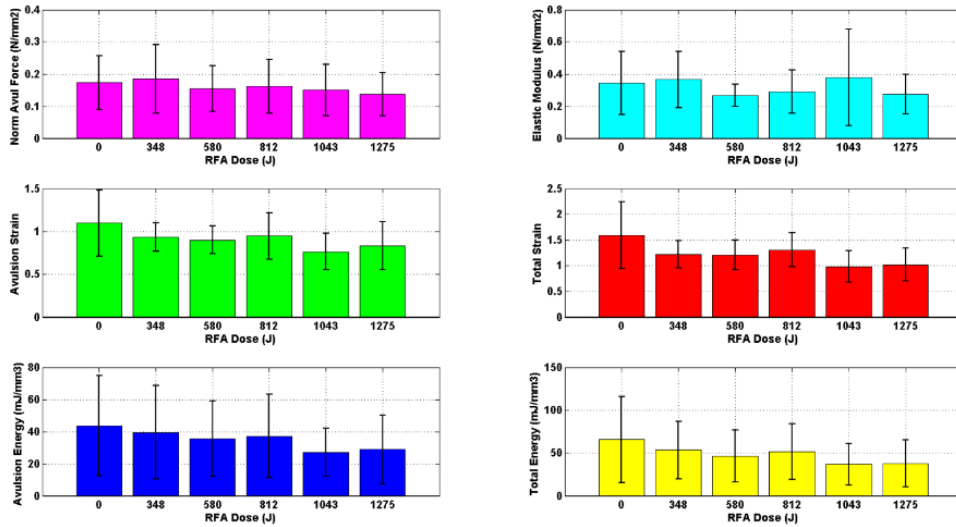
Figure 17:Dose effects of RFA on biomechanical properties of swine diaphragm muscle bundles, as compared with controls. RFA = radiofrequency ablation
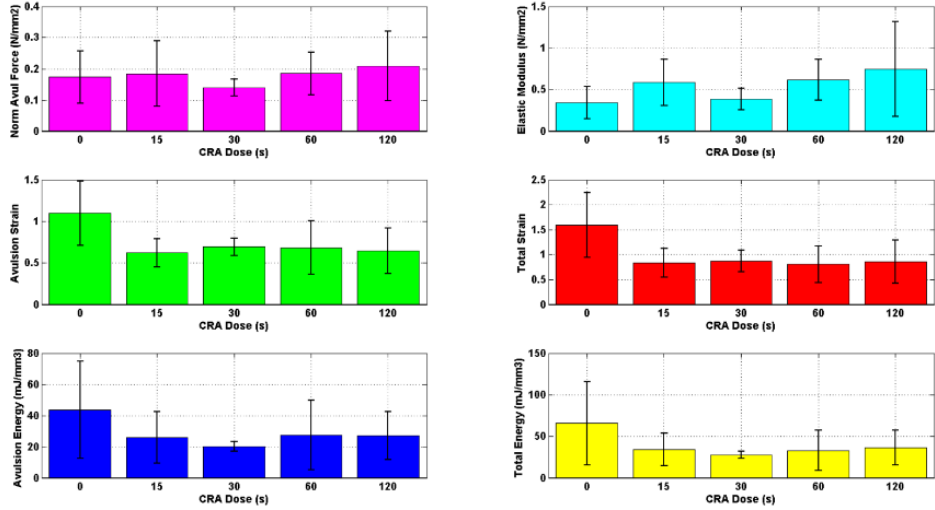
Figure 18:Dose effects of CRA on biomechanical properties of swine diaphragm muscle bundles, as compared with controls. CRA = cryoablation; s = seconds

Discussion

In this study, we demonstrated that both physiologic and biomechanical properties of

swine respiratory diaphragm are altered when subjected to 5 different ablative therapies.

The mechanisms of action of every ablative modality are unique and complex. RFA is a

form of alternating electrical current that dissipates within tissue and generates a lesion

by resistive (electrical) heating,[11] resulting in protein denaturation and coagulation

necrosis. CRA works by freezing tissue in a focused manner to destroy cells in a given

target location, forming a ball of ice that causes freezing, thawing, hemorrhage,

inflammation, fibrosis, and apoptosis.[21] HIFU works by focusing high-intensity

ultrasound waves in a small region of the target tissue, inducing deep hyperthermia and,

ultimately, tissue ablation, through 2 primary modes of tissue injury: thermal and

mechanical; the temperature at the transducer focus can reach over 65°C within seconds,

53

denaturing cellular proteins and causing coagulation necrosis.[31] MWA results in

dielectric heating of tissue when high-frequency electromagnetic radiation stimulates

oscillations of dipole water molecules within the cellular and extracellular medium,

converting the electromagnetic energy into oscillating kinetic energy; this energy is

dissipated as heat at the target location, resulting in thermal injury.[5] CHA uses chemical

agents at lethal concentrations to denature proteins and create focal tissue damage and

lesions, leading to tissue necrosis in the injection location.[24]

Reduced Strength of Contractions
For each of the 5 ablative modalities, we observed a dose-dependent sustained reduction

in PF. With the 4 thermal modalities (RFA, CRA, MWA, and HIFU), changes in

diaphragm tissue occurred at the cellular level when the 3-dimensional protein structure

was disrupted as a result of exposure to extreme temperatures; the proteins lost their

functionality and underwent denaturation.[3] Typically, *hyper*thermic temperatures cause

cell membrane collapse, protein denaturation, cessation in enzymatic function, and

mitochondrial dysfunction leading to coagulation necrosis.[7] Similarly, *hypo*thermic

temperatures cause direct cellular injury from ice-crystal formation, vascular ischemia,

and induced apoptosis.[29]

In contrast, with the chemical modalities (CHA) that we investigated, the diaphragm

tissue samples suffered dehydration, membrane lysis, protein denaturation, and disruption

of structural organization of proteins.[24] That cascade of events led to disruption of

essential proteins, including the contractile myofilaments and the intrinsic and extrinsic proteins of the cell.[21]

At the muscle level, the ability of the diaphragm muscle to elicit an electromechanical response resulting in contraction depended on the viability of the muscle fibers. Ablation resulted in immediate tissue injury leading to cell death, so tissue viability was compromised[7] and thus PF decreased. As expected, we found that higher doses resulted in an increase of cellular injury, consistent with the decreased PF. Yet, in some samples in our study, especially at lower doses, PF initially decreased, but then showed some recovery over the 3-hour measurement period. That pattern could be explained by the effects of skeletal muscle stunning that have been reported after ischemic injury.[19]

Compromised Cellular Function
Ischemic injury resulting from ablation is an impediment to cellular function and results in contractile dysfunction, further leading to PF reduction.[17] One of the proposed mechanisms involves the cell's inability to regulate transmembrane ionic concentration gradients affecting generation of action potentials and muscle contractions. Another mechanism involves accumulation of inorganic phosphates from breakdown of creatine phosphate reserves that inhibit contractile protein function.[28] Additionally, rapid fall of Intracellular pH inhibits Ca^{2+} from binding to troponin, further reducing contractility. The initial decrease in contractility during ablation is considered to be fully reversible if the ablative dose is well below the threshold of tissue injury. However, exceeding the

threshold window prevents the contractile function from returning to the baseline value, even if ablation was not associated with any obvious cell death. This phenomenon, known as "stunning," can slowly reverse over a period of time until a plateau is reached. Several interrelated mechanisms responsible for stunning include (1) sarcolemmal membrane disruption, resulting in loss of action potential and muscle contraction; (2) generation of reactive oxygen species; and (3) selective proteolysis of proteins by action of proteases as a result of increased cytosolic calcium levels.[28]

Increased Resting Muscle Tension

For each of the 5 ablative modalities, we observed an initial increase in the BF which decreased over the recovery period, with the exception of acetic acid. Transient increases in BF as a function of increasing ablative doses is attributed, in part, to stunning: the muscle cells become incapable of eliciting an electromechanical response. This physiologic contracture is caused by a lack of adenosine triphosphate (ATP) within the muscle fibers.[26] Low ATP levels impair SERCA function, hindering sequestration of Ca^{2+} ions into the sarcoplasmic reticulum, causing accumulation within the sarcoplasm. Additionally, a lack of ATP to bind the cross-bridges formed between myosin heads and actin myofilaments cannot release, resulting in contracture.[9] These effects result in elevated BF; in addition, the toxic overload of Ca^{2+} causes a variety of pathophysiologic changes, including necrosis and apoptosis.[2] A reversible increase in tonic resting muscle tension occurs at temperatures <50°C; the muscle shows evidence of irreversible contracture at temperatures >50°C (isotherm of irreversible tissue injury).[4,12] Induced

hypo- and hyperthermia cause Ca^{2+} accumulation within the muscle cells, leading to the overload of Ca^{2+} that has been confirmed with calcium-sensitive fluorescent studies.[10]

Interestingly, in our study, we observed microbubble droplets on the ablated region of muscle bundles subjected to acetic acid for about 30 minutes; we believe that those droplets were caused by excessive dehydration (Fig. S16, electronic supplementary material). Again, the mechanisms of CHA are based on the induction of intracellular dehydration, protein damage, and thromboischemic effects on the muscle cells,[1] eventually resulting in contracture, cellular injury, and protein denaturation and dehydration.

Biomechanical Response

We observed no dose-dependent responses to the 5 ablative therapies in any of the 6 biomechanical parameters we investigated. After internal testing, we determined that the doses we used for our physiologic assessment did not cause a significant change in the biomechanical properties of the diaphragm tissue. However, because we could not elicit any contractions, we could not perform our physiologic assessment of these muscle bundles at the higher doses of the 5 ablative modalities. So, we selected only doses that were clinically relevant and that also allowed us to sequentially administer the physiologic tissue bath tests and the biomechanical tests.

Technique Sensitivity

We found that the sensitivity of tissue baths and uniaxial stress tests were quite different. Significantly higher ablative energies were required to produce any appreciable changes in biomechanical properties of the diaphragm tissue. Clinically, in human patients, an increase in avulsion force means that a higher force would be required to cause tissue tear, primarily because of the denaturation of proteins, elastin, and collagen. In mammals, collagen is the most abundant structural protein; it is located within the extracellular matrix, providing a mechanical scaffold for cells.[27] Ablation causes coagulation necrosis of the tissue; during that process, collagen undergoes posttranslational changes that alter its organization and contribute to tissue stiffness.[20] Accordingly, in most of the 5 ablative modalities we investigated, we observed an increase in avulsion force. We found that ablation typically resulted in a localized tissue injury, which caused either a biomechanical "weakness" or a biomechanical "strengthening" near the ablated region. Furthermore, the muscle bundles typically avulsed at the ablated region or at the healthy ablated tissue interface.

Study Limitations

To our knowledge, no similar studies have been reported on this topic, so it was not possible for us to compare our results with the literature. However, our study certainly had some limitations.

First, we analyzed only samples of muscle bundles prepared from diaphragm biopsies. The tissue response could well be different in the intact whole diaphragm of a living organism. The intact diaphragm is susceptible to secondary collateral injury from ablative

procedures performed in a different region or organ. The extent of collateral injury

depends on the type of ablative energy used, its duration, and its proximity to the

diaphragm. Moreover, these injuries generally tend to be localized to a given region of

the diaphragm. Our experiments did mimic collateral injury by directly ablating the

diaphragm muscle bundles in localized regions with various ablative modalities.

Secondary collateral injury might damage the diaphragm in different ways than direct

injury would, yet we believe that the end result would likely be the same: namely,

cellular injury leading to diaphragm dysfunction.

Second, we looked at only 5 ablative modalities and performed only uniaxial stress tests.

Moreover, we did not use irrigated catheters to test RFA, cryoballoon ablation catheters,

phased-array HIFU transducers, or different MWA antenna designs, and/or different

chemical ablative agents, all of which could have resulted in different findings.

Third, we studied healthy swine tissue and investigated only the acute effects of ablation,

i.e., within hours after ablation, rather than the cumulative effects. Tissue injury is often

correlated with histopathologic examinations, which we were unable to perform (given

the destructive nature of biomechanical tests).

Nevertheless, despite our study's limitations, our results can be used to better understand

the impact of ablative therapies, the mechanisms of tissue injury, and device-tissue

interactions, thereby aiding in future medical device design and development.

Acknowledgments

Effects of Ablation (Radiofrequency, Cryo, Microwave) on Physiologic Properties of the Human Vastus Lateralis

Ashish Singal, Lars M. Mattison, Charles L. Soule, and Paul A. Iaizzo

Preface

Published in the Transactions on Biomedical Engineering (2018), here is a similar investigation to the previous section performed with human tissue. This helps to provide a translational aspect of the research to validate that data collected on pig skeletal muscle is similar to that of human tissue.

Synopsis

Objective: Ablative treatments can sometimes cause collateral injury to surrounding muscular tissue, with important clinical implications. In this study, we investigated the changes in muscle physiology of the human vastus lateralis when exposed to 3 different ablation modalities: radiofrequency ablation, cryoablation, and microwave ablation.

Methods: We obtained fresh vastus lateralis tissue biopsy specimens from 9 patients (age range: 29 to 73 years) who were undergoing testing for malignant hyperthermia. Using leftover tissue, we prepared 46 muscle bundles that were tested in tissue baths before and after ablation.

Results: After ablation with all 3 modalities, we noted dose-dependent sustained reductions in peak force (strength of contraction), as well as transient increases in baseline

force (resting muscle tension). But, over the subsequent 3-hr recovery period, peak force improved, and baseline force consistently recovered to below its pre-ablation levels.

Conclusion: The novel in vitro methodologies we developed to investigate changes in muscle physiology after ablation can be used to study a spectrum of ablation modalities and also to make head-to-head comparisons of different ablation modalities.

Significance: As the role of ablative treatments continues to expand, our findings provide unique insights into the resulting changes in muscle physiology. These insights could enhance the safety and efficacy of ablations and help individuals design and develop novel medical devices.

Introduction

The vastus lateralis is one of the largest muscles of the quadriceps femoris group of muscles that lies on the lateral side of the femur. It has been extensively used as a versatile donor site for microsurgical flap reconstruction in various parts of the body [32]. In addition, vastus lateralis tissue biopsy specimens are routinely used in the caffeine-halothane contracture test for the diagnosis of malignant hyperthermia (MH) [33], a condition that triggers a severe reaction (fast rise in body temperature and severe muscle contractions) to certain drugs used as anesthetics during surgery.

The expanding role of ablative treatments, such as radiofrequency ablation (RFA), cryoablation (CRA), and microwave ablation (MWA), has enabled the use of minimally invasive options to treat musculoskeletal deformities. For example, RFA [34], CRA [35],

and MWA [36] have been used clinically to treat osteoid osteomas with good outcomes. Thermal ablation of bone and soft tissues has been associated with a high success rate and a relatively low complication rate, yet, in some cases, it can cause unintended collateral injury to surrounding sensitive structures such as muscles and nerves [37]. Nervous structures are extremely sensitive to high and low temperatures, which can result in either transient or permanent neurologic damage. Similarly, excessive temperature gradients can cause collateral injury to surrounding muscular tissues, resulting in muscular atrophy, scarring, and deep burns. Thus, successful thermal ablation requires a fine-tuned balance between sufficient ablation volume and thermal protection of the surrounding vulnerable structures.

In this study, our primary objective was to gain new insights into changes in physiologic properties of the human vastus lateralis in response to applied ablative treatments. To do so, we used novel ablative methodologies that were developed in our laboratory and performed in vitro analyses on isolated human vastus lateralis muscle bundles. Despite the vast similarities between different muscles of the body, each muscle type may be unique in terms of its response to ablative treatments and the resulting changes in physiologic properties. Hence, using our novel ablative methodologies, we quantified the effects of ablation on physiologic properties of the human vastus lateralis.

The ablation modalities we utilized in this investigation were RFA, CRA, and MWA. The mechanisms of action of each ablation modality are unique and complex. Briefly, RFA

is a form of alternating electrical current that dissipates within the tissue and generates a lesion by resistive (electrical) heating [38], resulting in protein denaturation and coagulation necrosis. CRA works by freezing tissue in a discrete and focused manner to destroy cells in a target location; the application of cryoenergy forms an ice ball that causes freezing, thawing, hemorrhage, inflammation, fibrosis, and apoptosis [39]. MWA results in dielectric heating of tissue when high-frequency electromagnetic radiation stimulates oscillations of dipole water molecules in the cellular and extracellular medium, converting the electromagnetic energy into oscillating kinetic energy that is then dissipated as heat at the target location, ultimately causing thermal injury [40].

Though similar in purpose, each ablation modality we studied has specific and optimal indications. Choosing the most appropriate ablation modality is vital to the success of any clinical ablative treatment. Important factors include the type of tissue to be ablated, the regional blood flow, and the size of the desired lesion. Each ablation modality has unique advantages. For example, RFA has been used in practice for the longest time establishing its safety and efficacy profile. The CRA probe adheres to the target location by forming an ice ball, so it works well when catheter instability is high because of relative motion between the probe and the target tissue location. MWA offers noncontact therapy by electric field radiation and dielectric heating, thus it may be applicable to a broader spectrum of tissues; however, its long-term effectiveness still needs to be evaluated.

Although numerous studies have been performed with an individual ablation modality

64

as the focus, a review of the literature shows no investigations that have systematically investigated head-to-head comparative effects of ablation modalities on the same tissue/organ. We believe that such investigations will not only provide unique insights into the changes in tissue physiology as a result of ablation, but also enhance the safety and efficacy of ablation procedures by minimizing collateral injury.

Methods

This study was reviewed and approved by the institutional review board at the University of Minnesota. We obtained fresh vastus lateralis tissue biopsy specimens from 9 patients (7 men, 2 women, age range: 29 to 73 years) who were undergoing testing for MH. The tissue was considered waste tissue, i.e. it would have otherwise been discarded after each patient's clinical diagnostic contracture test for MH.

Using either local anesthesia or anesthetic agents not considered to trigger MH, the surgeon dissected a vastus lateralis muscle biopsy specimen about 40 mm long and 15 mm wide from each patient [41]. Then, the muscle biopsy was immediately placed in oxygenated Krebs-Ringer buffer solution and transported to our laboratory (within 10 min). There, we pinned the muscle biopsy in a dissection dish and further dissected it in oxygenated Krebs-Ringer buffer solution, making smaller muscle bundles along the fascicular borders, about 25 mm long and 2 mm in diameter, in an approximate cylindrical shape for the MH diagnostic contracture testing [42],[43]. After completion of the MH contracture test, we prepared additional muscle bundles from leftover tissue that was not required for testing.

Tissue Baths

The tissue baths we used (Fig. 19A) have been previously described [42],[43]. They enabled investigation of changes in physiologic properties of the vastus lateralis in response to different ablative modalities. We mounted muscle bundles in 16 parallel, 50 ml tissue baths (1 muscle bundle per tissue bath) containing Krebs-Ringer buffer solution at 37°C and gassed with 95% O_2 and 5% CO_2 to maintain tissue viability [43]. Each tissue bath was water jacketed and connected to a heater pump (Haake Model DC1, Germany) that maintained 37°C throughout the duration of the experiment. The lower end of the muscle bundle was secured to a fixed hook, while the upper end was attached to a force transducer (Model FT03 with peak capacity of 50 g, Natus Neurology, Warwick, RI, USA).
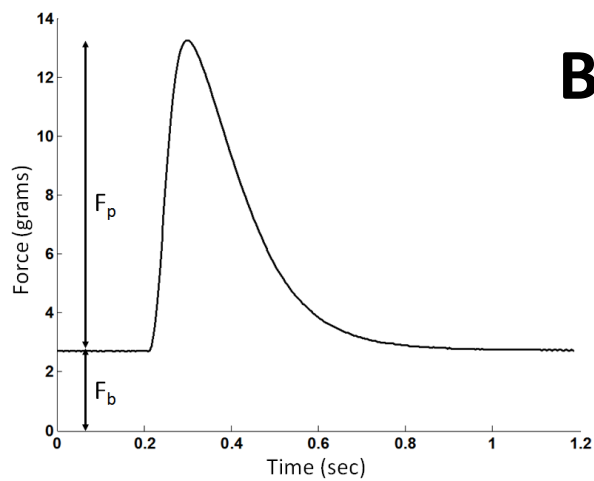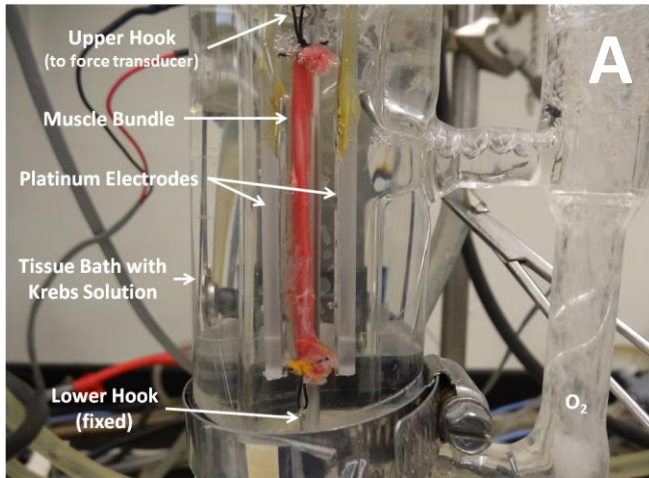
Figure 19 :A) Tissue bath system setup for performing physiologic studies, showing a representative vastus lateralis muscle bundle. B) Example of electromechanical stimulation response from a single muscle bundle, showing peak force (F_p, strength of contraction $= 13.0 - 2.8 = 10.2$ g), and baseline force (F_b, resting muscle tension $= 2.8$ g).

Using custom-built data acquisition software (LabVIEW, Austin, TX, USA), we amplified, digitized (using data acquisition card PCI-MIO-16E-4, National Instruments Corp., Austin, TX, USA), and saved the acquired data. We calibrated each force transducer at 2 settings: first, with no mass (0 g), and second, by hanging a 10 g mass and adjusting

the offset and gain of the amplifier before each experiment.

We collected in vitro force data from all 16 tissue baths simultaneously (representative example, Fig. 19B). After mounting the muscle bundles, we allowed them to stabilize for about 1 hr. During that hour, we optimized the stimulation voltage and length-tension relationship for each muscle bundle before starting the ablation protocol. We used the muscle bundle length resulting in maximum peak force (isometric twitch force) for the remainder of the study.

We assigned the muscle bundles to either the ablation group or the control group. For any given ablation modality, we tested each muscle bundle just once. We measured peak force (strength of contraction) and baseline force (resting muscle tension) both pre- and post-ablation for every muscle bundle. After each ablative treatment, tissues were allowed to recover for at least 3 hr, so that we could assess the relative tissue damage (necrosis) and recovery as a result of exposure to varying doses of different ablation modalities.

Stimulation Protocol
In each tissue bath, the muscle bundles were electrically stimulated simultaneously with a pair of bilateral platinum electrodes (50 mm long, 10 mm wide, and 0.3 mm thick). The electrodes were immersed within each tissue bath, positioned near to but not touching the muscle bundle (Fig. 19A). Muscle bundles were stimulated once every 10 sec with a square-wave pulse 1.0 ms wide throughout the duration of the experimental protocol,

except during ablation. The electrical field stimulation elicited an electromechanical twitch response, which was digitally recorded using a force transducer at a sampling rate of 250 Hz. If reproducible twitches could not be elicited with stimulation, or if the peak force was <1.0 g after the 1 hr stabilization period, we discarded that muscle bundle.

Change in Peak and Baseline Force

We acquired peak force and baseline force continuously for the duration of the experiment (Fig. 19B). We analyzed data at 14 unique time points, including immediately pre-ablation (2 min of data averaged just before ablation) and immediately post-ablation (2 min of data averaged just after ablation); the other 12 time points occurred at 15-min intervals during the 3-hr recovery period post-ablation (2 min of data averaged). We chose "2 min" so that we could calculate the mean value of peak force and baseline force from 12 individual data points obtained from muscle twitches; those 12 data points were deemed a reproducible representation of muscle physiology during that time period. To calculate the percent change in peak force and baseline force for all muscle bundles, we used the following formulae (where PF = peak force, BF = baseline force, t = at any given time point, Δ % = percent change):

$$\% \, \Delta \text{ Peak Force} = [(PF_t - PF_{\text{pre-ablation}})/(PF_{\text{pre-ablation}})] \times 100\%$$

(1)

$$\% \, \Delta \text{ Baseline Force} = [(BF_t - BF_{\text{pre-ablation}})/(BF_{\text{pre-ablation}})] \times 100\%$$

We analyzed all tissue bath data as the percent change in peak force and baseline force with respect to the pre-ablation time point; thus, every graph has 13 bars within each ablation dose (where the leftmost bar represents the percent change immediately post-ablation and every subsequent bar represents the percent change at 15-min intervals). To analyze comparative data, we grouped all muscle bundles exposed to the same ablation dose, and then calculated the mean ± standard deviation (SD) of the percent change in peak force and baseline force for each ablation modality.

Constant Catheter Force

Catheter contact force has been shown to be an important determinant affecting the quality of ablative energy delivered to the target tissue [44]. For example, in the case of RFA, a stronger electrode-tissue contact force increases the lesion size because of improved electrical coupling between the electrode-tissue interface, increased electrode contact surface area with the tissue, and reduced shunting of current in the form of convective energy losses [45]. In addition, a stronger contact force prevents relative motion between the electrode and tissue, resulting in more efficient RF energy coupling and delivery. However, excessive force can bury the electrode within the tissue, resulting in an increased probability of tissue charring, thereby reducing RF energy coupling and delivery.

Similarly, in the case of CRA, a stronger catheter tip contact force results in a faster rate of freezing because of compression of tissue and in decreased convection effects because of blood perfusion warming. Hence, stronger catheter tip pressure increases the lesion size

70

[46]. Thus, in order to perform a comparative assessment of ablation modalities, we selected a fixed value of catheter contact force. After gaining experience from pilot studies and referring to the literature, we selected a clinically relevant value of 0.1 N (10 g) to impart to the muscle bundle during ablation via a uniaxial machine.

Ablation Modalities
  In brief, the 3 ablation groups and 2 control groups were as follows:

•   *RFA group:* 484 KHz sinusoidal waveform at 3 ablation doses: 50°C, 60°C, and 70°C (corresponding to energy levels 312 J, 739 J, and 1169 J, respectively); 12 muscle bundles (n = 4 at each dose).

•   *CRA group:* Operated in the clinical mode, about -75°C at 3 ablation doses: 15, 30, and 60 sec; 9 muscle bundles (n = 3 at each dose).

•   *MWA group:* 1.3 GHz continuous sinusoidal waveform at 3 ablation doses: 410 J, 821 J, and 1231 J; 9 muscle bundles (n = 3 at each dose).

•   *Control–in bath group:* These 8 muscle bundles were left in the tissue bath throughout the duration of the testing protocol.

•   *Control–unmounted group:* These 8 muscle bundles were unmounted from the tissue bath and subjected to the same ablation conditions as the experimental ones but were not ablated.

RFA
  We used an RF Atakr II system (Medtronic, Minneapolis, MN, USA) that generates a sinusoidal waveform at a frequency of 484 KHz with a maximum power output of 100 W.

At such high frequencies, no tissue capture or unintended stimulation occurred; instead the energy was dissipated as heat in the tissue. In addition, we used an RF Contactr catheter (Medtronic; 8 mm electrode length; 7 Fr catheter diameter). The RF Atakr II generator provides high power output with the integral safety of closed-loop temperature control, given the embedded thermocouple in the ablation catheter. For all ablations, we used clinically relevant settings in the temperature mode; the system adjusted the power applied thereby achieving the user-set temperature and maintaining it for the duration of ablation. We set the system power at 50 W and ablation duration of 60 sec. The 3 different ablation doses we investigated were: 50°C, 60°C, and 70°C. During ablation, a laptop computer connected to the RF Atakr II generator via the serial communication port enabled digital recording of ablation parameters. For each sample, we recorded the average and maximum values of power and temperature. To calculate the average RF energy corresponding to each of the ablation temperatures investigated (312 J, 739 J, and 1169 J), we used the product of the average RF power and ablation duration. To apply a constant force of 0.1 N (10 g) on the muscle bundle, we used a special acrylic fixture (built to mount the RF catheter to the uniaxial machine's force transducer). Thus, we performed all ablations under a constant catheter force (Fig. 20).
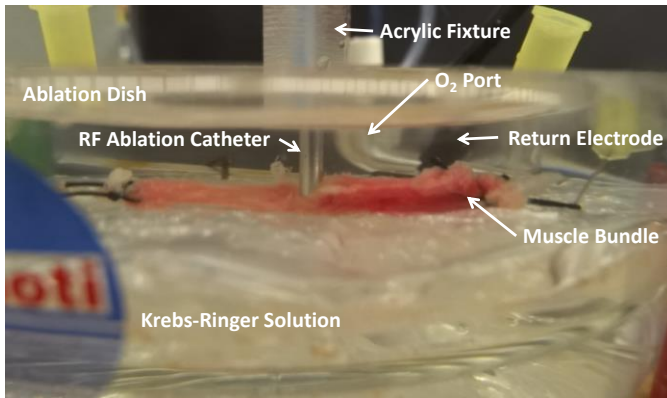
Figure 20: Vastus lateralis muscle bundle undergoing radiofrequency (RF) ablation near the center of the muscle bundle in the ablation dish, with the RF catheter imparting a force of 0.1 N (10 g) on the muscle bundle.

To perform RFA (always near the center of the muscle bundle), we first measured the muscle bundle's length, unmounted it from the tissue bath, pinned it in the ablation dish, and stretched it to the same length as in the tissue bath. RFA was then performed in the ablation dish. The total time the muscle bundle was in the ablation dish was typically <2 min. After ablation, we removed the muscle bundle from the ablation dish, mounted it back in the tissue bath, and stretched it to its original length. To study its recovery and post-ablation effects on muscle physiology, we collected data for another 3 hr.

CRA

We used CRA equipment from CryoCath (Medtronic) that uses a refrigerant (liquefied nitrous oxide, N_2O) to remove heat from a specific area in the tissue, thereby freezing and destroying the tissue at about -75°C. In addition, we used a Freezor MAX CRA catheter (Medtronic; 8 mm tip length, 9 Fr catheter diameter). A thermocouple integrated into the tip of the catheter allowed real-time temperature monitoring during ablation. For all ablations, we used clinically relevant settings, and the CRA system was operated in the

clinical mode. To study dose effects, we selected 3 different ablation durations: 15, 30, and 60 sec. To apply a constant force of 0.1 N (10 g) on the muscle bundle, we used a special acrylic fixture (built to mount the CRA catheter to the uniaxial machine's force transducer). Thus, we performed all ablations under a constant catheter force (Fig. 21).
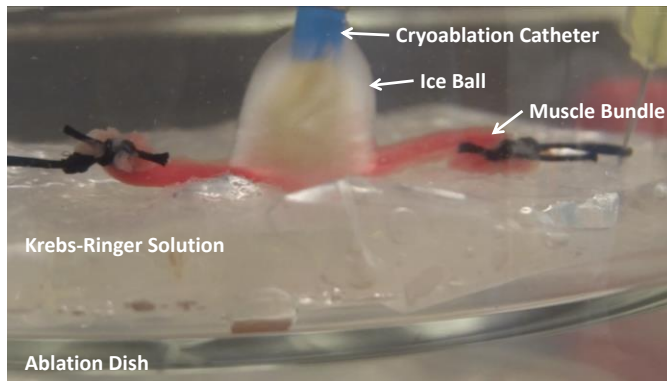
Figure 21:Vastus lateralis muscle bundle undergoing cryoablation near the center of the muscle bundle in the ablation dish, with the cryoablation catheter imparting a force of 0.1 N (10 g) on the muscle bundle. An ice ball almost twice the diameter of the catheter is observed that results in cryoinjury and tissue necrosis.

To perform CRA (center of the muscle bundle), we first measured the muscle bundle's length, unmounted it from the tissue bath, pinned it in the ablation dish, and stretched it to the same length as in the tissue bath. CRA was then performed in the ablation dish. After ablation, the ice ball was allowed to thaw (typically for 30 sec) so that the catheter-tip could become free and detached from the muscle bundle. The total time the muscle bundle was in the ablation dish was typically <2 min. We removed the muscle bundle from the ablation dish, mounted it back in the tissue bath, and stretched it to its original length. To study its recovery and the post-ablation effects on muscle physiology, we collected data for another 3 hr.

MWA

We custom-built the MWA system in our laboratory; the generator (Prostatron, 100 W maximum power) produced microwaves at 1.3 GHz. To ensure impedance matching for optimizing microwave energy delivery, we placed a stub-tuner between the MWA generator and the microwave antenna. To study dose effects, we selected microwave incident power of 20 W and ablation duration of 60 to 180 sec. To calculate the MWA energy during ablations, we used the product of average power (the difference between incident and reflected power) and ablation duration. After gaining experience from pilot studies, we selected 3 different doses in terms of ablation energy: 410 J, 821 J, and 1231 J. To apply a constant force of 0.1 N (10 g) on the muscle bundle, we used a special acrylic (built to mount the MWA antenna to the uniaxial machine's force transducer). Thus, all ablations were performed under constant force (Fig. 22).
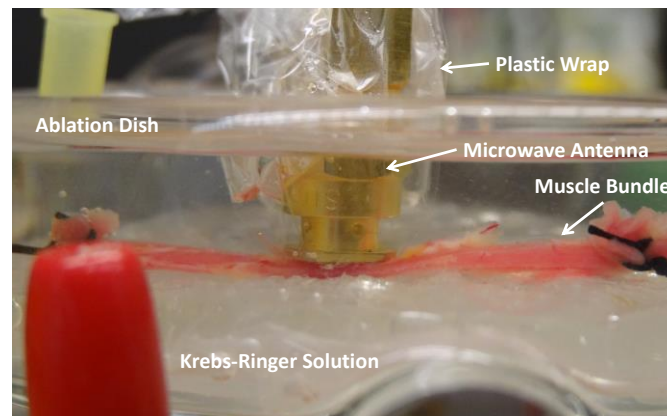
Figure 22: Vastus lateralis muscle bundle undergoing microwave ablation near the center of the muscle bundle in the ablation dish, with the microwave antenna imparting a force of 0.1 N (10 g) on the muscle bundle. A thin sheet of plastic film between the microwave antenna and the muscle bundle ensured ablation from electric field dielectric heating, and not from electrical conduction between the tissue and conductive Krebs-Ringer solution.

To perform MWA (center of the muscle bundle), we first measured the muscle bundle's length, unmounted it from the tissue bath, pinned it in the ablation dish, and stretched it to the same length as in the tissue bath. To ensure ablation from electric field dielectric heating, and not from electrical conduction between the tissue and conductive Krebs-Ringer solution, we placed a thin sheet of plastic film between the microwave antenna and the muscle bundle. MWA was then performed in the ablation dish. The total time the muscle bundle was in the ablation dish was typically <4 min. After ablation, we removed the muscle bundle from the ablation dish, mounted it back in the tissue bath, and stretched it to its original length. To study its recovery and post-ablation effects on muscle physiology, we collected data for another 3 hr.

Two Control Groups

The "control-in bath" group consisted of 8 muscle bundles left in the tissue bath throughout the duration of the testing protocol. The "control-unmounted" group included 8 muscle bundles that were unmounted from the tissue bath and subjected to the same ablation conditions as the experimental muscle bundles (including application of a constant catheter/ antenna force), except that they were not ablated.

Statistical Analysis

For all data analysis, we used Excel and Matlab software. All results are presented as the mean ± SD and $p < 0.05$ was considered statistically significant. To analyze peak force and baseline force (at each ablation dose and at each time point), we used analysis of variance

(ANOVA). To compare different levels for each fixed factor for each ablation modality, we used the Tukey test post hoc (GraphPad Prism). For each ablation modality and for both peak force and baseline force, we created a separate ANOVA model. The variables we entered into the ANOVA model were sample, time, and dose, where sample was treated as a random factor.

Results

We studied a total of 46 vastus lateralis muscle bundles in tissue baths. Of the 46 muscle bundles, 30 were in our 3 ablation groups: 12 RFA, 9 CRA, and 9 MWA, and 16 were in our 2 control groups. All muscle bundles were similar across the 5 groups, and any variation in size or dimensions was not significant, because we normalized all data to the physical characteristics of the muscle bundles.

The percent change (with respect to the pre-ablation time point) in peak force and baseline force in response to all ablation modalities is shown in Fig. 23 for RFA, Fig. 24 for CRA, and Fig. 25 for MWA. In the RFA group we observed significant ($p < 0.05$) dose-dependent reduction in peak force, while CRA and MWA showed different responses, but not significantly so. Transient increases in baseline force were also observed, but were only significant ($p < 0.05$) within ablation modalities for the RFA 70°C group. Note that, after RFA and MWA (but not CRA), peak force initially decreased, then somewhat improved over the subsequent 3-hr recovery period. This phenomenon of partial improvement in peak force was more pronounced at lower ablation doses. We observed smaller reductions in peak force after MWA versus RFA and CRA, which could be

attributed to less tissue injury resulting from a more focused lesion (Fig. 26). In contrast, CRA resulted in the maximum reduction in peak force because the voluminous ice ball destroyed a large section of the muscle bundle along its length (Fig. 21), resulting in cryoinjury (Fig. 26). Additionally, it is well accepted that the size of electrode determines the extent of tissue injury; because the RFA and CRA electrode sizes were similar in dimension to the muscle bundle diameter, the result was a transmural lesion covering the entire width of the muscle bundle (Fig. 26), manifesting in a higher level of tissue injury and in larger reductions in peak force.
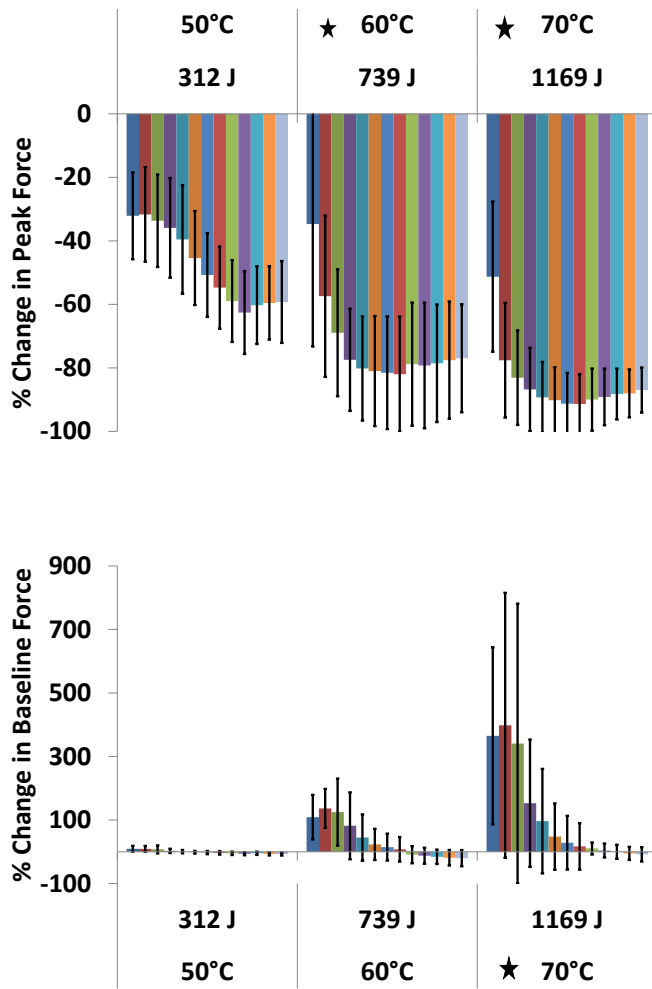
Figure 23:Dose effects of percent change in peak force and baseline force of vastus lateralis muscle bundles after radiofrequency ablation. The leftmost color bar for each ablation dose represents the percent change immediately after ablation; subsequent color bars represent the percent change at 15-min intervals. Entire groups that are statistically significant from control data are denoted by a star.
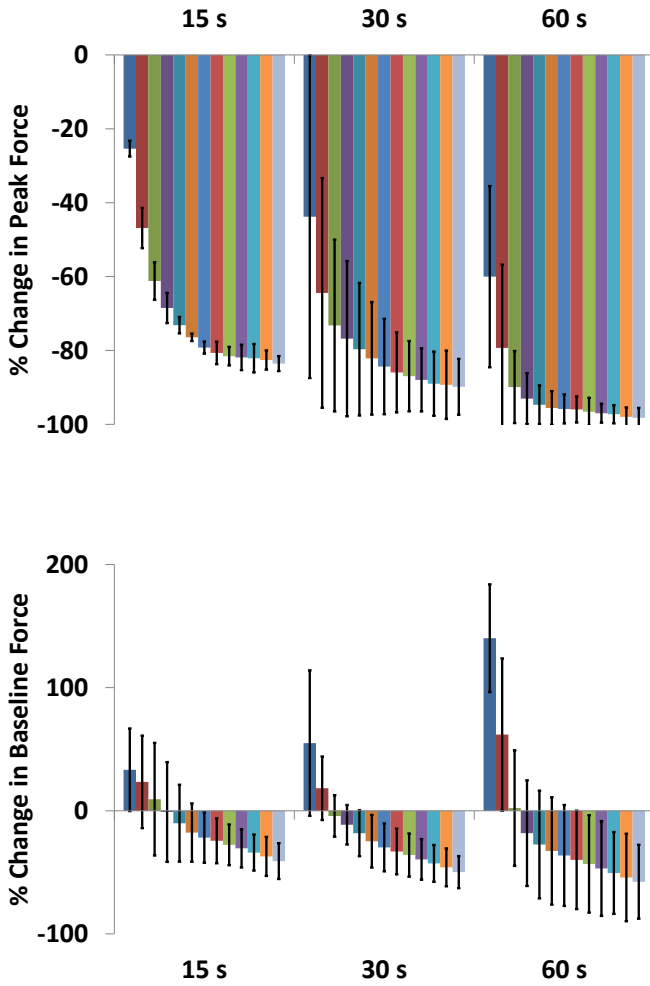
Figure 24: Dose effects of percent change in peak force and baseline force of vastus lateralis muscle bundles after cryoablation. The leftmost color bar for each ablation dose represents the percent change immediately after ablation; subsequent color bars represent the percent change at 15-min intervals.
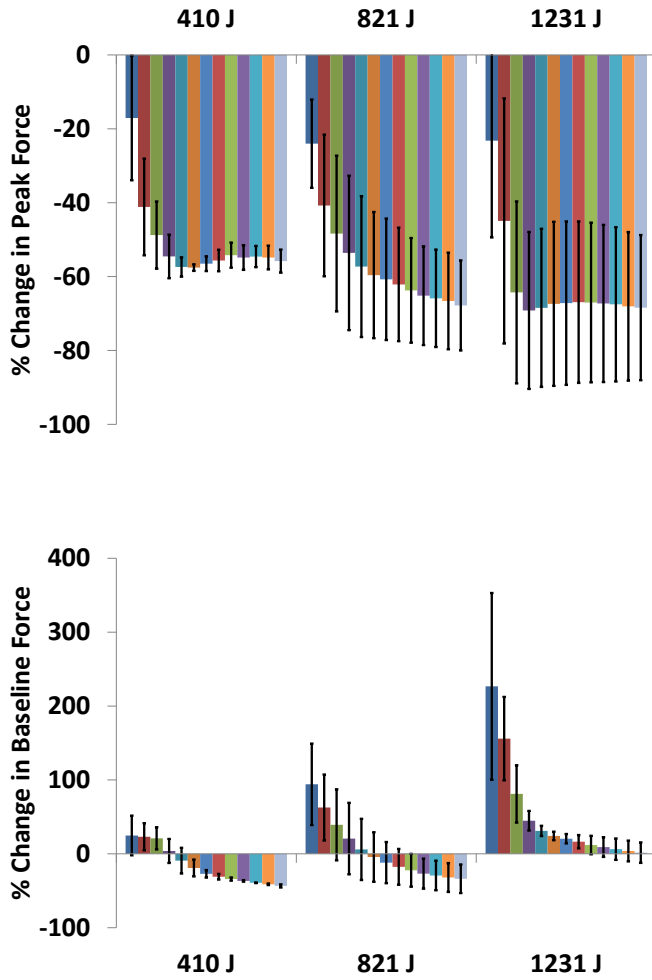
Figure 25: Dose effects of percent change in peak force and baseline force of vastus lateralis muscle bundles after microwave ablation. The leftmost color bar for each ablation dose represents the percent change immediately after ablation; subsequent color bars represent the percent change at 15-min intervals.

81
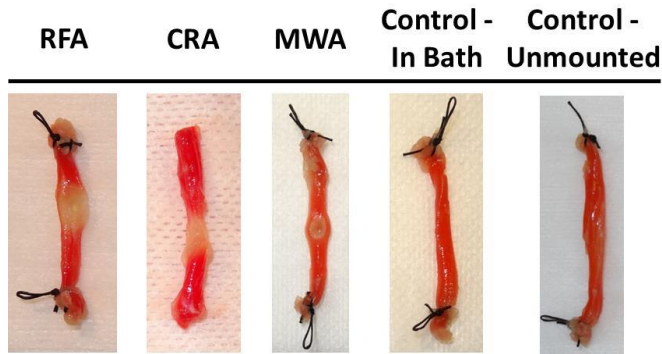
Figure 26: Representative example of acute tissue injury and lesion formation for 3 ablation groups and 2 control groups. The shape and size of electrodes govern the dissipation of thermal energy within the tissue. Microwave ablation (MWA) resulted in a focused lesion, but radiofrequency ablation (RFA) and cryoablation (CRA) resulted in a transmural lesion, because the ablation electrode size matched the muscle bundle diameter.

In all 3 ablation groups, we observed dose-dependent transient increases in baseline force, but its recovery during the 3-hr period was more pronounced in the CRA group, where it returned to pre-ablation levels within only about 30 min (versus 90 min in the other 2 ablation groups). The minimal changes in baseline force that we observed after RFA at 50°C align with the prediction that it is considered as the isotherm of irreversible tissue injury. Interestingly, in our head-to-head comparison of different ablation modalities, we found a consistent increase in baseline force after ablation with all 3 modalities as the energy deposited within the tissue (dose) increased. We attribute that increase in baseline force to the effects of tissue stunning and physiologic contracture, which causes an elevation in resting muscle tension.

In our 2 control groups ("control–in bath" and "control–unmounted"), we observed similar changes in peak force and baseline force (p > 0.05) suggesting that unmounting the muscle bundles from the tissue baths for application of ablative treatments had little or no impact

on the subsequent muscle physiologic response. For each of our 3 ablation groups, we prepared a comparative representative example of acute tissue injury and lesion formation at the end of the 3-hr recovery period (Fig. 26). All results reported here had a p-value of greater than 0.05 unless otherwise stated. Trending results are comments on the shapes of the graphs.

Discussion

In this study, we demonstrated that physiologic properties of the human vastus lateralis were altered when subjected to various ablative treatments.

For each ablation modality, we observed a dose-dependent sustained reduction in peak force. At the cellular level, when the 3-dimensional protein structure is disrupted after exposure to extreme temperatures (on either side of the scale) during ablations, the proteins lose their functionality and undergo denaturation [47]. Typically, *hyper*thermic temperatures cause cell membrane collapse, protein denaturation, cessation in enzymatic function, and mitochondrial dysfunction leading to coagulation necrosis [48]. Similarly, *hypo*thermic temperatures cause direct cellular injury from ice-crystal formation, vascular ischemia, and induced apoptosis [49],[50]. Both of those cascades of events disrupt essential proteins, including the contractile myofilaments and the intrinsic and extrinsic proteins of the cell [39]. At the muscle level, the ability of the muscle fibers to elicit an electromechanical response resulting in contraction is compromised [48]. The tissue injury leading to cell death causes reductions in peak force. As expected, higher ablative doses increase the level of cellular injury, which is consistent with the trends in reduction of peak

force that we observed in this study. Yet, in some cases, especially at lower doses, we observed that the peak force initially decreased, then showed some recovery over the 3-hr period. Our findings could be explained by the effects of skeletal muscle stunning that have been reported after ischemic injury [31].

Furthermore, ischemic injury resulting from ablations is a known impediment to cellular function and results in contractile dysfunction, which is another contributor to peak force reduction [52]. One proposed mechanism involves the cell's inability to regulate transmembrane ionic concentration gradients affecting generations of action potentials and muscle contractions. Another proposed mechanism involves accumulation of inorganic phosphates from breakdown of creatine phosphate reserves that inhibit contractile protein function [53]. Additionally, a rapid fall of intracellular pH inhibits Ca^{2+} from binding to troponin further reducing contractility. The initial decrease in contractility during ablations is considered to be fully reversible *if* the ablative dose is well below the threshold of tissue injury. However, exceeding the threshold window prevents return of contractile function to baseline levels, even with no obvious cell death. This phenomenon, termed "stunning," can slowly reverse, in some cases, until a plateau is reached. Several interrelated mechanisms are likely responsible for the stunning phenomenon: (1) sarcolemmal membrane disruption, resulting in loss of action potential and muscle contraction; (2) generation of reactive oxygen species; and (3) selective proteolysis of proteins by action of proteases as a result of increased cytosolic calcium levels [53].

Transient increases in baseline force as a function of increasing ablative doses have been attributed, in part, to the stunning phenomenon; the muscle cells become incapable of eliciting an electromechanical response, a condition called physiologic contracture. This condition is caused by the lack of adenosine triphosphate (ATP) within the muscle fibers [54]. Low ATP levels impair the sarco/endoplasmic reticulum Ca^{2+} ATPase (SERCA) function, hindering sequestration of Ca^{2+} ions into the sarcoplasmic reticulum and causing accumulation of Ca^{2+} within the sarcoplasm. Given the lack of ATP, it cannot be released to bind the cross-bridges formed between myosin heads and actin myofilaments, resulting in physiologic contracture [55]. Thus, physiologic contracture not only results in elevated baseline force, but also, because of the toxic Ca^{2+} overload, causes a variety of pathophysiologic changes, including necrosis and apoptosis [56]. A reversible increase in tonic resting muscle tension has been observed at temperatures $< 50°C$, however, at temperatures $> 50°C$ (the isotherm of irreversible tissue injury) the muscle shows evidence of irreversible contracture [57]. Induced hypo- and hyperthermia cause Ca^{2+} accumulation within the muscle cells leading to Ca^{2+} overload, as has been confirmed with calcium-sensitive fluorescent studies [58]. These events eventually result in: (1) contracture, causing a sustained increase in baseline force; (2) cellular injury, causing a reduction in peak force; and (3) protein denaturation and dehydration, causing stiffness.

Study Limitations
To our knowledge, no similar studies have been reported to date. Our study does have some limitations. First, we used only a selected number of clinically relevant ablation settings,

so we were unable to assess the cumulative effects of ablations. Second, we did not use irrigated catheters (in our RFA group), cryoballoon ablation catheters (in our CRA group), or different antenna designs (in our MWA group), all of which might have resulted in different findings. Third, we studied healthy human tissue and only investigated the acute effects of ablation, i.e., within hours after ablation. Fourth, we were unable to perform histopathologic assessment (whose results have often been correlated with tissue injury). Nevertheless, despite those limitations, our results can be used to better understand ablative treatments, mechanisms of tissue injury, and device-tissue interactions. We hope that our insights into the changes in muscle physiology with 3 different ablation modalities will enhance the safety and efficacy of ablations and will help individuals design and develop novel medical devices.

Conclusion

In this investigation, we used novel in vitro methodologies to assess how physiologic properties of freshly isolated functional vastus lateralis skeletal muscle bundles change as a result of exposure to 3 different ablation modalities. We believe that the methodologies we developed are applicable for analyzing a spectrum of ablation modalities, and for analyzing emerging techniques such as laser ablation and irreversible electroporation. To our knowledge, this is the first study of its kind comparing the effects of ablation modalities on skeletal muscle physiology. We observed unique dose responses for each ablation modality as well as therapeutic differences regarding the effects on muscle physiology. A better understanding of muscle tissue properties has wide applications, ranging from basic research to novel medical device design. Our unique data could provide important insights

for both clinicians and medical device designers. These results could be used to reduce complication rates, to minimize unintended collateral injury during clinical procedures, and to increase the safety, effectiveness and overall efficacy of ablative treatments. Moreover, increasing knowledge in this area will fuel the demand for introducing new procedures, modifying current ones, and reducing procedural time, with positive impacts on the efficiency and efficacy of ablative treatments.

Acknowledgement

Response of Skeletal Muscle to Electroporation

Preface

The methodology described in the previous two published papers was modified for the investigation of electroporation. Several different skeletal muscle types were investigated including swine diaphragm, human diaphragm, and human vastus lateralis. Functional assessment of twitch and baseline forces and tissue tensile properties were evaluated.

Methods

As previously described in this chapter, biopsies of skeletal muscle were obtained and dissected into bundles approximately 30x3x3mm in size. Swine diaphragm was obtained as waste tissue from a Yorkshire-cross swine from another, unrelated protocol. Human vastus lateralis was obtained as waste tissue from patients undergoing a caffeine

halothane contracture test and human diaphragm was obtained from organ donors who were donating their non-transplantable tissues for research to the Visible Heart Lab with the help of LifeSource. The bundles were promptly dissected, and a suture loop was tied to each end of the bundle. The bundles were then suspended in a heated, oxygenated muscle baths and submerged in a modified Krebs buffer. Electric field stimulation was applied every 10 seconds with a single 1ms pulse delivered at a supramaximal stimulation voltage. The bundles were stretched to their optimal length and allowed to stabilize before the baseline period recording was started.

Following the baseline recording period, the electroporation treatment was applied across the bundle with two needle electrodes 1cm in length. To place the electrodes, the bath was lowered, stimulation paddles removed, and a container with the same Krebs solution was placed around the bundle. The electrodes were placed parallel to the muscle bundle on either side and held in place as the delivery was applied. A custom fixture kept the needles placed at a consistent 1cm apart. The parameters were investigated based on the functionality of the NanoKnife generator.

The parameters that were investigated include:

Voltage (V): 500, 600, 700, 800, 900,1000, 1100, or 1200 (70 pulses, 90us, 1.5 or 4Hz)

Number of pulses: 10, 20, 30, 40, 50, 60, 70, 80, 90, 100 (500V, 90us, 4Hz)

Pulse width(us): 20, 30, 40, 50, 60, 70, 80, 90, or 100 (500V, 20 pulses, 4Hz)

Frequency (Hz): 1.5 or 4

Peak twitch force and baseline tension force were measured as previously outlined (figure 19B) and normalized to a pre-ablation period of 15 minutes to examine baseline function. For 3 hours following the application of the electroporation, the bundles were monitored.

Following the post ablation monitoring period, the bundles were measured and removed from the muscle bath fixture. They were then placed in the Instron Uniaxial Force Tester. Each muscle bundle was pulled in a quasistatic manner at a rate of 10 mm/min until failure. After failure, the bundle was massed and discarded. Only bundles with failures not originating from the suture were used for analysis (figure 13 and table 1).

All files were analyzed by a custom Matlab script that calculated 3-minute averages for peak and baseline force and normalized the data to a 15-minute pre-ablation period. The output was then analyzed using GraphPad Prism 8.0 (San Diego, CA).

Results

Swine Diaphragm

Voltage
To examine the effect of voltage on swine diaphragm, 117 bundles were treated across all voltages at 4 Hz and 79 bundles at 1.5 Hz. Functional peak force and baseline force was measured for three hours post ablation. At both frequencies an almost complete loss of twitch force was observed across all levels of treatment (figure 27). Bundles treated at the lowest level (500 V) showed some preserved function, but never recovered to more than 20% of its initial function.
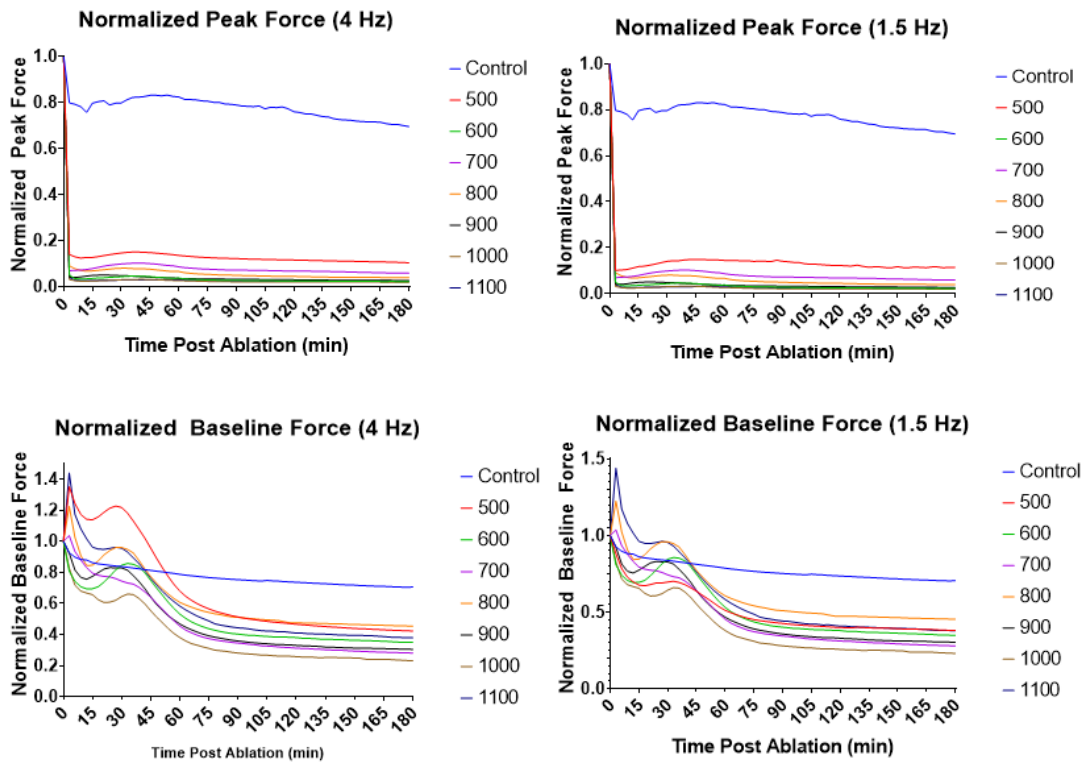
Figure 27: Normalized Peak Force and Normalized Base Force for swine diaphragm muscle showing the response to varying voltages and frequencies.

The baseline force shows that the bundles, again for both frequencies, go into a state of contracture following the application of energy and then immediately began to relax. It is interesting that the bundles across all treatment levels experience a second period of contracture, before a sustained period of relaxation. The treated bundles do relax to a level of 20-50% of the initial baseline force. This biphasic response could be due to the prolonged contracture due to the electroporation and the second contracture could be due to the influx of calcium following the treatment which eventually leads to cell death.

The avulsion force normalized to cross sectional area shows no difference between the treated groups (p>0.05) (figure 28). Similar values were obtained for both frequencies of application. In total 63 bundles were evaluated at 4 Hz, 53 at 1.5 Hz, and 135 control bundles.
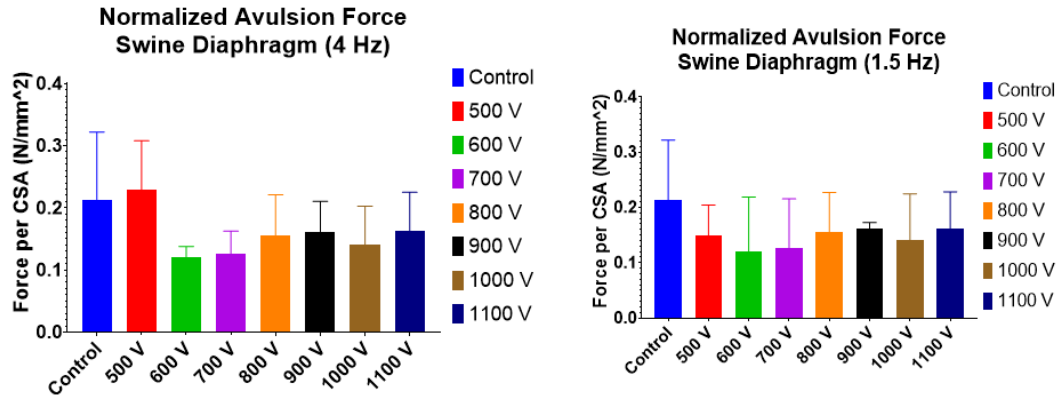
Figure 28: Normalized Avulsion force of Swine diaphragm to varying voltages and frequencies of electroporation.

Number of Pulses

A total of 242 bundles were examined to understand the effect of number of pulses on skeletal muscle. Despite initial stunning in all bundles, additional recovery was observed in the two lowest doses of 10 and 20 pulses (figure 29). At best, 10 pulses only regained 50% of its initial peak force generation. The investigated baseline force showed that the lower number of pulses primarily had diminished baseline force. There were a couple of exceptions as 60 pulses also decreased in baseline force while all other groups above 50 pulses showed an increase in baseline force.
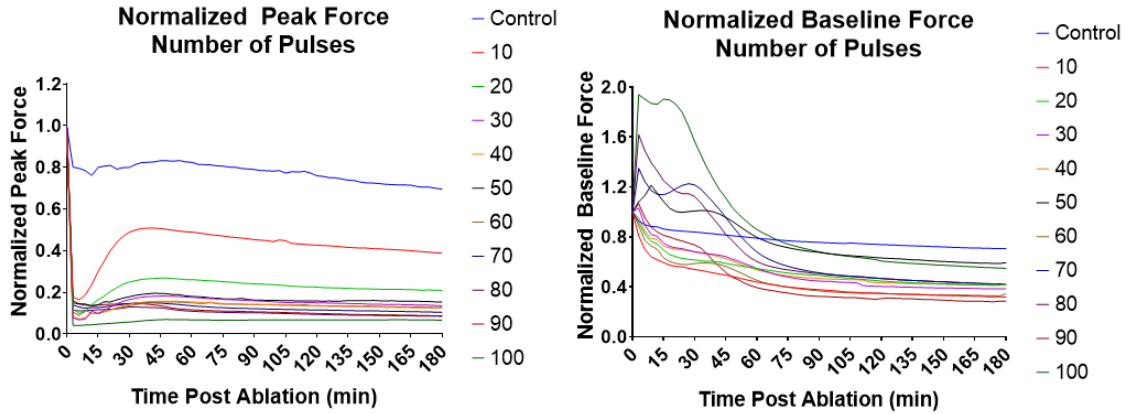
Figure 29: Normalized Peak Force and Baseline Force of Swine Diaphragm examining the effect of number of pulses on muscle function.

Again, the normalized avulsion force was not significant between groups (p>0.05). The values were very consistent between all the treated groups showing minimal variation between the different treatments.
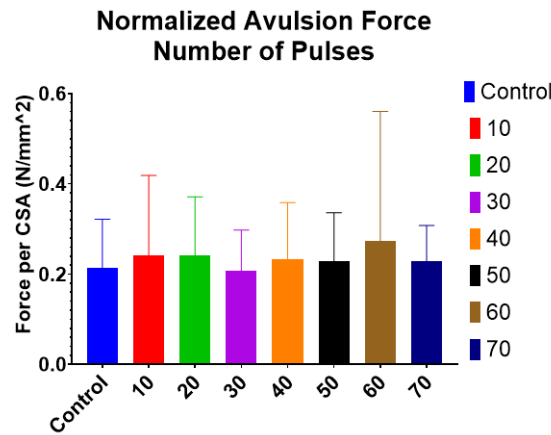
Figure 30: Normalized Avulsion force of Swine diaphragm to varying number of pulses of electroporation.

Pulse Length

The 131 bundles tested at various pulse lengths showed an initial stunning response, followed by a 3-hour period of recovery (figure 31). The initial stunning was more

severe with longer pulse lengths, but the was not indicative of the total recovery for the

bundles. After 45 minutes any decay in bundle function matched that of the control

bundles. Baseline force showed an initial period of contraction, followed by a decrease

to approximately 50% of baseline force. The 60 us group had one bundle that had an

elevated baseline, causing the average to shift well above the other bundles.
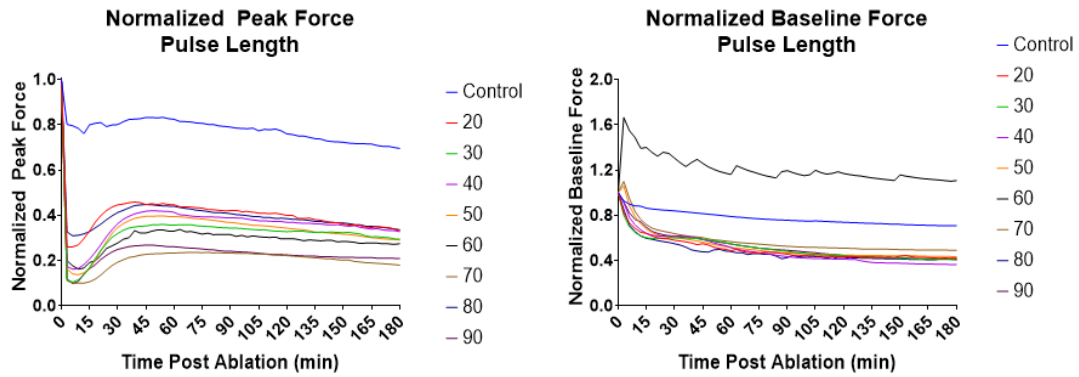
Figure 31: Normalized Peak Force and Baseline Force of Swine Diaphragm examining the effect of number of pulses on muscle function.

The normalized avulsion force was again consistent across all the bundles ($p > 0.05$)

(figure 32). Again the 60 us group had the most variability. These results suggest that

the structural integrity of the bundles was unaffected by the treatment.

93
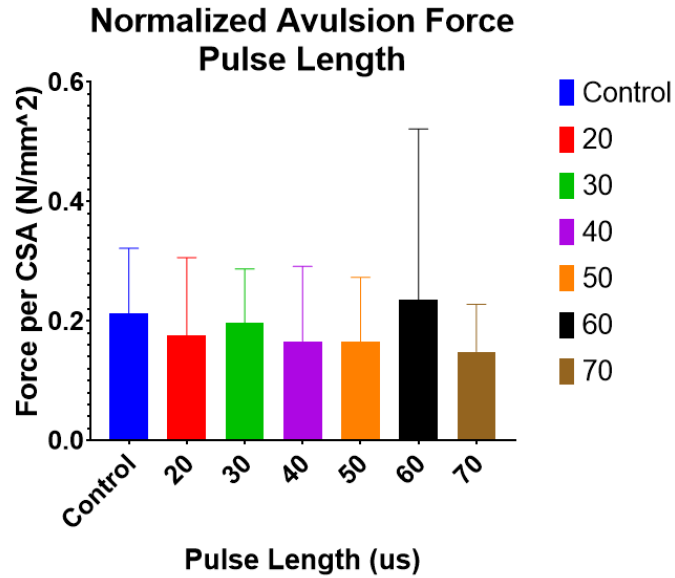
Figure 32: Normalized Avulsion force of Swine diaphragm to varying pulse lengths.

Human Diaphragm

Voltage

With only a few bundles to investigate (n=8), two levels of voltage were applied. As seen

in the swine diaphragm, a sustained drop in peak force was observed immediately

following the application of electroporation (figure 33). Baseline force dropped initially

followed by a short period of recovery. It then decreased again before remaining

constant after 45 minutes post ablation. No avulsion data was collected due to the small

sample size.
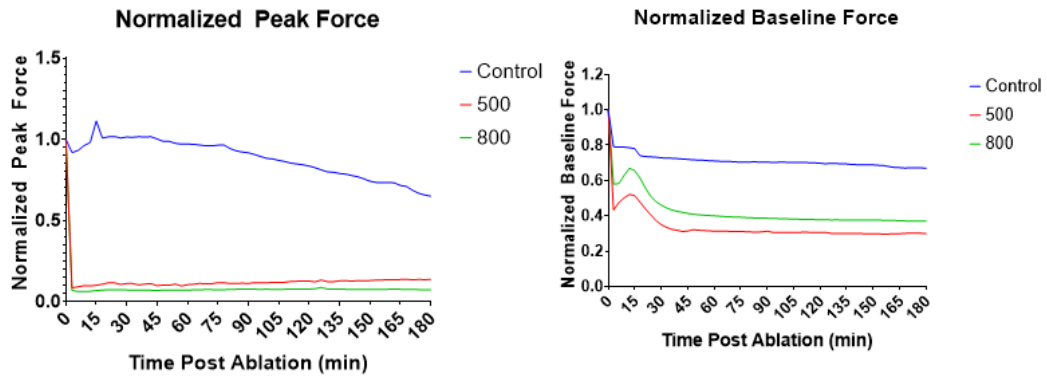
Figure 33: Normalized Peak Force and Baseline Force on Human Diaphragm examining the effect of voltage on muscle function.

Number of Pulses

Again, a small investigation due to limited access to human tissue (n=13) shows an interesting dose response of the diaphragm to the number of pulses applied. An initial stunning effect was observed, but a large amount of recovery was seen in all the doses except for the highest two (60 and 70 pulses). The baseline force also behaved differently as it decreased following energy application and stayed content following the initial change. No hypercontraction was observed across all the bundles.
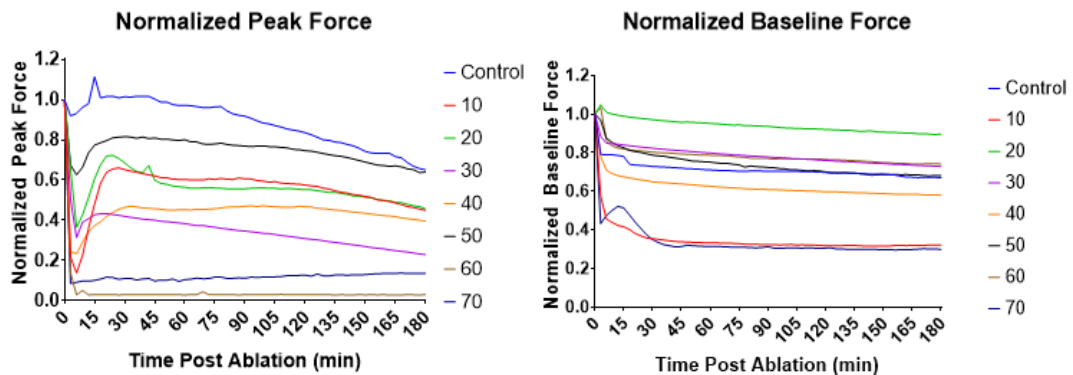
Figure 34: Normalized Peak Force and Baseline Force on human diaphragm examining the effect of number of pulses on muscle function.

95

Human Vastus Lateralis

Voltage

In total, 33 bundles were treated with various voltages to examine their response (figure 35). In a similar narrative to other skeletal muscle, function was immediately lost, and no recovery was observed. However, the baseline force response was different. A long period of contraction occurred starting 15 minutes after the ablation. Only the highest voltage had the bimodal response previously observed in skeletal muscle.
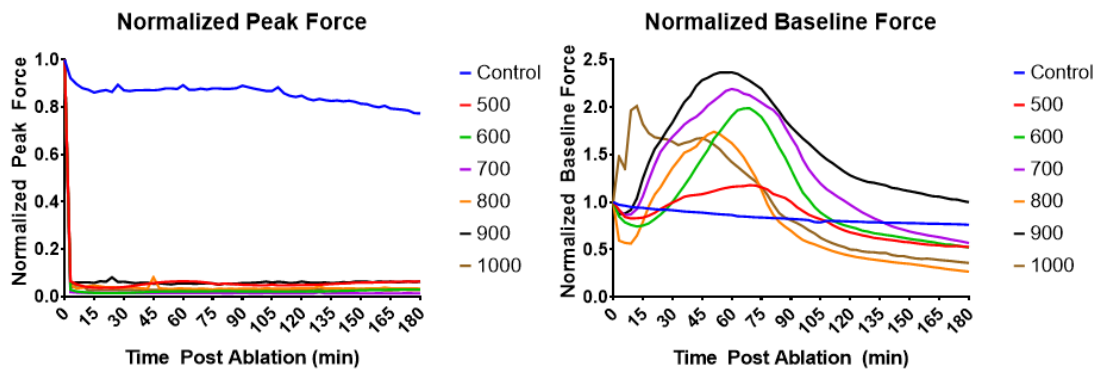
Figure 35: Normalized Peak Force and Baseline Force on human vastus lateralis examining the effect of voltage on muscle function.

Approximately half of the bundles failed in the middle of the bundle. Investigation of the differences between groups is difficult as 3 are only a single data point (600 V, 800 V, and 900 V) (figure 37). One note of interest is that on 2 occasions, the bundles failed in the middle during preparation (figure 36). Minimal force was applied, but in both cases, they were treated bundles.
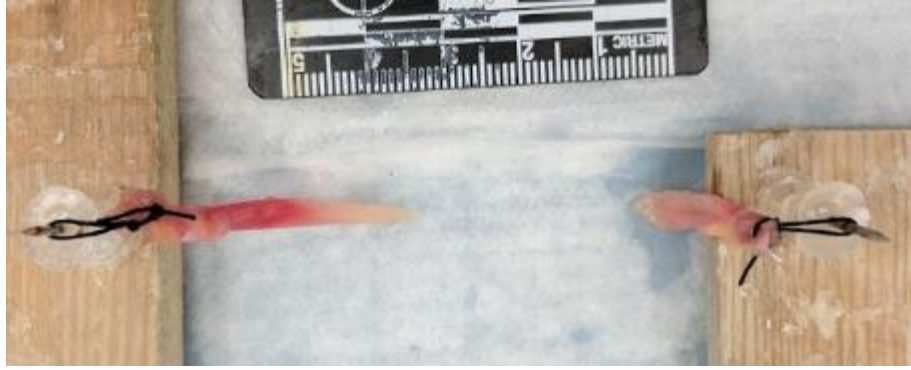
Figure 36: Image of a Vastus Lateralis muscle bundle that failed during preparation for uniaxial pulling.
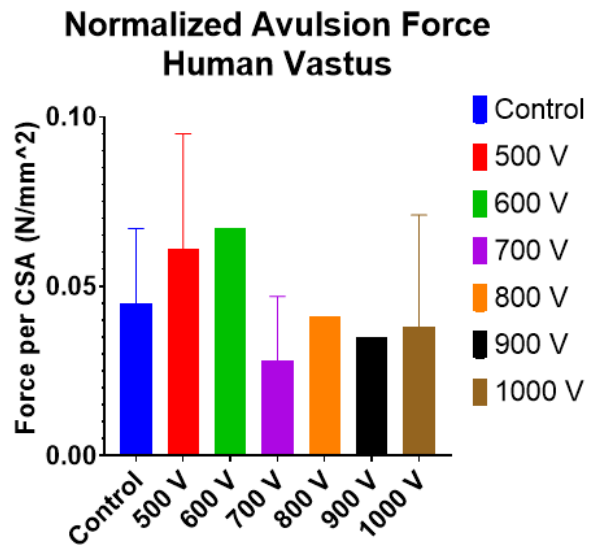
Figure 37: Normalized avulsion force response of human vastus lateralis to varying voltages.

Number of Pulses

Here a small sample (n=23) shows the response of vastus lateralis to fewer pulses that previously investigated (figure 38). The same response was observed with an immediate loss of function. However, the group that only had 10 pulses applied did appear to be

recovering. A longer study period would have allowed for a better understanding of this

response.
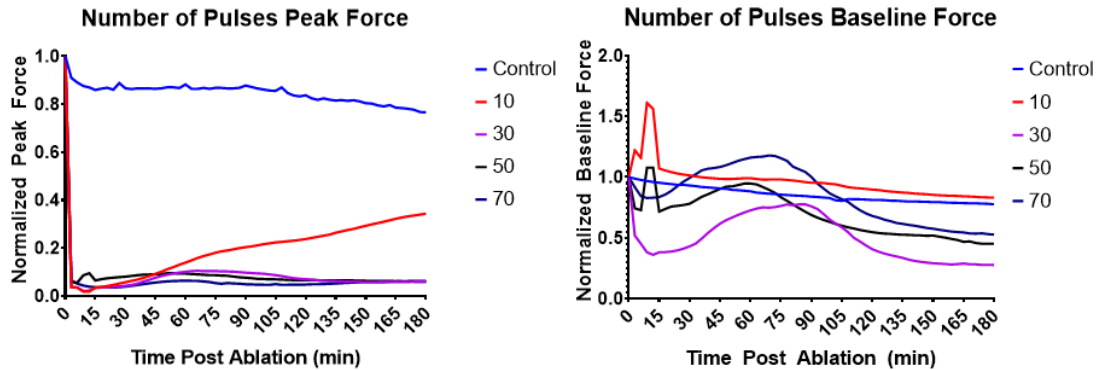
Figure 38: Normalized Peak Force and Baseline Force on human diaphragm examining the effect of number of pulses on muscle function.

Discussion

Skeletal muscle shows a very rapid response to electroporative therapies. Across the

board, when more than 20 pulses are applied, even at only 500 V, an immediate loss of

function is apparent and sustained. This is likely due to the nature of the skeletal muscle

cell. Long cells run the length of the bundle. If the middle of the bundle is completely

damaged, all the cells will have an area of damage causing decreased function. This is

not the case for other muscle types.

Between swine and human diaphragm, a larger recovery is observed within the human

tissue compared to swine with regards to peak force generation. Swine diaphragm tissue

also showed a period of hypercontraction which human diaphragm did not. This shows

that the swine diaphragm is a good way to compare the peak force response of the human

98

diaphragm. It is possible that the tissue properties of the human diaphragm presented here were altered due to the prolonged hypoxic period they were exposed to.

When comparing avulsion force normalized by cross sectional area, it is observed that the human vastus lateralis has a much smaller failure point compared to swine diaphragm. However, all the treated groups did not statistically vary compared to the baseline of the respective tissue, showing that tissue integrity is maintained following the application of electroporation.

Another aspect of this investigation is the potential for creating thermal lesions with the profiles used here. Previous work has shown that in tissue, thermal damage can be caused using needle electrodes, with a more profound effect at 4 Hz than 1.5 Hz[59]. We don't see that effect in these data as both frequencies showed similar results. Additionally, there is adequate cooling with a large fluid heat sink around the bundle.

There are limitations to this investigation. When the electroporation was applied, the tissue was submerged in a conductive Krebs buffer. However, the electric field applied to the tissue is different than was applied to the probes. This numbers presented in this work are therefore guidelines to what clinical numbers might be.

Conclusions
Here we were able to modify our previously established protocol to evaluate the functional and biomechanical response of various skeletal muscles to electroporation.

The more energy that was applied across the bundle, the larger the decrease in force that was observed. However, a larger force, sustained a decrease in contractile force in skeletal muscles. This property was not seen in other tissue types.

Chapter 3: Smooth Muscle Response to Ablative Therapies

Preface

Here we will use the methodology described in chapter 2 and modify it for the investigation of smooth muscle response to electroporation therapies. The smooth muscle that will be investigated is the esophagus as this is the primary smooth muscle in the cardiothoracic cavity.

Background

Smooth muscle is a different target tissue type compared to skeletal muscle. Within the cardiothoracic cavity, the esophagus is the primary smooth muscle running from the mouth to the stomach. Ablation of the esophagus can be used to treat various disease states such as Barrett's Esophagus. Groups have filled intellectual property on using irreversible electroporation to treat the disease.[1] Other groups have examined the use of electrochemotherapy for the treatment of esophageal cancer with good results.[2] This application for electrochemotherapy of these therapeutic pulses are within the range of those investigated here.

While there is positive success with esophageal treatment, the smooth muscle is an area of collateral damage in cardiac ablations. Given its proximity to the pulmonary veins and posterior wall of the left atrium, it can be damaged during an ablation. Incidence of atrial esophageal fistula has been reported in the range of 0.01-0.2% of all catheter ablation

cases[3]. Atrial esophageal fistula has been reported when using radiofrequency[4,5], cryo[6,7], and high intensity focused ultrasound[8] ablations. While this is an extremely rare occurrence, it is almost always fatal for the patient. Other investigations examining the direct treatment of electroporation onto the esophagus have shown that the chronically the tissue architecture remains unaffected 2 months following the ablation procedure[9]. While there was a visible lesion on the tissue, there were no signs of ulceration.

Here we will investigate the functional response of swine and human esophagus tissues to electroporation. The functional investigation will be coupled with examining the tissue properties after the application of the energy to better understand the changes to tissue properties as well.

Methods

The methods are similar to those previously described for skeletal muscle. Swine esophagus tissue was obtained as waste tissue from a Yorkshire-cross pig from another, unrelated protocol. Human esophagus was obtained from organ donors who were donating organs for research through a collaboration with LifeSource. Preparation of esophageal tissues differed slightly in that the submucosa and the muscularis propria were separated (figure 39). The submucosa was discarded, and circumferential bundles were prepared. The other modification to the experimental protocol was to change the electrical stimulus to every 30 seconds stimulating with 0.5 seconds of 15 Hz, 1ms pulses. This allowed for a larger, more pronounced smooth muscle response compared to the parameters used for skeletal muscles.
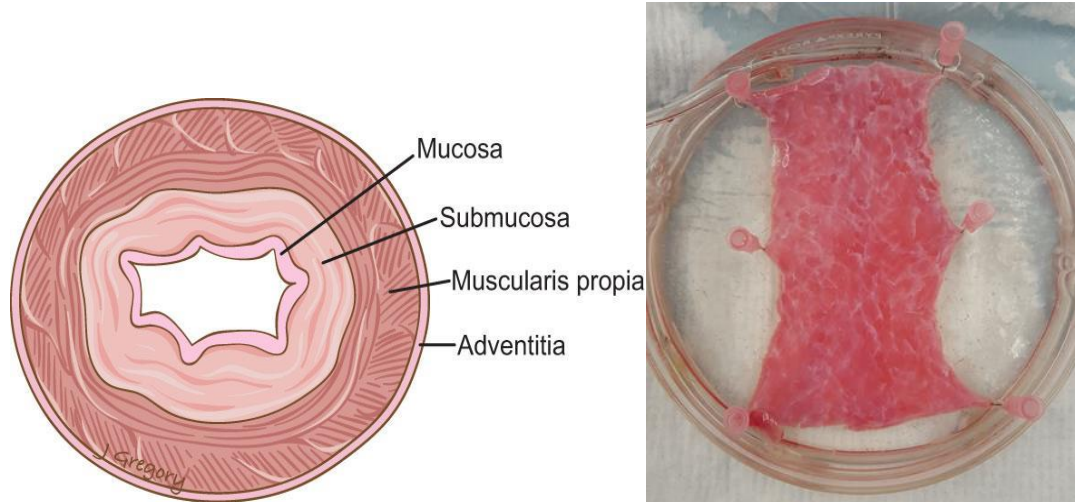
Figure 39: Left: Cross sectional anatomy of the esophagus. Right: Muscularis propria of the esophagus with the submucosa removed.

The same protocol was used for the application of electroporation to the esophageal tissue as reported in Chapter 2. In this case, only 3 parameters were investigated. The parameters that were investigated include:

Voltage (V): 500, 600, 700, 800, 900,1000, 1100, or 1200 (70 pulses 90us long at 1.5 or 4 Hz)

Number of Pulses: 10, 20, 30, 40, 50, 60, 70, 80, 90, 100 (500V, 90us pulses at 4Hz)

Frequency (Hz): 1.5 or 4

Peak twitch force and baseline tension force were measured as previously outlined (figure 19A) and normalized to a pre-ablation period of 15 minutes to examine baseline function. For 3 hours following the application of the electroporation, the bundles were monitored.

After completion of the post ablation monitoring period, the bundles were measured and removed from the muscle bath fixture. They were then placed in the Instron uniaxial pull machine. Each muscle bundle was pulled in a quasistatic matter until failure at a rate of 10 mm/min. Following this, the bundle was massed and discarded. Only bundles that failed in the center were used for analysis (figure 13 and table 1).

All files were analyzed by a custom Matlab script that calculated 3-minute averages and normalized the data to a 15-minute baseline period. The output was then analyzed using GraphPad Prism.

Results

Swine Esophagus
Voltage and Frequency

Functional twitch force data was collected from 87 muscle bundles across all voltages 4 Hz and 28 muscle bundles at 1.5 Hz. These data show an initial drop in function immediately following the application of all energies with very little to no recovery in the 3 hours of monitoring after the ablation. Baseline force shows the bundles go into contracture of increasing severity with higher energies. This period of contracture lasts for a period of 90 minutes. These data are shown in figure 40. No difference was observed between the different frequencies of applications.
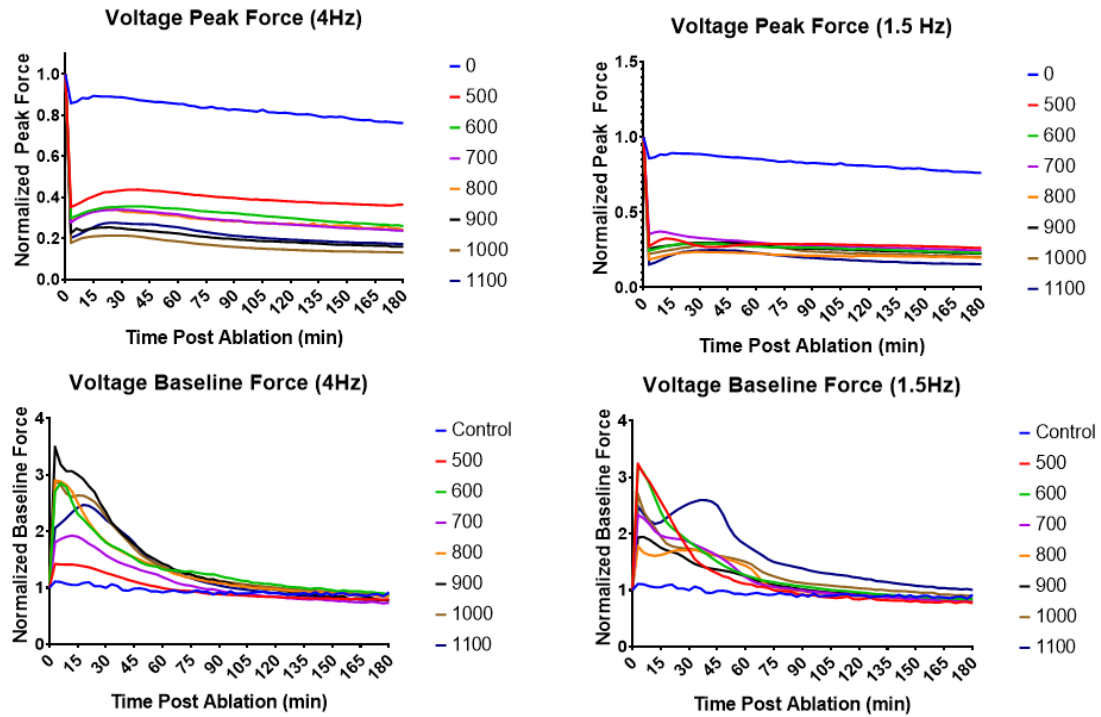
Figure 40: Normalized Peak Force and Baseline Force on swine esophagus examining the effects of applied voltage and frequency on muscle function.

In examination of the effects of number of pulses of electroporative therapy, 125 bundles were examined (figure 41). A dose response was observed showing that an increased number of pulses causes increasing damage to the bundles ability to contract. An initial drop in force generation was observed across all doses, with larger decreases in larger number of pulses applied. Change in baseline force shows a large increase (greater than 2 times) when more than 60 pulses are applied. This period of contracture is relatively transient at these levels as a return to baseline is observed within 30 minutes post ablation.
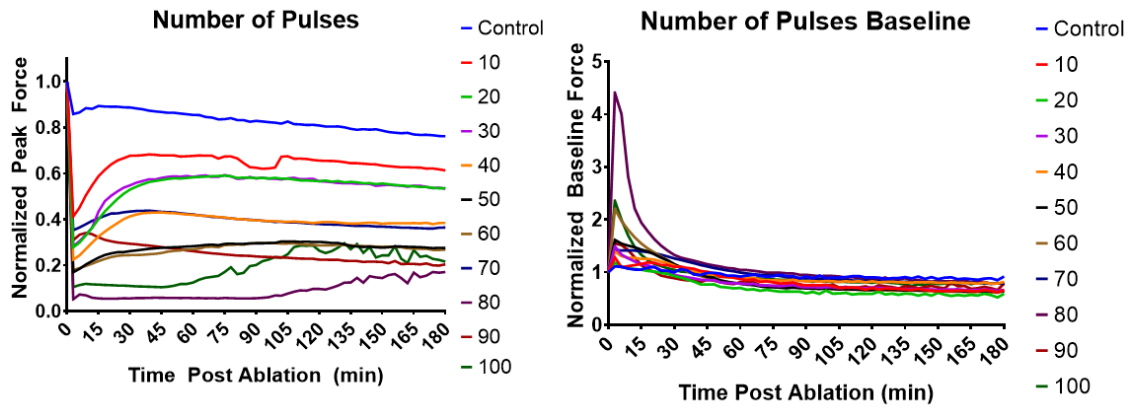
Figure 41: Normalized Peak Force and Baseline Force on swine esophagus examining the effects of number of pulses on muscle function.

Insufficient quality data was collected to examine the biomechanical properties of swine esophagus data.

Human Esophagus

Voltage and Frequency

Ninety-nine bundles were hung and treated with various voltages at 4 Hz, and 79 bundles were hung and treated with doses of 1.5 Hz. Baseline and Peak force data were calculated for the bundles (figure 42).

106
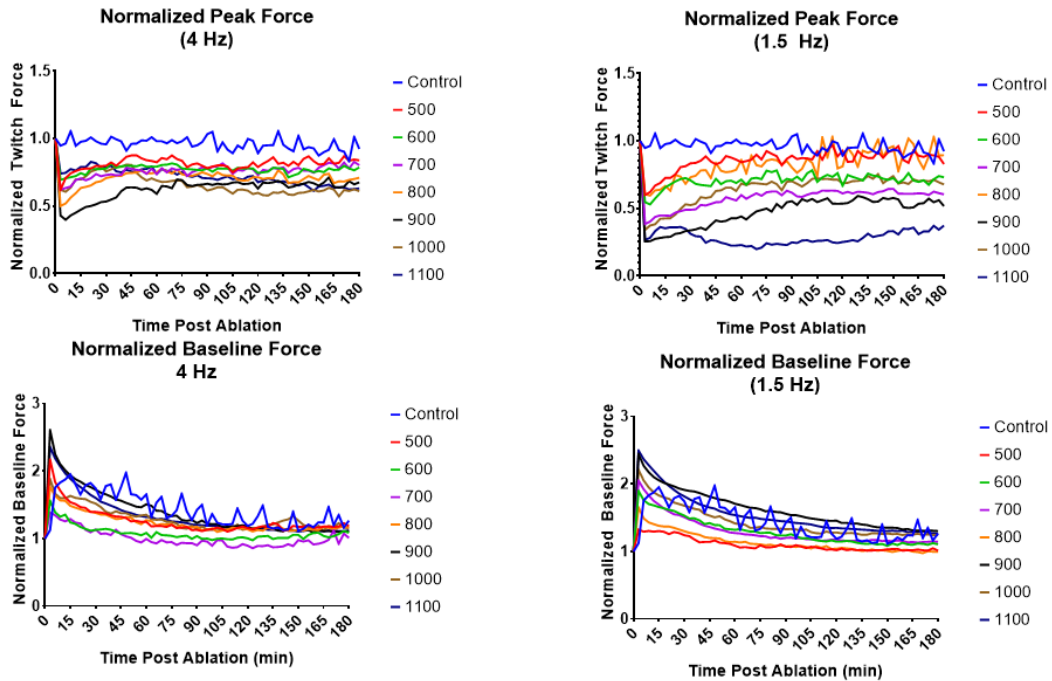
Figure 42: Normalized Peak Force and Baseline Force on human esophagus examining the effects of applied voltage and frequency on muscle function.

A dose response was also observed for both treatment groups. A larger decrease in force was observed for 1.5 Hz application compared to 4 Hz data. Eventual recovery was observed for all groups, except for 1100 V and 1.5 Hz group where force appears to recover faster with 4 Hz data as well. Baseline force data was almost identical across both groups. In general, bundles went into a state of contracture which slowly returned to initial baseline around 90 minutes.

In addition, avulsion force was normalized to the cross-sectional area of each bundle; determined by measuring orthogonal diameters of each bundle. Both 1.5 Hz and 4 Hz samples had 42 samples in each group (figure 43). The 1100 V, 1.5 Hz group did not

have any failures not initiated by the sutures. Regardless of treatment applied the

bundles, similar results were observed. A one-way ANOVA showed no difference from

the control group (p>0.05).
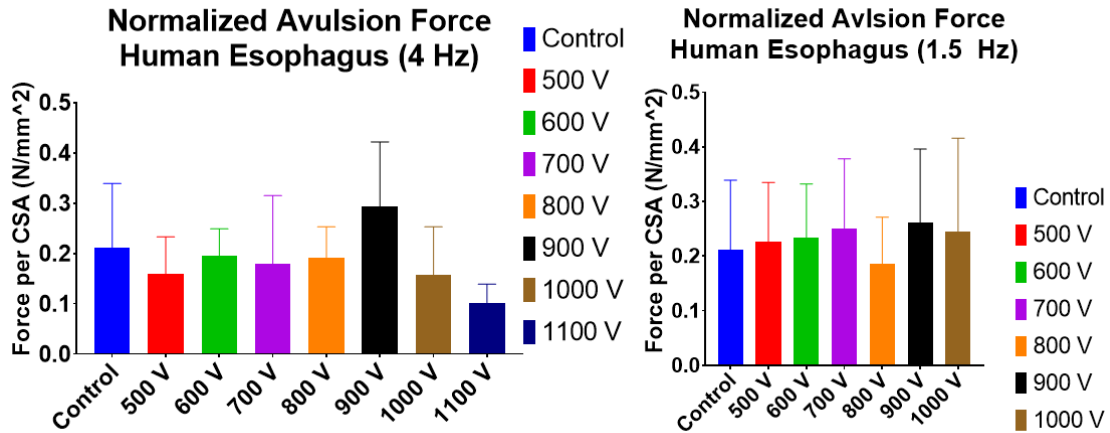
Figure 43: Normalized Avulsion force response of human esophagus to varying voltages.

Discussion

Both human and swine tissue showed similar responses to electroporative therapies. In

general, swine esophagus showed a more severe response to the therapy. This makes

sense as swine esophagus contains a higher percentage of skeletal muscle when compared

to human esophagus. The sharp drop in function mimics the response seen in chapter 2,

but to a lesser extent. The human esophagus has some skeletal muscle for the first third,

but otherwise transitions to primarily smooth muscle[10].

We should also consider the structure of smooth vs skeletal muscle. Skeletal muscle

consists of long fibers that are run the entire length of the muscle. Smooth muscle is a

series of a smaller array of cells that aren't all subjected to the electric field. Thus, where

108

skeletal muscle might have a more all or none response to electroporation, smooth muscle could mute this response, especially in this experimental set up.

Both swine and human tissue show a large increase in baseline force when exposed to the electric field that eventually resolves completely down to the initial baseline level around 90 minutes post ablation and is maintained for the rest of the experiment. The implications of this show that if exposed to an electroporative electric field, the esophagus could experience a prolonged period of contracture. For patients receiving therapy, this could cause intense discomfort unless a muscle relaxant had been previously administered.

Conclusions

Here we have shown that we can evaluate both swine and human esophagus tissue for both functional and structural changes following the application of electroporation. We show that the esophagus is more resilient to electroporation therapy than skeletal muscle. Since swine esophageal muscle has more similarities to skeletal muscle, the results were more severe for loss of function. Contractures were observed for both samples which should be considered during a procedure as well. Overall, these samples of human and swine esophageal presented with similar properties.

Chapter 4: Cardiac Tissue Response to Electroporation

This chapter examines cardiac tissue and its response to electroporative therapies. Cardiac tissue is the primary target for atrial fibrillation ablations. The interest in using electroporation for cardiac applications has greatly increase in the past few years. In 2018, two review articles were published on using irreversible electroporation as a treatment for atrial arrythmias (1-2). These articles advocate for the mounting evidence suggesting that the safety profile of electroporation is favorable compared to existing technologies (3). Additionally, preliminary results from the use of electroporation in humans for pulmonary vein isolation has been published (4). Using either an endocardial or epicardial approach, acute pulmonary vein isolation was achieved.

In examining the safety profile of electroporation there are reports that it does not cause stenosis in blood vessels (5,6) as typically seen in RF lesions, that it is nerve sparing (7), and that the structural integrity of the esophagus is maintained following energy application (8). All of these create a very attractive treatment option for cardiac ablation. Additional targets have also been suggested, such as the ganglion plexus of the heart (9). This could provide a new, novel way to treat atrial arrythmias.

All this excitement around the field of catheter-based electroporation therapies, has generated a lot of interest in novel catheter design (1,4,8,10,11). Catheters range in design from large plate electrodes (8), to balloon base options for pulmonary vein

isolation (10). Options for both endocardial and epicardial transcatheter delivery options have been presented as well (4,12).

Understanding the response of cardiac tissue is important as damage to this tissue is required for an efficacious ablation. Swine cardiac tissue was analyzed, as well as tissue from a single human heart. Future work in the field can be informed based on the results presented here on the response of cardiac tissue to irreversible electroporation.

Physiological Assessment of Cardiac Muscle Post-Irreversible Electroporation Therapy

Lars M Mattison, Paul A Iaizzo PhD FHRS

Preface
This paper was originally published as a technical brief at the Design of Medical Devices 2017 conference. It has been updated to include additional data and discussion. Using the same methodology as the smooth and skeletal muscles, cardiac trabeculations from the ventricles were evaluated. An additional section has been added at the end to include the biomechanical response of swine cardiac tissue as well.

Background
Ablations have become the gold clinical standard of drug resistant atrial fibrillation (AF). AF is projected to affect 50 million people by the year 2050.[13] Today, two primary methods of ablation are used clinically: radio frequency and cryoablation. These ablation

technologies are equally effective, but still cause complications[14]. Most of these

complications arise from the fact that both technologies require a thermal change in the

tissue to cause cell death. Thermal change of the tissue while effective, can be subject to

many different variables that may result in collateral damage. These include levels of

focal blood flow, location of vessels near the ablation site, and/or adjacent tissue damage

causing clinical issues such as esophageal fistulas or phrenic nerve injury. Irreversible

Electroporation serves as a possible non-thermal alternative. This therapy is a train of

high voltage (>500V/cm) short DC pulses that causes increased permeability of the cell

membrane. If a large enough electric field is applied, then the cell membrane can be

permanently damaged resulting in cell death. To date, most of the irreversible

electroporation research that has been done has examined the use of this approach for

treating cancerous tumors in the skin, prostate, and liver. Very little study of this potential

treatment relating to the heart has been done other than synchronizing delivery of the

therapy with the heartbeat to not induce ventricular fibrillation. The appeal of a

potentially more predictable lesion would be highly desired in this clinical realm. Here

we present initial investigations as to the functional response of cardiac tissue to

electroporative energy via the NanoKnife.

Methods
Yorkshire-cross swine were intubated and anesthetized using approved protocols by the

institutional animal care and use committee (IACUC). Upon completion of another

unrelated protocol, the heart was excised and trabeculae from both the left and right

ventricle were carefully dissected. Following procurement and dissection of tissue, a

previously described setup was used.[15,16] In short, loops of suture were tied onto either end of isolated bundles: these were then suspended between a stationary support rod and a force transducer. This setup was then submerged in a temperature controlled, carbogen gassed chamber, containing a modified Krebs-Henseleit buffer maintained at 37°C. Laterally placed platinum electrodes were used to supramaximally stimulate the bundles to contract every 10 seconds. The force data was then recorded using a custom LabView program. Optimal muscle function was obtained i.e. length-tension relationships and stimulus amplitude. Following this, the stimulating electrodes were removed from either side of the muscle bundle and replaced with 1 cm long NanoKnife (Angiodynamics, Latham, NY) needles. Once in place, an FDA approved treatment of irreversible electroporation varying from 500 V to 1100 V a pulse rate of 1.5 Hz (n=19) or 4 Hz (n=140) PPM using a 90µs pulse width and 70 total pulses were applied to the bundles. The viability of the bundles was then monitored for three hours following the applied therapy.
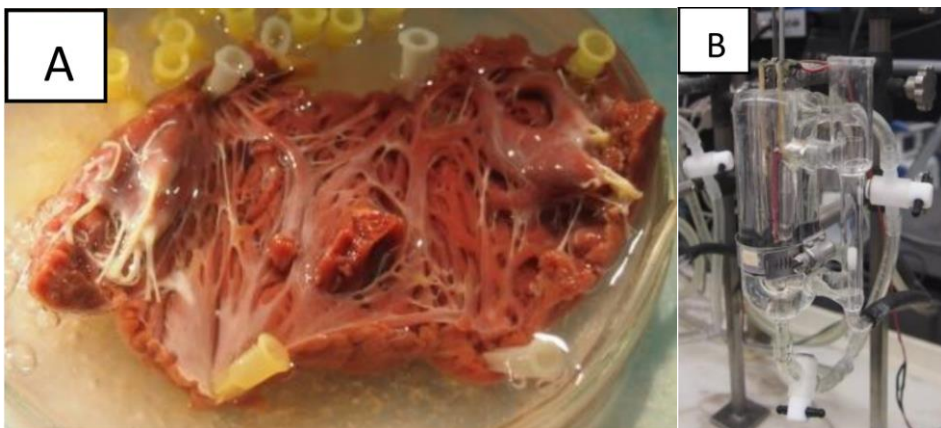
Figure 44: A) Cardiac trabeculae for dissection B) Muscle Bath set up with electrodes and tissue suspended between them.

Results

The data showed the normalized to baseline function of the bundles as they recover over the 3 hours following the ablation. Baseline force was defined as average twitch force for 15 minutes prior to application of the therapy. The control group received no therapy and serves as a reference to functional decay of the tissue over time. Figure 45 shows the dose responses of the tissue to 1.5 Hz and 4 Hz. The faster the pulse rate the more initial stunning.   For the 1.5 Hz bundles, only 150 minutes of data was collected across all bundles which is reflected in results. Also, voltages above 800 V show a larger functional decrease, while the lower voltages show an initial decrease, but long-term trends follow the control group. This suggests that the faster pulse rate causes more initial stunning of the tissue when compared to the slower pulse rate, but the voltages deliver similar results across the different pulse rates. Overall, the higher the voltage the larger decrease in function of cardiac muscle, without respect to pulse rate.
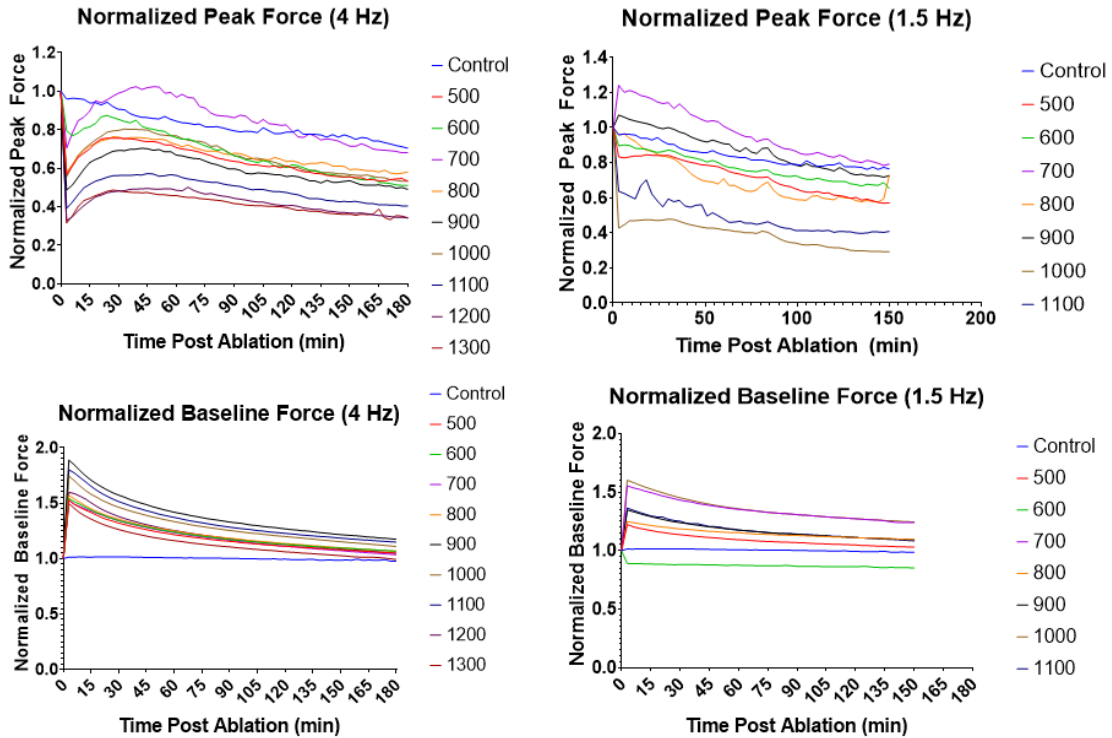
Figure 45: Normalized Peak Force and Baseline Force on swine cardiac tissue examining the effects of applied voltage and frequency on muscle function.

Interpretation

These data suggest that irreversible electroporation can effectively cause a decrease in function of cardiac muscle. The exact minimum dose needed for this functional decrease in force is between 800V and 900V. Seeing this decrease in function suggests that lesions are created in cardiac tissue allowing this technology to be used for cardiac ablations. As this is a relatively new technology, there is still a need to develop a better understanding of how different tissue types respond to the therapy. Future work should include a larger sample sizes and looking at other factors of irreversible electroporation such as pulse length and number of pulses.

115

Swine Biomechanical Data

Of the muscles that were tested in the muscle bath set up, only those exposed to the higher pulse rate (4 Hz) underwent uniaxial testing (figure 46). Of the 140 bundles tested, only 32 had failures that were not initiated by the suture. This caused small groups at the individual applied levels. None of the groups showed significant difference from the control group using ANOVA ($p > 0.05$), but a larger dataset would provide more confidence in this assessment. These data suggest that the biomechanical integrity of the tissue is maintained despite the application of electroporation.
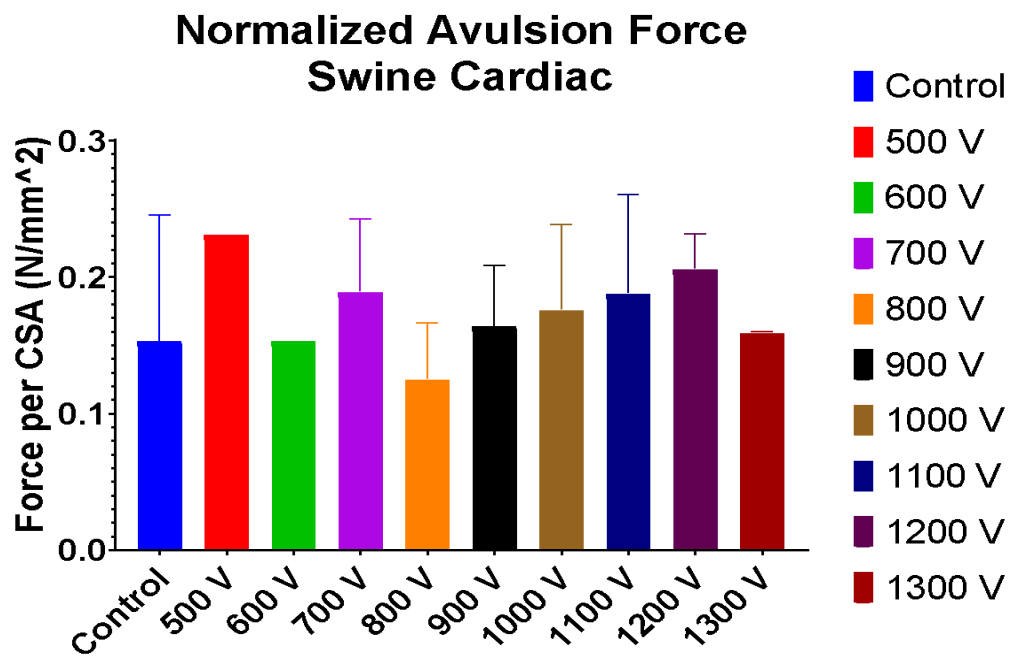
Figure 46: Normalized Avulsion Force of swine cardiac tissue with different voltages applied at 4 Hz.

Human Cardiac Tissue

Fresh human cardiac tissue was obtained from organ donors through a collaboration with

LifeSource. Tissue that was not useable for transplant would be procured and donated

for research. The same methods as described for swine cardiac muscle were used. In this section, tissue from a single heart was dissected into 16 bundles, 8 from each ventricle. Thus, the results are only meant to facilitate discussion of swine vs human tissue.

Results

A total of 16 bundles provided viable data for analysis. Each treatment group had 1 sample from the right ventricle (RV) and left ventricle (LV) for 2 bundles being treated at each voltage level of electroporation. The peak force and normalized baseline trends can be observed in figure 47. Peak force showed an initial drop followed by a period of recovery.
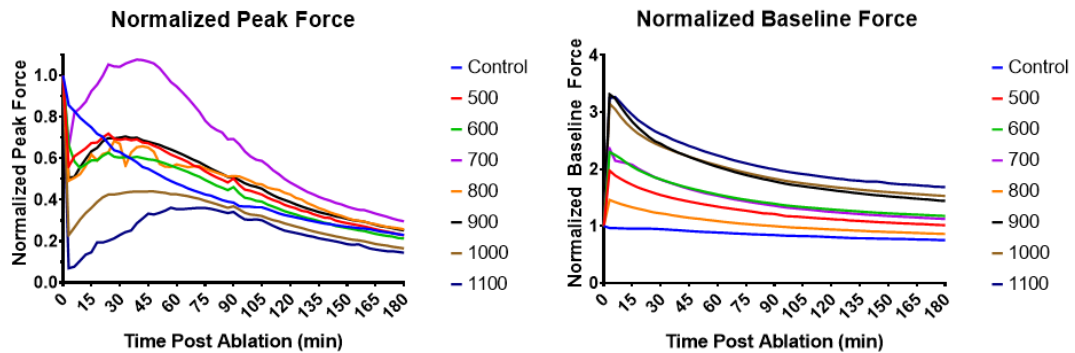
Figure 47: Normalized Peak Force and Baseline Force on human cardiac tissue examining the effects of applied voltage and frequency on muscle function.

Uniaxial pulls were performed and energy per volume was reported in figure 48. Pull tests showed an unexpected peak in energy required for 700 V application. None of the groups were significantly different compared to the control group ($p > 0.05$).

117
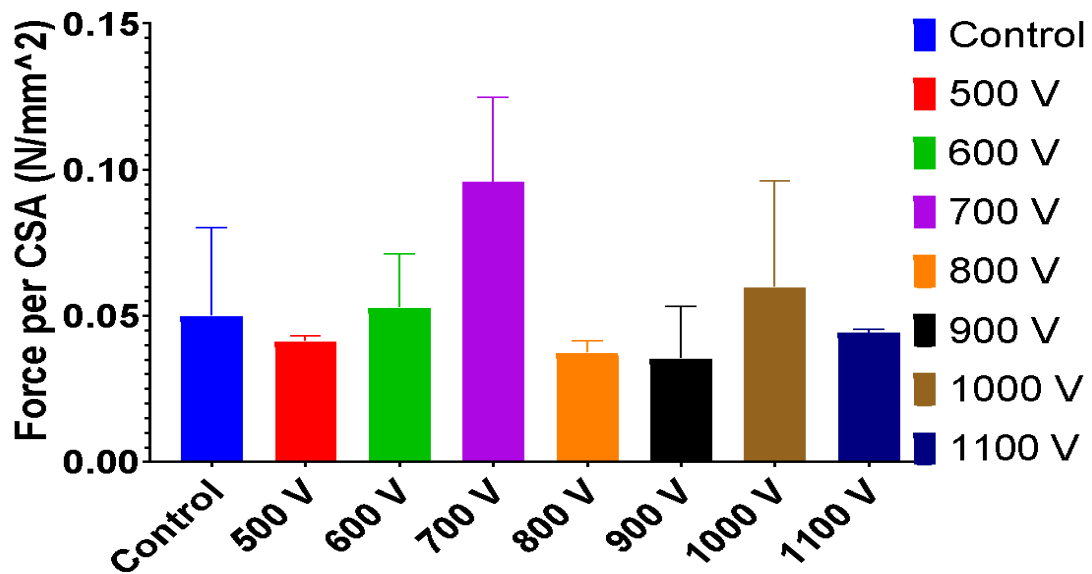
Figure 48: Normalized Avulsion Force for human cardiac tissue with different voltages applied at 4 Hz.

Discussion

Overall, we can begin to compare the differences and similarities between swine and human tissue. Where the results suggest that the biomechanical integrity of the tissue of both samples is maintained despite the application of electroporation.

One observation was the human cardiac normalized peak twitch force appears to return to baseline around the 90-minute time point. This result could be due to the hypoxic damage caused to the tissue prior to arriving in lab. Additionally, the lack of perfusion of the tissue could cause the core of the bundle to receive less oxygen than needed. The theory of hypoxic damage is also suggested by the prolonged elevated baseline period.

118

It is noted that a large increase in the baseline force is caused by the application of electroporation. This initiated a prolonged contracture that could be observed in cardiac ablation procedures. If a similar energy is applied, the tissue might go into contracture and take an extended period of time to relax and return to full function, even if it has minimal damage.

 The avulsion force data was reported regardless of location of the failure. This means that even if the suture caused the failure, the data is still presented here as it was such a small data set. Even though none of the data was statistically significant from the control group, the 700 V group is observed to have a higher force per cross sectional area failure value. This is due to one of the bundles being the moderator band, which has previously shown higher failure forces compared to other ventricular trabeculae[15]. This is due to it being a standalone structure with a more singular fiber orientation compared to other dissected trabeculations. Thus, the avulsion force was similar for all samples indicating no difference between biomechanical structure.

Also, applied fields that the tissue is exposed to is important to understand. The Krebs buffer is a conductive medium with different properties compared to that of similar tissue or blood. Modeling of the electric field would help to better understand exactly what field that bundles were exposed to, establishing more exact therapy delivery targets.

When comparing swine and human tissues, similar trends were observed in the baseline force for both tissues, but functionality post treatment is different. Peak twitch force showed a similar effect between swine and cardiac muscle when applied at 4Hz, with an initial decrease followed by a period of recovery. But there was a larger loss of function occurred with the human cardiac tissue compared to swine tissue. Both swine and human tissue did respond to treatment.

Conclusions

Human and swine cardiac ventricular trabeculae can both be damage by electroporation therapy. Cardiac tissue being more receptive to a loss of function compared to swine tissue. Following treatment, a 90-minute tissue contracture was observed which should be monitored during cardiac ablation procedures. Also, tissue death did not change the force required for avulsion following treatment. This continues to support that electroporation is an effective therapy that can be used to treat cardiac tissue in a safe manner that does not change the structural integrity of cardiac tissue.

Chapter 5: Responses of Nervous Tissue to Irreversible Electroporation

Phrenic nerve injury is the most common, non-access site related procedural complication of cryoablation procedures. There is no treatment once the nerve is damaged, leaving patients to wait and hope for recovery. Previous reports have suggested that electroporation is nerve sparing, but this has only been reported in terms of clinical function and histology. To better understand this response, compound action potentials (CAPs) from isolated nerves were used to evaluate the response of the phrenic nerves to electroporative therapies.

Synopsis
Background

Phrenic nerve injury (PNI) can result from various ablative therapies used for pulmonary vein isolation to treat drug resistant atrial fibrillation. If induced, PNI is considered unlikely to treat and recovery can take anywhere from hours to years, thus prevention is key. Irreversible electroporation (IRE), a new ablation modality, is being investigated as a replacement therapy for cryoablation and/or radiofrequency ablation in such patients.

Objective

In this study, our objective was to examine how swine phrenic nerves, eliciting compound action potentials, will respond to direct application of IRE.

Methods

We dissected phrenic nerves (n = 56) from the pericardium of a swine. After placing the nerves into a recording chamber, we recorded baseline compound action potentials,

stimulating the nerves with a 1 mV square wave (0.1 ms). We recorded relative nerve function at 3 sites along the nerve. Then we applied IRE, after which we recorded nerve function every 15 minutes for 2 hours.

Results

The nerve experienced a period of initial stunning of increasing severity with increasing the dose of electroporation. Increasing the dose caused reduced CAP amplitude suggesting that not all nerve fibers recover. All but one nerve had some function at the final assessment at 2 hours.

Conclusion

Based on the results presented here, nerves should not be exposed to excessively large fields of electroporation as they are subject to stunning followed by reduced function.

Keywords: ablation, irreversible electroporation, atrial fibrillation, phrenic nerve injury, phrenic nerve palsy, compound action potential

Abbreviations:

CAP – compound action potential

PNI – phrenic nerve injury

PTP – peak-to-peak

RF – radiofrequency

TTP – time to peak

Introduction

The two most common ablation modalities for treating patients with drug-resistant arrhythmias are radiofrequency (RF) ablation and cryoablation. RF ablation uses electric energy delivered to the tissue to generate focal resistive heating (Joule heating); thereby causing protein denaturation and cell death. Cryoablation uses very low temperatures to freeze the target tissue, forming focal ice within the tissue that causes membrane hemorrhage, cellular inflammation, apoptosis and ultimately fibrosis. In other words, both of these ablation modalities cause cellular death by exposing tissue to extreme temperatures. The degree of tissue damage due to the thermal field is affected with many factors, such as: local blood flow, levels of tissue perfusion, and/or unfavorable anatomies. Importantly, these thermal ablative procedures applied near the pulmonary views within the left atrium, have also been associated with well-documented clinical complications, including atrioesophageal fistula and phrenic nerve injury (PNI).[1-6]

In contrast, renewed use of the ablation modality referred to as irreversible electroporation (IRE) causes cell death by exposing tissue to an electric field *without* generating lethal thermal fields. The exact mechanisms of action of IRE are not fully understood, but the most widely accepted theory is that the large electric field creates temporary pores within cell membranes.[7, 8] If the pores are large enough, the ion balances within the cell can no longer be maintained, eventually leading to cell death.

It is considered that the uses of IRE may prevent some complications induced by either RF ablation or cryoablation. Unlike both of those thermal ablation modalities, IRE is not

considered to be largely affected by regional blood flow; instead, lesion formations are considered to be controlled by the proper placement of the electric field. Additionally, IRE does not affect extracellular matrices, since it targets cell membranes. And unlike RF ablation and cryoablation, IRE also is not thought to not cause stenosis of blood vessels. Importantly, these therapeutic qualities have reignited interest in pursuing IRE as a potential form for cardiac ablations.[9]

In our swine study, we focused on functional effects of applying IRE to isolated phrenic nerves, which innervate the diaphragm. This is of importance because PNI, which sometimes manifests as phrenic nerve palsy, can lead to breathing difficulties. PNI remains today as the most common complication of pulmonary vein isolation; as noted above a procedure used to treat atrial fibrillation by electrically isolating the pulmonary veins from the left atria.[10] We hypothesized that IRE could prevent PNI due to previous investigators utilizing experimental procedures where they observed no functional damage to nervous tissue and minimal complications.[11-15]

Our objective was to examine how isolated phrenic nerves would respond to direct application of IRE, with the worst-case scenario where there was no atrial or surrounding tissues lying between the delivery electrodes and the nerves. Specifically, we analyzed the thresholds in vitro for inducing temporary or permanent damage to phrenic nerve function, in order to determine the safe ranges of applied therapeutic IRE voltages.

124

Methods

The experimental procedure that we employed in this study was based on previous protocols developed in our laboratory, in which we examined the responses of phrenic nerve to cryothermal therapies.[6] Phrenic nerves were carefully isolated from anesthetized Yorkshire-cross swine that had undergone a median sternotomy as part of another, unrelated protocol which was approved by the University of Minnesota's Institutional Animal Care and Use Committee. Using blunt dissection, we extracted the left and right phrenic nerves ($n = 56$) from the pericardium, making all cuts superior to the heart and as close to the diaphragm as possible. Then, we placed the extracted nerves in a modified Krebs-Henseleit buffer solution and carefully dissected them from the surrounding connective and fatty tissues. Doing so allowed for optimized nerve recordings.   Next, we placed the nerves in a bath of modified, oxygenated Krebs-Henseleit buffer solution at 37°C, for a minimum of 20 minutes; allowing the nerves to recover from the mechanical stresses they were subjected to during procurement and dissection. Subsequently, we placed each nerve onto a modified electrode ladder (ML T016, ADInstruments Inc., Dunedin, New Zealand), where we stimulated, so action potentials would travel orthodromically and from the proximal end with a 1 mV square wave (0.1 ms) (S48, Grass Technologies, Middleton, WI, USA). We sequentially recorded the resultant bipolar compound action potentials (CAPs) at 3 different sites down the nerve: site 1, site 2, and site 3 (Figure 49).
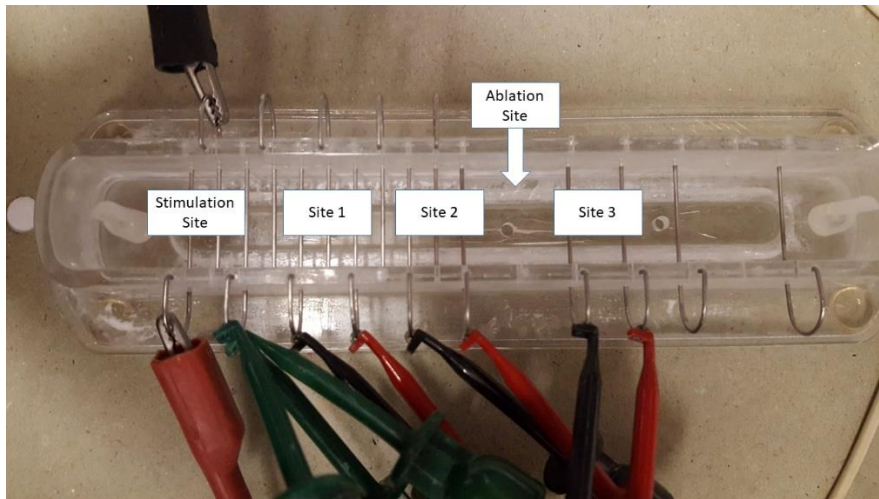
Figure 49: Nerve recording setup showing the stimulation site, the 3 recording sites, and the ablation site

To record these waveforms, we used a PowerLab 16/30 with LabChart 7 software,

(ADInstruments Inc.) (Figure 50). At each time point, we made 4 recordings per nerve, in

order to ensure consistent data collection and to establish baseline function.
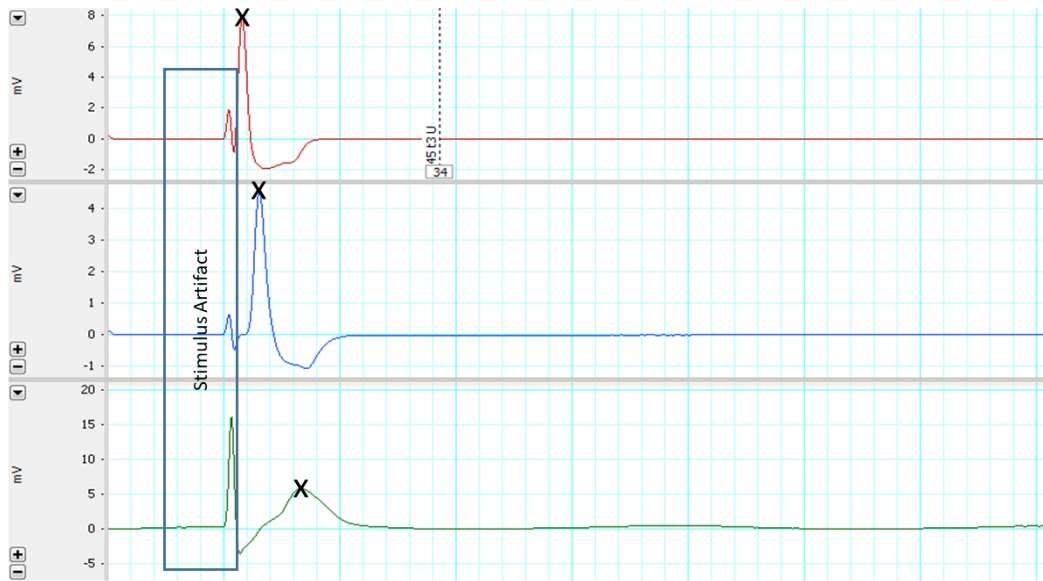
Figure 50: Typical baseline recording of nerve function across all 3 sites from top to bottom (X = peak amplitude; red = site 1 recording, blue = site 2 recording, green = site 3 recording); stimulation artifact observed before the recording of the compound action potential.

After establishing baseline action potential parameters, we applied IRE to the nerve between recording sites 2 and 3. We utilized a NanoKnife generator and a pair of needle-based electrodes (AngioDynamics, Latham, NY, USA). After placing the nerves on the electrode ladder, we submerged them in the modified Krebs-Henseleit buffer solution. We placed probes on either side of the nerve and then applied electric fields of 0, 500, 1000, 1500, 2500, or 2750 V. We randomly assigned these voltages, testing 8 nerves in each electric field and 4 in each probe orientation. All other IRE parameters were constant: 240 pulses per minute, a total of 70 pulses (delivered in series of 10), and a pulse width of 90 µS. During select deliveries, thermal measurements were recorded using a FLIR IR camera to evaluate the thermal effects of the IRE applications.

After applying IRE, we immediately assessed each phrenic nerve function (as described above), and then every 15 minutes for the next 2 hours. Between each assessment, the nerve was placed in the recovery bath of warmed and oxygenated krebs buffer.

Raw data was exported to MATLAB (MathWorks, Natick, MA, USA) for analysis. We used a custom MATLAB script in order to obtain CAP amplitude and time to peak. Time to peak was used as an analog for conduction velocity. Data were analyzed with an ANOVA test and the Tukey honest significant difference test. Statistical analysis was performed using GraphPad Prism version 7.04 (GraphPad Software, La Jolla, CA, USA).

Results
We were able to elicit CAPs from all 56 nerves, with successful measurements at all 3 recording sites. All nerves were considered viable as the waveforms recorded from sites 1 and 2 did not differ from baseline ($P > 0.05$) for the entire assessment. The percentage of nerves showing a CAP from site 3 following the ablation was reported in Table 5. Functionality reported here does not directly equate to clinical functionality, as even small amplitude CAPs were still considered functional.

Time to peak and CAP amplitude were calculated for the 3rd recording site and the results are presented in figures 51 and 52. In general, the time to peak was faster at higher energies, with all energies 1500 V and above showing statistically significant higher TTP values (p < 0.05).

The analyzed thermal data showed that the effects were negligible as the maximum

temperatures remained well below 65°C.

Table 4: Percentage of nerves with function at each timepoint and treatment

Voltage	Pre	0	15	30	45	60	75	90	105	120
Control	100%	100%	100%	100%	100%	100%	100%	100%	100%	100%
500	100%	43%	100%	100%	100%	100%	100%	100%	100%	100%
1000	100%	50%	88%	100%	100%	100%	100%	100%	100%	100%
1500	100%	38%	63%	88%	100%	100%	100%	100%	100%	100%
2000	100%	38%	100%	100%	100%	100%	100%	100%	100%	100%
2500	100%	13%	63%	100%	100%	100%	100%	100%	100%	100%
2750	100%	0%	38%	100%	100%	100%	88%	100%	100%	88%
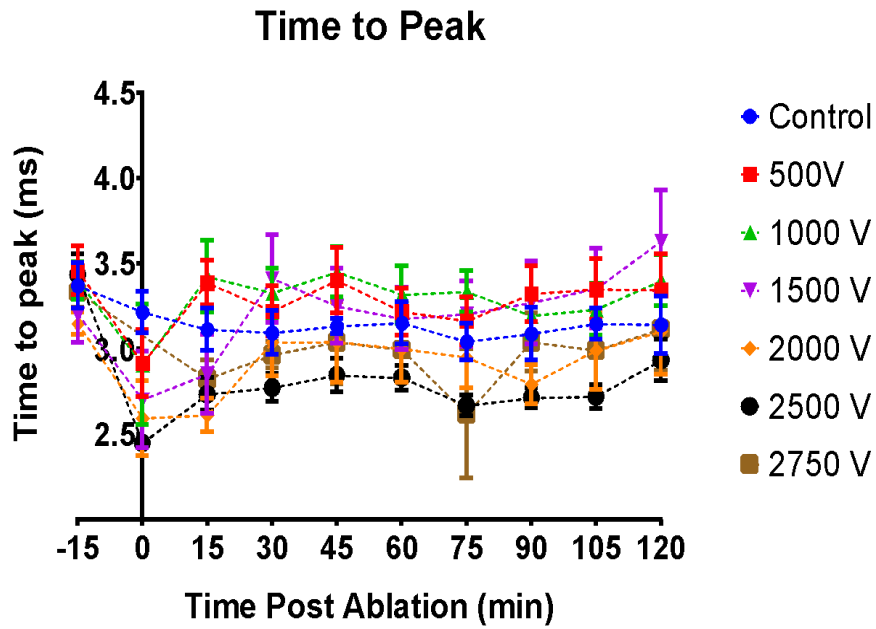
Figure 51: Time to peak measurements following the ablation period. Nerves that were non-functional were excluded from the analysis to only measure functional nerves.

Normilized CAP Amplitude
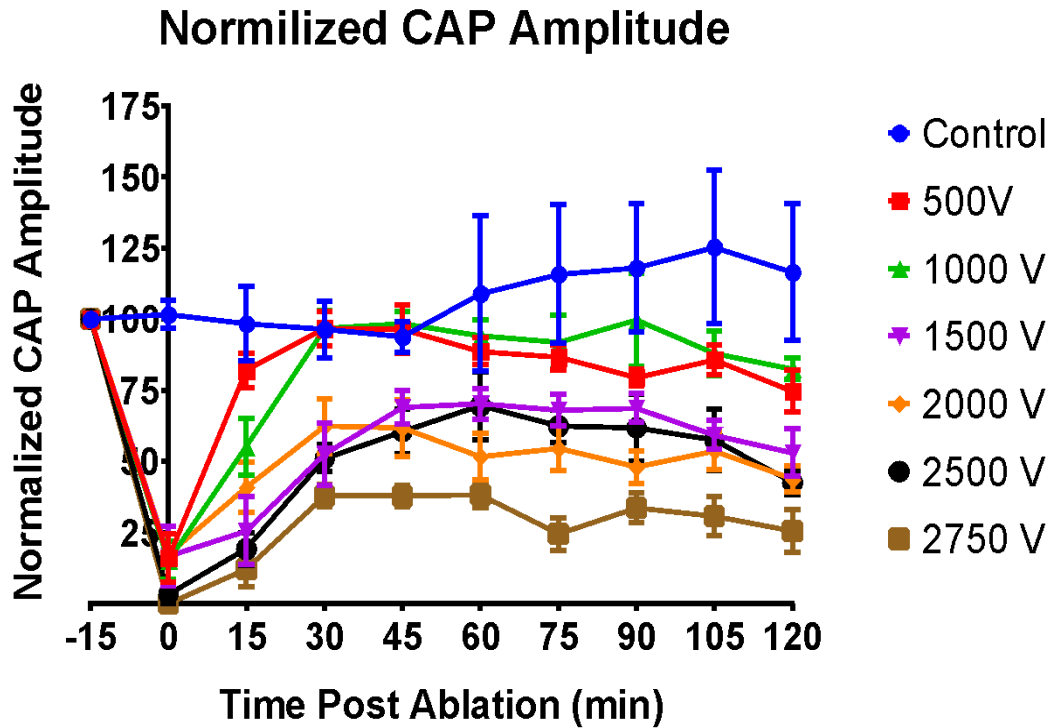
Figure 52: Normalized CAP Amplitude showing the recovery of function following the application of electroporation.

Discussion

Across all energies, some effect was observed in the CAP amplitude. A stunning effect

was observed to last only 15-30 minutes following the application of the energy and after

the 30 minutes, only minimal additional recovery occurred. Higher doses caused a longer

stunning period with only the highest dose of 2750 V causing stunning in all the nerves.

These decreased CAP amplitudes at the higher doses shows that some damage occurred

as CAP are measures of the number of neurons firing at a given point. While the clinical

implications of CAP amplitudes is difficult to understand it is understood some decrease

in function might occur. After the 1-hour time point, all nerves but 1 had sustained

130

function. The one nerve had intermittent function for the 1 to 2-hour study. This demonstrates that at this point the nerve is starting to undergo irrecoverable damage.

Examination of time to peak shows that following treatment, nerves that have maintained function conduct faster than untreated nerves. This phenomenon suggests that the larger fibers, which conduct faster, maintain their function while the smaller fibers are damaged at the lower doses. This shows that the phrenic nerve should be very resistant to electorporative therapies compared to other surrounding tissues, while other peripheral nerves that are smaller or non-myelinated could be more susceptible to the therapy.

The results here are in line with what has been reported by Neven et al. Clinical insights gained from this study show that an initial stunning of the nerve can be expected, but recovery should be expected within 30 minutes of the application of energy. The robust response of nerves with the additional potential of pulmonary vein stenosis and lack of esophageal response to the therapy suggest that electroporation is an ideal energy for ablations.

One limitation to this study is that this setup has two needle electrodes placed on either side of the nerve surrounded by a conductive medium. This will alter the expected electric field that is applied across the nerves. Electric field modeling would help to better understand exactly what electric field the nerves were exposed to. This would help to compare the results of this study to other applications electroporation therapy.

Another limitation is the accuracy of the thermal measurements. Infrared imaging only

measures the surface temperature, so actual temperatures might be higher that reported.

It is difficult to get accurate temperature measurements as placing a probe by the nerve

will distort the electric field, which could change the effect of the electroporation

treatment. While not a perfect method, the IR camera does provide insight as to any

thermal effects that occur.

Conclusion

To our knowledge, this is the first comprehensive study to analyze the functional

response of isolated phrenic nerves to an IRE therapy. We observed that nerves can

maintain some level of function following direct application of irreversible

electroporation. Nerve stunning is observed for up to 30 minutes when using energies

above what is needed to treat cardiac tissue. Importantly, for permanent lesion formation,

we know that swine phrenic nerves as compared with their myocardial tissues, require the

application of higher-intensity IRE fields. Thus, we believe that the use of IRE as

ablation treatment for arrhythmias might lead to fewer complications relative to phrenic

nerve dysfunctions.

Chapter 6 -Thesis Conclusions

The principal research goal of this thesis was to understand the response of different cardiothoracic tissues to irreversible electroporation when compared to currently utilized thermal ablation technologies. This thesis outlines protocols developed to evaluate several different tissue types including: diaphragm, esophagus, myocardium and nerve bundles from both swine and human subjects as well as human vastus lateralis tissue. Both physiological responses of twitch force and baseline tension as well as each tissue's biomechanical properties have been reported for all the muscle groups. In total, over 3000 bundles of muscle were prepared and tested to help understand these responses.

This body of work has shown that skeletal muscle exhibits sensitivity to electroporative therapies with regards to contraction force generation, while smooth and cardiac tissues are more resilient. Using square wave pulses, like those generated by the NanoKnife, showed prolonged periods of contracture in all muscle types at high energies. However, despite this apparent loss of function, the biomechanical properties of all tissue types tested remain unchanged following the application of irreversible electroporation. In addition, these results have shown that nervous tissue, although damaged by electroporation, will continue to function at a diminished level.

Ultimately, the application of irreversible electroporation to treat atrial fibrillation will not provide an infallible therapy for the disease. However, when compared to existing technologies used in clinical practice today it shows great promise as a technique for controlled cardiac ablation. The response of various cardiothoracic tissues to electroporative

therapies presented here can be used to inform future device design, procedural development and clinical best practices for these novel electroporation-based therapies.

References

Thesis Summary and Chapter 1

1. January CT, Wann LS, Alpert JS, Calkins H, Cigarroa JE, Cleveland JC Jr, et al. 2014 AHA/ACC/HRS guideline for the management of patients with atrial fibrillation. *Journal of the American College of Cardiology*. 2014;64(21):2246–80.

2. Neven, K., Driel, V. Van, Wessel, H. Van, Es, R. Van, Pré, B. Du, Doevendans, P. A., & Wittkampf, F. (2014). Safety and feasibility of closed chest epicardial catheter ablation using electroporation. *Circulation: Arrhythmia and Electrophysiology*, *7*(5), 913–919. https://doi.org/10.1161/CIRCEP.114.001607

3. Nollet, J. A. (1754). *Recherches sur les causes particulieres des phénoménes électriques*.

4. Fuller, G.W.: Report on the investigations into the purification of the Ohio river water at Louisville Kentucky. D. Van Nostrand Company, New York (1898)

5. Mir, L. M., Orlowski, S., Belehradek, J., & Paoletti, C. (1991). Electrochemotherapy potentiation of antitumour effect of bleomycin by local electric pulses. *European Journal of cancer*, *27*(1), 68-72.o

6. Davalos, R. V., Rubinsky, B., & Mir, L. M. (2003). Theoretical analysis of the thermal effects during in vivo tissue electroporation. *Bioelectrochemistry*, *61*(1–2), 99–107. https://doi.org/10.1016/j.bioelechem.2003.07.001

7. Edd, J. F., Horowitz, L., Davalos, R. V., Mir, L. M., & Rubinsky, B. (2006). In vivo results of a new focal tissue ablation technique: Irreversible electroporation. *IEEE Transactions on Biomedical Engineering*, *53*(7), 1409–1415. https://doi.org/10.1109/TBME.2006.873745

8. Jiang, Chunlan, et al. "Irreversible Electroporation of Cardiovascular Cells and Tissues." *Journal of Medical Devices* 7.3 (2013): 030903.

9. Ibey, B. L., Ullery, J. C., Pakhomova, O. N., Roth, C. C., Semenov, I., Beier, H. T., … Pakhomov, A. G. (2014). Bipolar nanosecond electric pulses are less efficient at electropermeabilization and killing cells than monopolar pulses. *Biochemical and Biophysical Research Communications*, *443*(2), 568–573. https://doi.org/10.1016/j.bbrc.2013.12.004

10. Siddiqui, I. A., Latouche, E. L., DeWitt, M. R., Swet, J. H., Kirks, R. C., Baker, E. H., … McKillop, I. H. (2016). Induction of rapid, reproducible hepatic ablations using next-generation, high frequency irreversible electroporation (H-FIRE) in vivo. *Hpb*, *18*(9), 726–734. https://doi.org/10.1016/j.hpb.2016.06.015

11. Campana, L. G., Marconato, R., Valpione, S., Galuppo, S., Alaibac, M., Rossi, C. R., & Mocellin, S. (2017). Basal cell carcinoma: 10-year experience with electrochemotherapy. *Journal of Translational Medicine*, *15*(1), 1–12. https://doi.org/10.1186/s12967-017-1225-5

12. Okino, M., Mohri, H. Effects of a high-voltage electrical impulse and an anticancer drug on in vivo growing tumors. Japanese Journal of Cancer Research 78, 1319–1321(1987).

13. Kloth, L. C., & Feedar, J. A. (1988). Acceleration of wound healing with high voltage, monophasic, pulsed current Phys Ther 1989 Aug;69(8):702. *Physical Therapy*, *68*(4), 503–508. Retrieved from http://onlinelibrary.wiley.com/o/cochrane/clcentral/articles/246/CN-00652246/frame.html

14. Carley, P. J., & Wainapel, S. F. (1985). Low Intensity Direct Current for Wound Healing - Carley. *Archives of Physical Medicine and Rehabilitation*, *66*(May), 443–446. https://doi.org/10.13140/RG.2.1.3359.8324

15. Ferguson, M., Byrnes, C., Sun, L., Marti, G., Bonde, P., Duncan, M., & Harmon, J. W. (2005). Wound healing enhancement: Electroporation to address a classic problem of military medicine. *World Journal of Surgery*, *29*(SUPPL. 1), 55–59. https://doi.org/10.1007/s00268-004-2062-2

16. Kos, S., Vanvarenberg, K., Dolinsek, T., Cemazar, M., Jelenc, J., Préat, V., … Vandermeulen, G. (2017). Gene electrotransfer into skin using noninvasive multi-electrode array for vaccination and wound healing. *Bioelectrochemistry*, *114*, 33–41. https://doi.org/10.1016/j.bioelechem.2016.12.002

17. Sessions, J. W., Armstrong, D. G., Hope, S., & Jensen, B. D. (2017). A review of genetic engineering biotechnologies for enhanced chronic wound healing. *Experimental Dermatology*, *26*(2), 179–185. https://doi.org/10.1111/exd.13185

18. Scheffer, H. J., Nielsen, K., De Jong, M. C., Van Tilborg, A. A., Vieveen, J. M., Bouwman, A., … Meijerink, M. R. (2014). Irreversible electroporation for non-thermal tumor ablation in the clinical setting: A systematic review of safety and

efficacy, *37*((Scheffer, De Jong, Van Tilborg, Van Kuijk, Meijerink) Radiology
and Nuclear Medicine, VU University Medical Center, Amsterdam, Netherlands),
S316–S317. Retrieved from

http://ovidsp.ovid.com/ovidweb.cgi?T=JS&PAGE=reference&D=emed16&NEW
S=N&AN=71618241

19. Van Driel, V. J. H. M., Neven, K. G. E. J., Van Wessel, H., Du Pré, B. C., Vink,
A., Doevendans, P. A. F. M., & Wittkampf, F. H. M. (2014). Pulmonary vein
stenosis after catheter ablation electroporation versus radiofrequency. *Circulation:
Arrhythmia and Electrophysiology*, *7*(4), 734–738.
https://doi.org/10.1161/CIRCEP.113.001111

20. A. Singal, L. M. Mattison, C. L. Soule and P. A. Iaizzo, "Effects of Ablation
(Radiofrequency, Cryo, Microwave) on Physiologic Properties of the Human
Vastus Lateralis," in *IEEE Transactions on Biomedical Engineering*, vol. PP, no.
99, pp. 1-1. doi: 10.1109/TBME.2017.2787041

21. Mattison, L. M., & Iaizzo, P. A. (2017, April). Physiological Assessment of
Cardiac Muscle Post-Irreversible Electroporation Therapy. In *2017 Design of
Medical Devices Conference* (pp. V001T01A018-V001T01A018). American
Society of Mechanical Engineers.

22. Mattison, Lars M, Apran Patil, Paul A Iaizzo. "Physiological Response of
Skeletal and Smooth Muscle to Irreversible Electroporation" 2nd World Congress
on Pulsed Electric Fields   in Biology, Medicine and Food & Environmental
Technologies. September 2017.

23. Mattison, Lars M, Maria A Burbano, Paul A Iaizzo. "Afferent vs Efferent Response of the Phrenic Nerve to Irreversible Electroporation" 2nd World Congress on Pulsed Electric Fields   in Biology, Medicine and Food & Environmental Technologies. September 2017.

24. Mattison, Lars M, Matthew R Yoder, Charles L Soule, Paul A Iaizzo "Physiological and Biomechanical Response of Skeletal Muscle to Electroporation" 1st World Congress on Electroporation.

25. Robert E. Neal II ; Paulo A. Garcia ; John L. Robertson ; Rafael V. Davalos. *Experimental Characterization and Numerical Modeling of Tissue Electrical Conductivity during Pulsed Electric Fields for Irreversible Electroporation Treatment Planning.* IEEE Transactions on Biomedical Engineering, Volume: 59 Issue: 4, 2012.

26. Davalos, R.V., Mir, L.M. & Rubinsky, B. *Tissue Ablation with Irreversible Electroporation.* Ann Biomed Eng (2005) 33: 223. https://doi.org/10.1007/s10439-005-8981-8.

27. Li W, Fan Q, Ji Z, Qiu X, Li Z (2011) *The Effects of Irreversible Electroporation (IRE) on Nerves.* PLoS ONE 6(4): e18831. doi:10.1371/journal.pone.0018831

28. Maor E., Ivorra A., Leor J., Rubinsky B., *Irreversible Electroporation Attenuates Neointimal Formation after Angioplasty.* IEEE TRANSACTIONS ON BIOMEDICAL ENGINEERING, VOL. 55, NO. 9, SEPTEMBER 2008

29. Maor E., Ivorra A., Leor J., Rubinsky B., *The Effect of Irreversible Electroporation on Blood Vessels*. Technology in Cancer Research and Treatment. Volume 6, Number 4, August 2007. ISSN 1533-0346

30. Valerio, M., Dickinson, L., Ali, A., Ramachadran, N., Donaldson, I., Mccartan, N., … Emberton, M. (2017). Nanoknife Electroporation Ablation Trial: A Prospective Development Study Investigating Focal Irreversible Electroporation for Localized Prostate Cancer. *Journal of Urology*, *197*(3), 647–654. https://doi.org/10.1016/j.juro.2016.09.091

31. Charpentier, K. P., Wolf, F., Noble, L., Winn, B., Resnick, M., & Dupuy, D. E. (2011). Irreversible electroporation of the liver and liver hilum in swine. *Hpb*, *13*(3), 168–173. https://doi.org/10.1111/j.1477-2574.2010.00261.x

32. Vorobiev, E., & Lebovka, N. (2010). Enhanced extraction from solid foods and biosuspensions by pulsed electrical energy. *Food Engineering Reviews*, *2*(2), 95–108. https://doi.org/10.1007/s12393-010-9021-5

33. Barba, F. J., Galanakis, C. M., Esteve, M. J., Frigola, A., & Vorobiev, E. (2015). Potential use of pulsed electric technologies and ultrasounds to improve the recovery of high-added value compounds from blackberries. *Journal of Food Engineering*, *167*, 38–44. https://doi.org/10.1016/j.jfoodeng.2015.02.001

Chapter 2

1. Ahmed, M. and S. N. Goldberg. Image-guided tumor ablation: basic science. In: Tumor Ablation: Principles and Practice, edited by E. van Sonnenberg, W.

McMullen, and L. Solbiati. New York: Springer Science + Business Media, Inc., 2005, p. 24.

2. Berchtold, M. W., H. Brinkmeier, and M. Müntener. Calcium ion in skeletal muscle: its crucial role for muscle function, plasticity, and disease. Physiol. Rev. 80:1215-1265, 2000.

3. Bischof, J. C. and X. He. Thermal stability of proteins. Ann. N Y Acad. Sci. 1066:12-33, 2005.

4. Boutilier, R. G. Mechanisms of cell survival in hypoxia and hypothermia. J. Exp. Biol. 204, Pt. 158:3171-3181, 2001.

5. Brace, C. L. Microwave tissue ablation: biophysics, technology, and applications. Crit. Rev. Biomed. Eng. 38:65-78, 2010.

6. Chow, M. J. and Y. Zhang. Changes in the mechanical and biochemical properties of aortic tissue due to cold storage. J. Surg. Res. 171:434-442, 2011.

7. Chu, K. F. and D. E. Dupuy. Thermal ablation of tumours: biological mechanisms and advances in therapy. Nat. Rev. Cancer 14: 199-208, 2014.

8. Downey, R. Anatomy of the normal diaphragm. Thorac. Surg. Clin. 21:273-279, 2011.

9. Endo, M. Calcium-induced calcium release in skeletal muscle. Physiol. Rev. 89:1153-1176, 2009.

10. Everett 4th, T. H., S. Nath, C. Lynch 3rd, J. M. Bech, J. G. Whayne, and D. E. Haines. Role of calcium in acute hyperthermic myocardial injury. J. Cardiovasc. Electrophysiol. 12:563-569, 2001.

11. Haemmerich, D. Biophysics of radiofrequency ablation. Crit. Rev. Biomed. Eng. 38:53-63, 2010.

12. Haines, D. E. Biophysics of radiofrequency lesion formation. In: Catheter Ablation of Cardiac Arrhythmias, 2nd edition, edited by S. K. S. Huang and M. A. Wood. Philadelphia: Saunders (Elsevier), 2011, p. 3.

13. Head, H. W., G. D. Dodd 3rd, N. C. Dalrymple, S. R. Prasad, F. M. El-Merhi, M. W. Freckleton, and L. G. Hubbard. Percutaneous radiofrequency ablation of hepatic tumors against the diaphragm: frequency of diaphragmatic injury. Radiology 243:877-884, 2007.

14. Hiraki, T., H. Gobara, H. Fujiwara, H. Ishii, K. Tomita, M. Uka, S. Makimoto, and S. Kanazawa. Lung cancer ablation: complications. Semin. Intervent. Radiol. 30:169-175, 2013.

15. Iaizzo, P. A. and F. Lehmann-Horn. The in vitro determination of susceptibility to malignant hyperthermia. Muscle Nerve 12: 184-190, 1989.

16. Iaizzo, P. A., D. J. Wedel, and W. J. Gallagher. In vitro contracture testing for determination of susceptibility to malignant hyperthermia: a methodologic update. Mayo Clin. Proc. 66:998-1004, 1991.

17. Kandarian, S. C. and T. P. White. Force deficit during the onset of muscle hypertrophy. J. Appl. Physiol., vol. 67, no. 6, pp. 2600-2607, 1989.

18. Kato, T., T. Yamagami, T. Hirota, T. Matsumoto, R. Yoshimatsu, and T. Nishimura. Transpulmonary radiofrequency ablation for hepatocellular carcinoma

under real-time computed tomography-fluoroscopic guidance.
Hepatogastroenterology 55;1450-1453, 2008.

19. Keller, M. W. Arteriolar constriction in skeletal muscle during vascular stunning: role of mast cells. Am. J. Physiol. 272:H2154-2163, 1997.

20. Kjaer, M. Role of extracellular matrix in adaptation of tendon and skeletal muscle to mechanical loading. Physiol. Rev. 84:649-698, 2004.

21. Lustgarten, D. L., D. Keane, and J. Ruskin. Cryothermal ablation: mechanism of tissue injury and current experience in the treatment of tachyarrhythmias. Prog. Cardiovasc. Dis. 41:481-498, 1999.

22. Mori, T., K. Kawanaka, Y. Ohba, K. Shiraishi, K. Iwatani, K. Yoshimoto, and Y. Yamashita. Diaphragm perforation after radio-frequency ablation for metastatic lung cancer. Ann. Thorac. Cardiovasc. Surg. 16:426-428, 2010.

23. Moriondo, A., F. Boschetti, F. Bianchin, S. Lattanzio, C. Marcozzi, and D. Negrini. Tissue contribution to the mechanical features of diaphragmatic initial lymphatics. J. Physiol. 588:3957-3969, 2010.

24. Rehman, J., J. Landman, C. Sundaram, and R. V. Clayman. Tissue chemoablation. J. Endourol. 17:647-657, 2003.

25. Schwartz, A., G. Desolneux, M. Desjardin, S. Evrard, and D. Bechade. Symptomatic diaphragmatic hernia after pulmonary radiofrequency ablation. J. Visc. Surg. 150:157-158, 2013.

26. Sink, J. D., G. L. Pellom, W. D. Currie, W. R. Chitwood Jr, R. C. Hill, and A. S. Wechsler. Protection of mitochondrial function during ischemia by potassium cardioplegia: correlation with ischemic contracture. Circulation 60:158-163, 1979.

27. Smith, L. R. and E. R. Barton. Collagen content does not alter the passive mechanical properties of fibrotic skeletal muscle in mdx mice. Am. J. Physiol. Cell Physiol. 306:C889-898, 2014.

28. Steenbergen, C. and N. G. Frangogiannis. Ischemic heart disease. In: Muscle: Fundamental Biology and Mechanisms of Disease, edited by J. Hill and E. Olson. Boston: Elsevier, 2012, p. 497.

29. Whittaker, D. K. Mechanisms of tissue destruction following cryosurgery. Ann. R. Coll. Surg. Engl. 66:313-318, 1984.

30. Wood, T. F., D. M. Rose, M. Chung, D. P. Allegra, L. J. Foshag, and A. J. Bilchik. Radiofrequency ablation of 231 unresectable hepatic tumors: indications, limitations, and complications. Ann. Surg. Oncol. 7:593-600, 2000.

31. Zhou, Y. Generation of uniform lesions in high intensity focused ultrasound ablation. Ultrasonics 53:495-505, 2013.

32. M. G. Sardesai et al., "Vastus lateralis muscle-only free flap: defining its role in head and neck reconstruction," *J. Otolaryngol. Head Neck Surg.*, vol. 37, no. 2, pp. 230-234, Apr. 2008.

33. A. T. Berman et al., "Muscle biopsy: proper surgical technique," *Clin. Orthop. Relat. Res.*, vol. 198, pp. 240-243, Sep. 1985.

34. A. J. Huang, "Radiofrequency ablation of osteoid osteoma: difficult-to-reach

places," *Semin. Musculoskelet. Radiol.*, vol. 20, no. 5, pp. 486-495, Nov. 2016.

35. M. J. Whitmore et al., "Cryoablation of osteoid osteoma in the pediatric and adolescent population," *J. Vasc. Interv. Radiol.*, vol. 27, no. 2, pp. 232-237, Feb. 2016.

36. C. Prud'homme et al., "Prospective pilot study of CT-guided microwave ablation in the treatment of osteoid osteomas," *Skeletal Radiol.*, vol. 46, no. 3, pp. 315-323, Mar. 2017.

37. D. K. Filippiadis et al., "Percutaneous image-guided ablation of bone and soft tissue tumours: a review of available techniques and protective measures," *Insights Imaging*, vol. 5, no. 3, pp. 339-346, June 2014.

38. D. Haemmerich, "Biophysics of radiofrequency ablation," *Crit. Rev. Biomed. Eng.*, vol. 38, no. 1, pp. 53-63. 2010.

39. D. L. Lustgarten et al., "Cryothermal ablation: mechanism of tissue injury and current experience in the treatment of tachyarrhythmias," *Prog. Cardiovasc. Dis.*, vol. 41, no. 6, pp. 481-498, May-June 1999.

40. C. L. Brace, "Microwave tissue ablation: biophysics, technology, and applications," *Crit. Rev. Biomed. Eng.*, vol. 38, no. 1, pp. 65-78. 2010.

41. F. Lehmann-Horn and P. A. Iaizzo, "Resealed fiber segments for the study of the pathophysiology of human skeletal muscle," *Muscle Nerve*, vol. 13, no. 3, pp. 222-231, Mar. 1990.

42. P. A. Iaizzo and F. Lehmann-Horn, "The in vitro determination of susceptibility to malignant hyperthermia," *Muscle Nerve,* vol. 12, no. 3, pp. 184-190, Mar. 1989.

43. P. A. Iaizzo et al., "In vitro contracture testing for determination of susceptibility to malignant hyperthermia: a methodologic update*," Mayo Clin. Proc.*, vol. 66, no. 10, pp. 998-1004, Oct. 1991.

44. A. Thiagalingam et al., "Importance of catheter contact force during irrigated radiofrequency ablation: evaluation in a porcine ex vivo model using a force-sensing catheter," *J. Cardiovasc. Electrophysiol.*, vol. 21, no. 7, pp. 806-811, July 2010.

45. K. Yokoyama et al., "Novel contact force sensor incorporated in irrigated radiofrequency ablation catheter predicts lesion size and incidence of steam pop and thrombus," *Circ. Arrhythm. Electrophysiol.*, vol. 1, no. 5, pp. 354-362, Dec. 2008.

46. A. Ikeda et al., "Increasing contact force increases lesion size during cryo-ablation," *Circulation*, vol. 118, Suppl. 18, pp. S829-830, 2008 (abstract). Oct. 2008.

47. J. C. Bischof and X. He, "Thermal stability of proteins," *Ann. N Y Acad. Sci.,* vol. 1066, pp. 12-33, Dec. 2005.

48. K. F. Chu and D. E. Dupuy, "Thermal ablation of tumours: biological mechanisms and advances in therapy," *Nat. Rev. Cancer*, vol. 14, no. 3, pp. 199-208, Mar. 2014.

49. D. K. Whittaker, "Mechanisms of tissue destruction following cryosurgery," *Ann.*

R. Coll. Surg. Engl., vol. 66, no. 5, pp. 313-318, Sep. 1984.

50. R. G. Boutilier, "Mechanisms of cell survival in hypoxia and hypothermia," *J. Exp. Biol.,* vol. 204, no. 18, pp. 3171-3181, Sep. 2001.

51. M. W. Keller, "Arteriolar constriction in skeletal muscle during vascular stunning: role of mast cells," *Am. J. Physiol.,* vol. 272, no. 5, Pt 2, pp. H2154-2163, May 1997.

52. S. C. Kandarian and T. P. White, "Force deficit during the onset of muscle hypertrophy," *J. Appl. Physiol.,* vol. 67, no. 6, pp. 2600-2607, Dec. 1989.

53. C. Steenbergen and N. G. Frangogiannis, "Ischemic heart disease," in *Muscle: Fundamental Biology and Mechanisms of Disease.* Boston: Elsevier, 2012, p. 497.

54. J. D. Sink et al., "Protection of mitochondrial function during ischemia by potassium cardioplegia: correlation with ischemic contracture," *Circulation,* vol. 60, no. 2, Pt 2, pp. 158-163, Aug. 1979.

55. M. Endo, "Calcium-induced calcium release in skeletal muscle," *Physiol. Rev.,* vol. 89, no. 4, pp. 1153-1176, Oct. 2009.

56. M. W. Berchtold et al., "Calcium ion in skeletal muscle: its crucial role for muscle function, plasticity, and disease," *Physiol. Rev.,* vol. 80, no. 3, pp. 1215-1265, July 2000.

57. D. E. Haines, "Biophysics of radiofrequency lesion formation," in *Catheter Ablation of Cardiac Arrhythmias.* 2nd ed., Philadelphia: Saunders (Elsevier), 2011, p. 3.

58. T. H. Everett 4th et al., "Role of calcium in acute hyperthermic myocardial injury," *J. Cardiovasc. Electrophysiol.,* vol. 12, no. 5, pp. 563-569, May 2001.

59. Kranjc, M., Zupanic, A., Miklavcic, D., & Jarm, T. (2010). Numerical analysis and thermographic investigation of induction heating. *International Journal of Heat and Mass Transfer*, *53*(17-18), 3585-3591.

Chapter 3

1. 1 Hamilton Jr, William C., and Mark Ortiz. "Irreversible electroporation (ire) for esophageal disease." U.S. Patent Application No. 12/755,517.

2. Egeland, C., Baeksgaard, L., Johannesen, H. H., Löfgren, J., Plaschke, C. C., Svendsen, L. B., ... & Achiam, M. P. (2018). Endoscopic electrochemotherapy for esophageal cancer: a phase I clinical study. Endoscopy international open, 6(06), E727-E734.

3. 3.. Marc O. Siegel, David M. Parenti, Gary L. Simon; Atrial-Esophageal Fistula after Atrial Radiofrequency Catheter Ablation, *Clinical Infectious Diseases*, Volume 51, Issue 1, 1 July 2010, Pages 73–76, https://doi.org/10.1086/653425

4. Ghia KK, Chugh A, Good E, Pelosi F, Jongnarangsin K, Bogun F, Morady F, Oral H. A nationwide survey on the prevalence of atrioesophageal fistula after left atrial radiofrequency catheter ablation. J Interv Card Electrophysiol. 2009 Jan;24(1):33-6.

5. Gilcrease GW, Stein JB. A delayed case of fatal atrioesophageal fistula following radiofrequency ablation for atrial fibrillation. J Cardiovasc Electrophysiol. 2010 Jun 1;21(6):708-11.

6. Stöckigt F, Schrickel JW, Andrié R, Lickfett L. Atrioesophageal fistula after cryoballoon pulmonary vein isolation. J Cardiovasc Electrophysiol. 2012 Nov;23(11):1254-7.

7. Kawasaki R, Gauri A, Elmouchi D, Duggal M, Bhan A. Atrioesophageal Fistula Complicating Cryoballoon Pulmonary Vein Isolation for Paroxysmal Atrial Fibrillation. J Cardiovasc Electrophysiol. 2014 Apr 4.

8. Borchert B, Lawrenz T, Hansky B, Stellbrink C. Lethal atrioesophageal fistula after pulmonary vein isolation using high-intensity focused ultrasound (HIFU). Heart Rhythm. 2008 Jan;5(1):145-8.

9. Neven, K., van Es, R., van Driel, V., van Wessel, H., Fidder, H., Vink, A., ... & Wittkampf, F. (2017). Acute and long-term effects of full-power electroporation ablation directly on the porcine esophagus. *Circulation: Arrhythmia and Electrophysiology*, *10*(5), e004672.

10. Yazaki, E., & Sifrim, D. (2012). Anatomy and physiology of the esophageal body. *Diseases of the Esophagus*, *25*(4), 292-298

Chapter 4

1. Wittkampf, F. H., van Es, R., & Neven, K. (2018). Electroporation and its relevance for cardiac catheter ablation. *JACC: Clinical Electrophysiology*.

2. Sugrue, A., Maor, E., Ivorra, A., Vaidya, V., Witt, C., Kapa, S., & Asirvatham, S. (2018). Irreversible electroporation for the treatment of cardiac arrhythmias. *Expert review of cardiovascular therapy*, *16*(5), 349-360.

3. Neven, K., van Driel, V., van Wessel, H., van Es, R., du Pré, B., Doevendans, P. A., & Wittkampf, F. (2014). Safety and feasibility of closed chest epicardial

catheter ablation using electroporation. *Circulation: Arrhythmia and Electrophysiology*, CIRCEP-114.

4. Reddy, V. Y., Koruth, J., Jais, P., Petru, J., Timko, F., Skalsky, I., ... & Funosako, M. (2018). Ablation of Atrial Fibrillation With Pulsed Electric Fields: An Ultra-Rapid, Tissue-Selective Modality for Cardiac Ablation. *JACC: Clinical Electrophysiology*, 674.

5. Du Pré, B. C., van Driel, V. J., van Wessel, H., Loh, P., Doevendans, P. A., Goldschmeding, R., ... & Vink, A. (2012). Minimal coronary artery damage by myocardial electroporation ablation. *Europace*, *15*(1), 144-149.

6. van Driel, Vincent JHM, et al. "Pulmonary vein stenosis after catheter ablation: electroporation versus radiofrequency." *Circulation: Arrhythmia and Electrophysiology* (2014): CIRCEP-113.

7. Van Driel VJHM, Neven K, Van Wessel H, Vink A, Doevendans PAFM, Wittkampf FHM: Low vulnerability of the right phrenic nerve to electroporation ablation. Heart Rhythm [Internet] Elsevier, 2015; 12:1838–1844. Available from: http://dx.doi.org/10.1016/j.hrthm.2015.05.012

8. Neven, K., van Es, R., van Driel, V., van Wessel, H., Fidder, H., Vink, A., ... & Wittkampf, F. (2017). Acute and long-term effects of full-power electroporation ablation directly on the porcine esophagus. *Circulation: Arrhythmia and Electrophysiology*, *10*(5), e004672.

9. DeSimone, C. V., Kapa, S., & Asirvatham, S. J. (2014). Electroporation: past and future of catheter ablation.

10. Wittkampf, F. H., van Driel, V. J., van Wessel, H., Neven, K. G., Gründeman, P. F., Vink, A., ... & Doevendans, P. A. (2012). Myocardial lesion depth with circular electroporation ablation. *Circulation: Arrhythmia and Electrophysiology*, CIRCEP-111.

11. DeSimone, C. V., Ebrille, E., Syed, F. F., Mikell, S. B., Suddendorf, S. H., Wahnschaffe, D., ... & Asirvatham, S. J. (2014). Novel balloon catheter device with pacing, ablating, electroporation, and drug-eluting capabilities for atrial fibrillation treatment—preliminary efficacy and safety studies in a canine model. *Translational Research*, *164*(6), 508-514.

12. Hong, J., Stewart, M. T., Cheek, D. S., Francischelli, D. E., & Kirchhof, N. (2009, September). Cardiac ablation via electroporation. In *Engineering in Medicine and Biology Society, 2009. EMBC 2009. Annual International Conference of the IEEE* (pp. 3381-3384). IEEE.

13. Miyasaka, Yoko, et al. "Secular trends in incidence of atrial fibrillation in Olmsted County, Minnesota, 1980 to 2000, and implications on the projections for future prevalence." Circulation 114.2 (2006): 119-125.

14. Kuck, Karl-Heinz, Josep Brugada, Alexander Fürnkranz, Andreas Metzner, Feifan Ouyang, KR Julian Chun, Arif Elvan et al. "Cryoballoon or radiofrequency ablation for paroxysmal atrial fibrillation." New England Journal of Medicine (2016).

15. Singal, Ashish. The Comparative Assessment of Clinical Ablative Therapies: Effects on Physiological and Biomechanical Properties of Contractile Tissues in

Response to Therapeutic Doses. Thesis. University of Minnesota, 2014. N.p.: n.p., n.d. Print.

16. Iaizzo PA, Lehmann-Horn F: The in vitro determination of susceptibility to malignant hyperthermia. Muscle and Nerve 12: 184-190, 1989. PMID: 2725548

Chapter 5

References

1. Packer DL, Kowal RC, Wheelan KR, Irwin JM, Champagne J, Guerra PG, Dubuc M, Reddy V, Nelson L, Holcomb RG, Lehmann JW: Cryoballoon Ablation of Pulmonary Veins for Paroxysmal Atrial Fibrillation First Results of the North American Arctic Front (STOP AF) Pivotal Trial. J Am Coll Cardiol [Internet] Elsevier Inc., 2013; 61:1713–1723. Available from: http://dx.doi.org/10.1016/j.jacc.2012.11.064

2. Koruth JS, Reddy VY, Miller MA, Patel KK, Coffey JO, Fischer A, Gomes JA, Dukkipati S, D'Avila A, Mittnacht A: Mechanical esophageal displacement during catheter ablation for atrial fibrillation. J Cardiovasc Electrophysiol 2012; 23:147–154.

3. Preis O, Digumarthy SR, Wright CD, Shepard JOM: Atrioesophageal Fistula After Catheter Pulmonary Venous Ablation for Atrial Fibrillation: Imaging Features. 2007; 22:283–285.

4.   Ghia KK, Chugh A, Good E, Pelosi F, Jongnarangsin K, Bogun F, Morady F, Oral
        H: A nationwide survey on the prevalence of atrioesophageal fistula after left atrial
        radiofrequency catheter ablation. J Interv Card Electrophysiol 2009; 24:33–36.

5.   Stöckigt F, Schrickel JW, Andrié R, Lickfett L: Atrioesophageal fistula after
        cryoballoon pulmonary vein isolation. J Cardiovasc Electrophysiol 2012; 23:1254–
        1257.

6.   Goff RP, Bersie SM, Iaizzo PA: In vitro assessment of induced phrenic nerve
        cryothermal injury. Hear Rhythm [Internet] Elsevier, 2014; 11:1779–1784.
        Available from: http://dx.doi.org/10.1016/j.hrthm.2014.06.022

7.   Stampfli, R: Reversible electrical breakdown of the excitable membrane of a
        Ranvier node. *An Acad Brasil Ciens* 30 (1958): 57-63. 8.

8.   Kotnik T, Kramar P, Pucihar G, Miklavčič D, Tarek M: Cell membrane
        electroporation - Part 1: The phenomenon. IEEE Electr Insul Mag 2012; 28:14–23.

9.   Neven K, Driel V Van, Wessel H Van, Es R Van, Pré B Du, Doevendans PA,
        Wittkampf F: Safety and feasibility of closed chest epicardial catheter ablation
        using electroporation. Circ Arrhythmia Electrophysiol 2014; 7:913–919.

10.   Sánchez-Quintana D, Cabrera JA, Climent V, Farré J, Weiglein A, Ho SY: How
        close are the phrenic nerves to cardiac structures? Implications for cardiac
        interventionalists. J Cardiovasc Electrophysiol 2005; 16:309–313.

11. Van Driel VJHM, Neven KGEJ, Van Wessel H, Du Pré BC, Vink A, Doevendans PAFM, Wittkampf FHM: Pulmonary vein stenosis after catheter ablation electroporation versus radiofrequency. Circ Arrhythmia Electrophysiol 2014; 7:734–738.

12. Maor E, Ivorra A, Leor J, Rubinsky B: The effect of irreversible electroporation on blood vessels. Technol Cancer Res Treat 2007; 6:307–312.

13. Neven K, Van Es R, Van Driel V, Van Wessel H, Fidder H, Vink A, Doevendans P, Wittkampf F: Acute and Long-Term Effects of Full-Power Electroporation Ablation Directly on the Porcine Esophagus. Circ Arrhythmia Electrophysiol 2017; 10:1–8.

14. Van Driel VJHM, Neven K, Van Wessel H, Vink A, Doevendans PAFM, Wittkampf FHM: Low vulnerability of the right phrenic nerve to electroporation ablation. Heart Rhythm [Internet] Elsevier, 2015; 12:1838–1844. Available from: http://dx.doi.org/10.1016/j.hrthm.2015.05.012

15. Schoellnast H, Monette S, Ezell PC, Deodhar A, Maybody M, Erinjeri JP, Stubblefield MD, Single GW, Hamilton WC, Solomon SB: Acute and subacute effects of irreversible electroporation on nerves: experimental study in a pig model. Radiology [Internet] 2011; 260:421–427. Available from: http://www.ncbi.nlm.nih.gov/pubmed/21642418

Appendix A – Publications

Original Articles

1. Duan, Shanzhong, **Lars M Mattison**, and Teresa Binkley, 2012, "Multibody Dynamics Model for Analysis of Human Body Response to Vibrations" ASME IMECE 2012.
2. **Mattison, Lars M**, Shawn Duan, and Teresa Binkley, 2012,"Translation of Vibration from a Vibrational Plate to the Human Body," South Dakota State University Journal of Undergraduate Research, 10 (2012)
3. **Mattison, Lars M**, Taylor N. Suess, Michael P. Twedt, Stephen P. Gent. "Comparison of Theoretical and Experimental Corn Drying Profiles Within a Cross-Flow Column Dryer" ASME IMECE 2013.
4. **Mattison, Lars M,** John R Spratt, Brian Howard, Shancy Augustine, Semal Musleh, and Paul A. Iaizzo. "A Simplified Model for the Assessment of Ex Vivo Lung Perfusion Methodologies and Treatments" Journal of Medical Devices May 2016.
5. **Mattison, Lars M,** Paul A Iaizzo. "A Device to Aid in Quantifying Lung Compliance and Edema" Journal of Medical Devices May 2016.
6. Loor, Gabriel, Brian T Howard, John R Spratt, **Lars M Mattison**, Angela Panoskaltsis-Mortari, Roland Z Brown, Tinen L Iles, Carolyn M Meyer, Haylie Helms, Andrew Price, Paul A Iaizzo. "Prolonged EVLP Using OCS Lung: Cellular and Acellular Perfusates." *Transplantation* (2017). PMID: 28009782
7. Iles, Tinen L, Timothy G Laske, David L Garshelish, **Lars M Mattison**, Brian Lee, Val Eisele, Erik Gaassedelen, Paul A Iaizzo. "Medtronic Reveal LINQ Devices to Better Understand Hibernation Physiology in the American Black Bear (Ursus americanus) Journal of Medical Devices 2017.
8. **Mattison, Lars M** and Paul A. Iaizzo. "Physiologic Assessment of Cardiac Muscle Post Irreversible Electroporation Therapy" Journal of Medical Devices June 2017.
9. John R Spratt MD, MA, **Lars M Mattison, BS**, Paul A. Iaizzo, PhD, Roland Z Brown, BA, Haylie Helms, Tinen L Iles, MS, Brian Howard, PhD, Angela Panoskaltsis-Mortari, PhD, and Gabriel Loor, MD. "An experimental study of the recovery of injured procine lungs with prolonged normothermic cellular ex vivo lung perfusion following donation after circulatory death." Transplant International September 2017. PMID: 28493634
10. Schmitz, Anthony**, Lars M Mattison**, Tinen L Iles, Paul A Iaizzo. "Novel visualization of coronary stenting techniques and subsequent 3D modeling and printing of deployed devices" European Society of Cardiology Clinical Case Gallery March 2017.
11. Spratt, John R, **Lars M Mattison**, Paul A Iaizzo, Gabriel Loor. The ABCs of Autologous Blood Collection for Ex Vivo Organ Preservation. *The Journal of Thoracic and Cardiovascular Surgery*. January 2018. PMID: 29129423

12. Holm, Mikayle, **Lars M Mattison**, Pierce Vatterott, Paul A Iaizzo. "Direct visualization of the removal of chronically implanted pacing leads from an unfixed human cadaver" Heart Rhythm Case Reports Feb 2018. PMID: 29915710
13. Singal, Ashish, **Lars M Mattison**, Charles L. Soule, Paul A Iaizzo. "Effects of Ablation (Radiofrequency, Cryo, Microwave) on Physiologic Properties of the Human Vastus Lateralis" Transactions on Biomedical Engineering 2018. PMID: 29989956
14. Singal, Ashish, **Lars M Mattison**, Charles L Soule, John R Ballard, Eric N Rudie, Erik N K Cressman, Paul A Iaizzo. "Assessment of Ablative Therapies in Swine: Response of Respiratory Diaphragm to Varying Doses" Annals of Biomedical Engineering March 2018. PMID: 29594687
15. **Mattison, Lars M**, Chloe Johnson and Paul A. Iaizzo. "Biomechanical Response of Swine Esophagus Tissue to Irreversible Electroporation" Journal of Medical Devices 2018.
16. Holm, Mikayle A, Alex Mattson, **Lars M Mattison**, Erik Gaasedelen, Jorge Zhingre Sanchez, and Paul A. Iaizzo. "Portable Ex Vivo Heart Perfusion Apparatus – Visible Heart Mobile" Journal of Medical Devices 2018.
17. Spratt, John R, **Lars M Mattison, BS**, Paul A Iaizzo, PhD, Carolyn Meyer, BS, Roland Z Brown, BA, Tinen Iles, MS, Angela Panoskaltsis-Mortari, PhD, Gabriel Loor, MD. Lung Transplant after Prolonged Ex Vivo Lung Perfusion: Predictors of Allograft Function in Swine. Journal of Surgical Research. Transplant International (Accepted).
18. Seewald, Maria S., Erik N. Gaasedelen, Tinen L. Iles, **Lars M Mattison**, Alexander R. Mattson, Megan M Schmidt, Ruediger C. Braun-Dullaeus, and Paul A. Iaizzo. "Adenosine triphosphate dosages in a swine heart model: implications for ex vivo perfusion devices and cardiac transplants" Journal of Cardiovascular Translational Research (Submitted).
19. **Mattison, Lars M**, Maria Burbano-Salazar, and Paul A Iaizzo. 'In Vitro Assessment of Phrenic Nerve Responses to Irreversible Electroporation" (Submitted to Heart Rhythm 2018).
20. Gill, Lisa**, Lars M. Mattison**, Arpan Patel, and Paul A. Iaizzo, PhD "Effects of human adiponectin on stimulated human myometrial contractility in vitro" (Submitted May 2018).
21. Zhingre Sanchez, Jorge, **Lars M Mattison**, Michael G Bateman, and Paul A Iaizzo .Computational Simulations of Ventricular Outflow Tract Obstructions Associated With Varied Replacement Valve Geometries. 2018 Journal of Medical Devices.

Book Chapters

1. **Mattison, Lars M**, Tim G Laske, and Paul A Iaizzo. "Transcather Valve Replacement" The Handbook of Cardiac Anatomy, Physiology, and Devices 3rd Edition. 2015.
2. Shaffer, Andrew, **Lars M Mattison,** John R Spratt, Tinen L Iles, Natalie Kerns, Stephen Huddleston, Michael G Bateman, and Paul A Iaizzo. "A New Era for

Improving Cardiothoracic Transplantations" Engineering in Medicine: Advances and Opportunities. 2018.

3. **Mattison, Lars M,** Brian T Howard, Paul A Iaizzo "Applications of Electroporation for the treatment of soft tissue in the Human Body" Engineering in Medicine: Advances and Opportunities. 2018.

Invited Lectures and Presentations

1. "Ex-Vivo Lung Perfusion" Second Chance for Life Annual Meeting. August 2015.

2. "Device to Quantify Lung Compliance and Edema" Three in Five Competition, Design of Medical Devices Conference 2016, University of Minnesota. April 13, 2016.

3. "Computational Modeling in the Visible Heart Lab" Dassault Systems Innovation Conference. University of Minnesota. April 15, 2016.

4. "Uncontrolled DCD with Prolonged Ex Vivo Lung Perfusion: A Feasibility Model for Donor Lung Recovery and Allocation" Surgery Transplant Conference, University of Minnesota. May 11, 2016.

5. "A Simplified Model for the Assessment of Ex-Vivo Lung Perfusion Post Treatments" Minnesota Surgical Society, September 30, 2016.

6. **"**Physiological Response of Human Esophagus to Irreversible Electroporation" 2nd World Congress on Pulsed Electric Fields in Biology, Medicine and Food & Environmental Technologies." September 2017.

7. "Biophysical Responses of Cardiothoracic Tissues to Irreversible Electroporation Therapy" Design of Medical Devices Conference. April 10, 2018.

Presented Abstracts

1. Maas, Danise L, **Lars M Mattison**, Macie Michelson, Bradley Bowser. "The effects of fatigue on vertical loading during running" American Society of Biomechanics Conference 2013.
2. Quallich, Stephen G, Mark A Benscoter, **Lars M Mattison**, Megan M Schmidt, Salah J El Haddi, Paul A Iaizzo. "Assessing Iatrogenic Atrial Septal Defect Formation with Novel Transseptal Puncture Device" TCT 2014 Washington, DC.
3. Loor, Gabriel, Brian Howard, Tinen Iles, **Lars M Mattison,** Phillip Meyer, Travis Day, Angela Panoskaltsis-Mortari, Rosemary Kelly, and Paul A Iaizzo. Prolonged Lung Preservation at 24 Hours Using Donor Whole Blood Perfusion in the Organ Care System (OCS). ISHLT 2015.
4. **Mattison, Lars M**, Paul A Iaizzo "Phrenic Nerve Response to Cryoablation

Therapies" American College of Cardiology 2015.

5. **Mattison, Lars M,** Matthew R Yoder, Charles L Soule, Paul A Iaizzo "Physiological and Biomechanical Response of Skeletal Muscle to Electroporation" 1st World Congress on Electroporation.

6. Spratt, John. R., **Lars M Mattison,** Paul A Iaizzo, Tinen L Iles, William Payne, and Gabriel Loor. "Uncontrolled DCD with Prolonged Ex Vivo Lung Perfusion (EVLP): A Feasible Model for Donor Lung Recovery and Allocation" ISHLT 2016.

7. Thomas, Katheryn N., Charles L Soule, **Lars M Mattison,** and Paul A Iaizzo. "Assessing Muscle Protection with Pharmacological Post-Conditioning Agents in an Acute Ischemia Reperfusion Model" *The FASEB Journal*,*30*(1 Supplement).

8. Bandschapp, Oliver, Asensio Gonzalez, Tinen Iles, **Lars M Mattison**, Megan Schmidt, Charles Soule, Paul A Iaizzo "Influence of Prior Statin Intake on Masseter Muscle Force During an Induced Malignant Hyperthermia Episode in Swine." Anethesiology Annual Meeting 2016.

9. **Mattison, Lars M**, Gabriel Loor, John R Spratt, Brian T Howard, Tinen L Iles, Phillip Meyer, Travis Day, Angela Panoskaltsis-Mortari, Marshal Hertz, Paul A Iaizzo, "A Comparison of Prolonged Swing Lung Preservation Using Packed Red Blood Cells, Donor Whole Blood, And Acellular Solution Using the Organ Care System (OCS™)" Thomas L. Petty Lung Conference 2016.

10. **Mattison, Lars M**, Sydney Newton, Nana Mitsuishi, and Paul A Iaizzo. "Phrenic Nerve Response to Irreversible Electroporation Therapies" BMES 2016.

11. Seewald, Maria, Erik Gaasedelen, Tinen Iles, **Lars M Mattison**, Alexander Mattison, Megan Schmidt, and Paul A Iaizzo. "Improving Cardiac Transplantation Using an Ex Vivo Perfusion Model and Pharmacological Posttreatment" BMES 2016.

12. Burbano, Maria, **Lars M Mattison**, and Paul A Iaizzo. "Effects of Cardiac and Respiration Movements on Relative Phrenic Nerve Displacements" BMES 2016.

13. Johnson, Evan, **Lars M Mattison**, Alex Mattison, and Paul A Iaizzo. "A Perfusion Apparatus to Image Semilunar Valve Anatomies in Perfusion-Fixed Human Hearts" BMES 2016.

14. **Mattison, Lars M**, Maria A Burbano, Paul A Iaizzo. "Effect of Irreversible Electroporation Probe Orientation on Phrenic Nerve Function Post Therapy" Minnesota Neuromodulation Symposium 2017.

15. Spratt, John R, **Lars M Mattison**, Paul A Iaizzo, Carolyn Meyer, Tinen L Iles, Angela Panoskaltsis-Mortari and Gabriel Loor. "Lung Transplantation from DCD Donors After Prolonged Normothermic Portable EVLP" ISHLT 2017.

16. Spratt, John R, Gabriel Loor, **Lars M Mattison**, Angela Panoskaltsis-Mortari. "In Vitro Analysis of RBC-Mediated Lung Injury in Prolonged Ex Vivo Lung Perfusion" ISHLT 2017.

17. **Mattison, Lars M**, Pierce Vatterott, Michael D. Eggen, Paul A. Iaizzo. "Novel visualizations of lead extractions employing multimodal imaging in perfusion-fixed human hearts." Heart Rhythm Society 2017.

18. **Mattison, Lars M, Apran Patil, Paul A Iaizzo. "Physiological Response of**

Skeletal and Smooth Muscle to Irreversible Electroporation" 2nd World Congress on   Pulsed Electric Fields   in Biology, Medicine and Food & Environmental Technologies. September 2017.

19. **Mattison, Lars M, Maria A Burbano, Paul A Iaizzo. "Afferent vs Efferent Response of the Phrenic Nerve to Irreversible Electroporation" 2nd World Congress on   Pulsed Electric Fields   in Biology, Medicine and Food & Environmental Technologies.** September 2017.

20. Gill, Lisa, **Lars M Mattison**, Arpan Patel, Paul A. Iaizzo "Adiponectin and human myometrial contractility in vitro" Society for Maternal and Fetal Medicine Pregnancy Conference. January 2018.

21. Gill, Lisa, **Lars M Mattison**, Arpan Patel, Paul A. Iaizzo "Myometrial Contractility in Gestational Diabetes" Society for Reproductive Investigation. March 2018.

22. Gurevich, Sergey G., **Lars M Mattison,** Anthony Prisco, Paul A Iaizzo, and Ganesh Raveendran. "3D Printing and Computer Modeling to Predict Paravalvular Leak in Transcatheter Aortic Valve Replacement" JACC Cardiovascular Interventions. Feb 2018.

23. Spratt, John R., **Lars M Mattison**, Natalie K. Aldrich, Stephen J. Huddleston, Linette Meyer, Gabriel Loor, and Paul A. Iaizzo. "Prolonged Extracorporeal Preservation and Evaluation of Human Lungs with Portable Normothermic Ex Vivo Perfusion" ISHLT 2018.

Poster Symposia

1. **Mattison, Lars M** and Shadi F. Othman. "Design of a Next Generation Bioreactor" Nebraska SROP Presentation 2012, Lincoln, NE.

2. **Mattison, Lars M**, Daniel A. Rajewski, Eugene S. Takle, Jerry L. Hatfield, and John H. Prueger. "Effects of Wind Turbine Wakes on Micrometeorological Conditions over a Crop Canopy" Iowa State REU Poster Session 2010.

3. **Mattison, Lars M**, Matthew R Yoder, Charles L Soule, Paul A Iaizzo "Biomechanical Response of Skeletal Muscle to Electroporation" Minnesota Muscle Symposium 2015.

4. Segurra, Jamilisse, **Lars M Mattison**, Paul A Iaizzo "Effects of Laser-Cutting in Muscle Tissue Biomechanics" LSSUP Poster Session 2016.

5. **Mattison, Lars M**, Matt R. Yoder, Jeremy M. Stimack, Paul A. Iaizzo PhD "A Comparison of Physiological Response of Muscle Tissues to Electroporation" Minnesota Muscle Symposium 2016.

6. **Mattison, Lars M,** Gabriel Loor, John R Spratt, Brian T Howard, Tinen L Iles, Phillip Meyer, Travis Day, Angela Panoskaltsis-Mortari, Marshal Hertz, Paul A. Iaizzo, "A Comparison of Prolonged Swing Lung Preservation Using Packed Red Blood Cells, Donor Whole Blood, And Acellular Solution Using the Organ Care System (OCS™)" University of Minnesota Department of Research Day 2017.

7. **Mattison, Lars M**, Michael G Bateman, and Alex J Hill "CoreValve Frame Analysis from Post Implant Clinical CTs" Medtronic S&T Conference October 24-27, 2017.

8. **Mattison, Lars M**, Arpan Patil, and Paul A Iaizzo PhD "Physiological Response of Skeletal Muscle to Irreversible Electroporation" Minnesota Muscle Symposium May 2017.
9. **Mattison, Lars M** Arpan Patil, and Paul A Iaizzo PhD "Physiological Assessment of Cardiac Muscle Post-Irreversible Electroporation Therapy" Department of Surgery Research Day 2017.
10. **Mattison, Lars M**, Julianne Spencer, Michael G Bateman, and Alex J Hill "TAV Frame Analysis in Bicuspid Patients from Post Implant CTs" Medtronic S&T Conference October 17-19, 2017.

Appendix B – Supplementary Figures for Assessment of Ablative Therapies in Swine: Response of Respiratory Diaphragm to Varying Doses
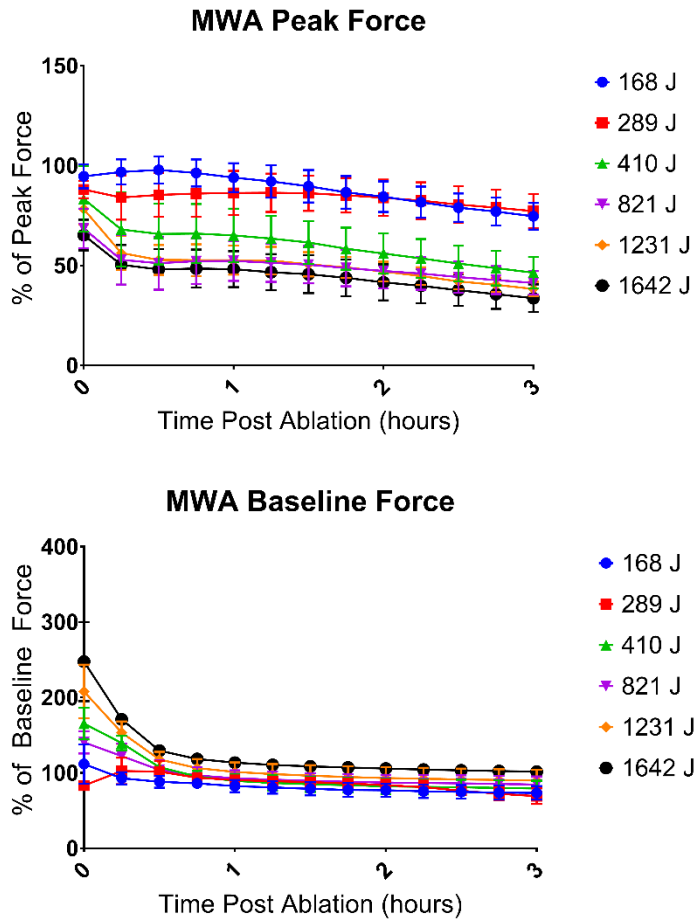

Fig. S1: Dose effects of percent change in peak force (top) and baseline force (bottom) of swine diaphragm muscle bundles post **microwave ablation**.

Fig. S2: Dose effects of percent change in peak force (top) and baseline force (bottom) of swine diaphragm muscle bundles post **HIFU ablation**.

163

Fig. S3: Dose effects of percent change in peak force (top) and baseline force (bottom) of swine diaphragm muscle bundles post **acetic acid ablation**.

Fig. S4: Dose effects of percent change in peak force (top) and baseline force (bottom) of swine diaphragm muscle bundles post **ethyl alcohol ablation**.

NaCl Peak Force

NaCl Baseline Force

Fig. S5: Dose effects of percent change in peak force (top) and baseline force (bottom) of swine diaphragm muscle bundles post **sodium chloride ablation**.
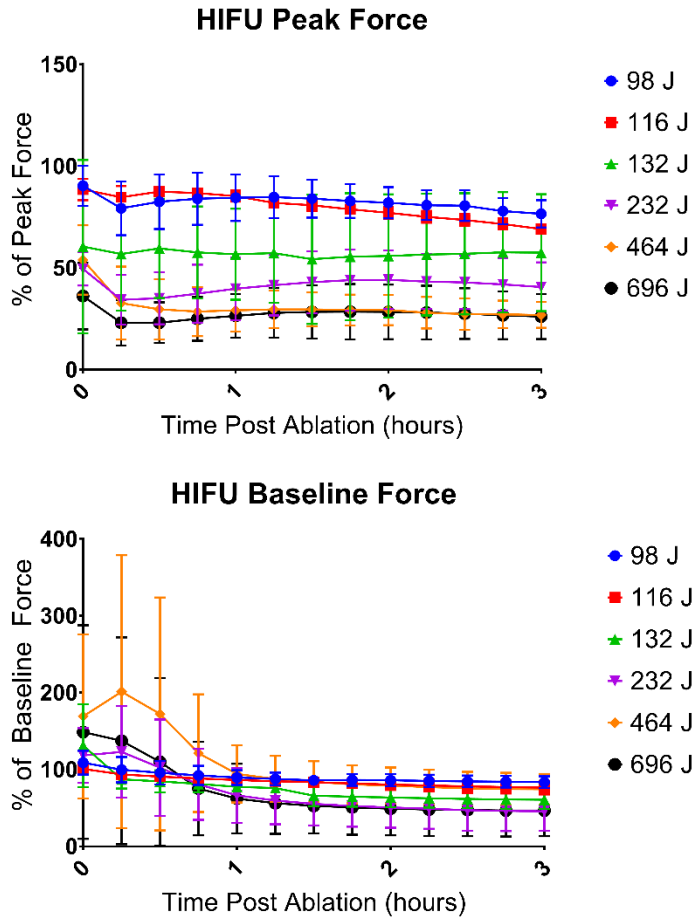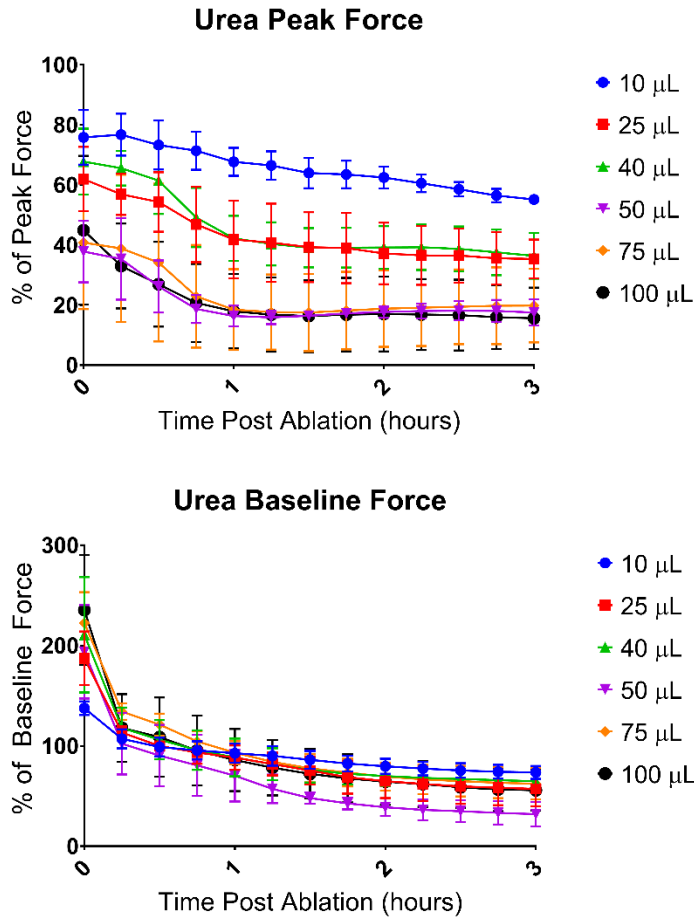
Fig. S6: Dose effects of percent change in peak force (top) and baseline force (bottom) of swine diaphragm muscle bundles post **urea ablation**.
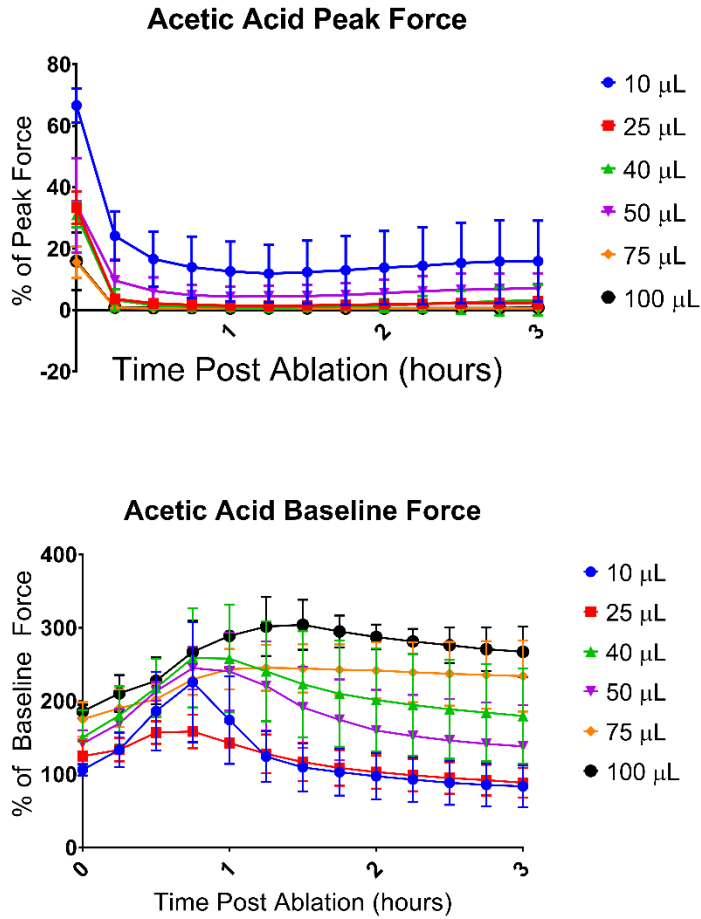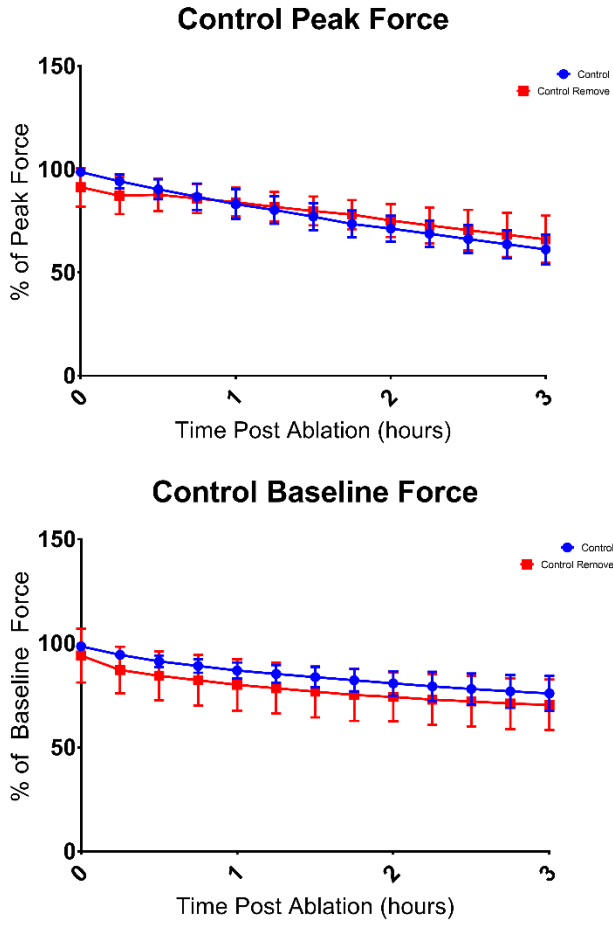
Fig. S7: Percent change in peak force (top) and baseline force (bottom) of "control-in bath" and "control-unmounted" swine diaphragm muscle bundles.
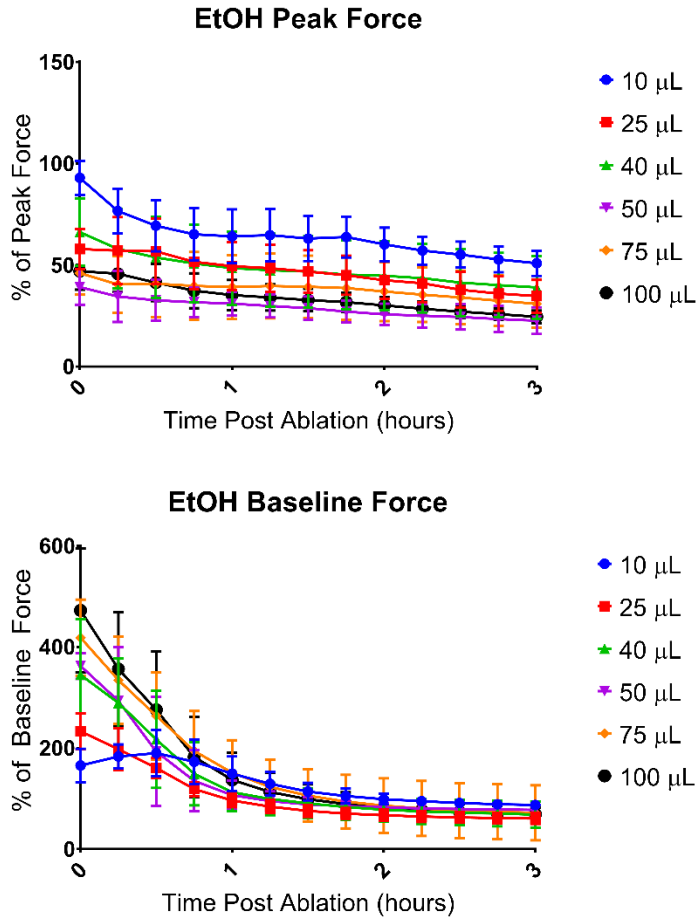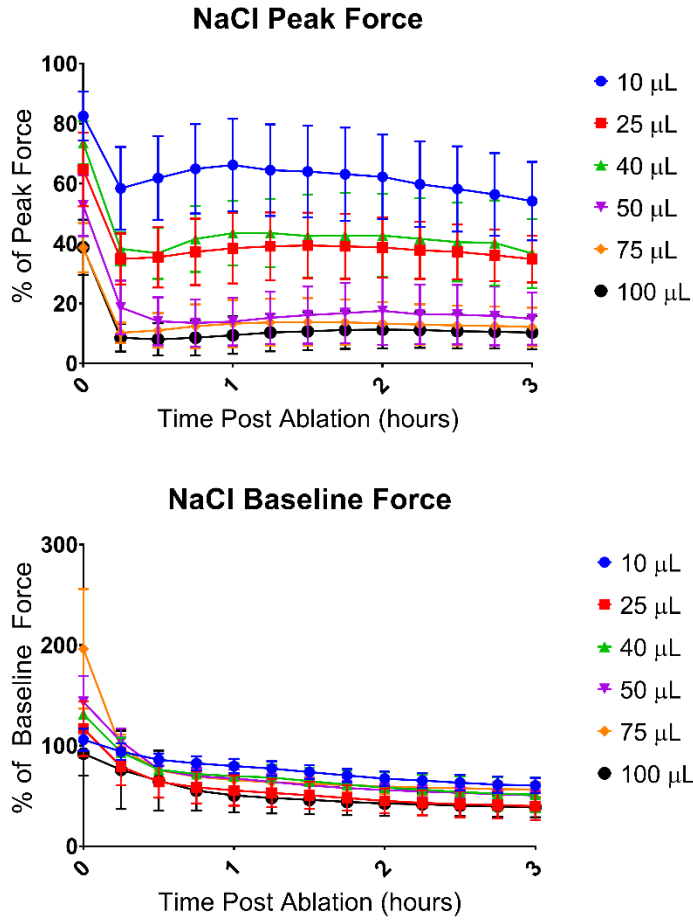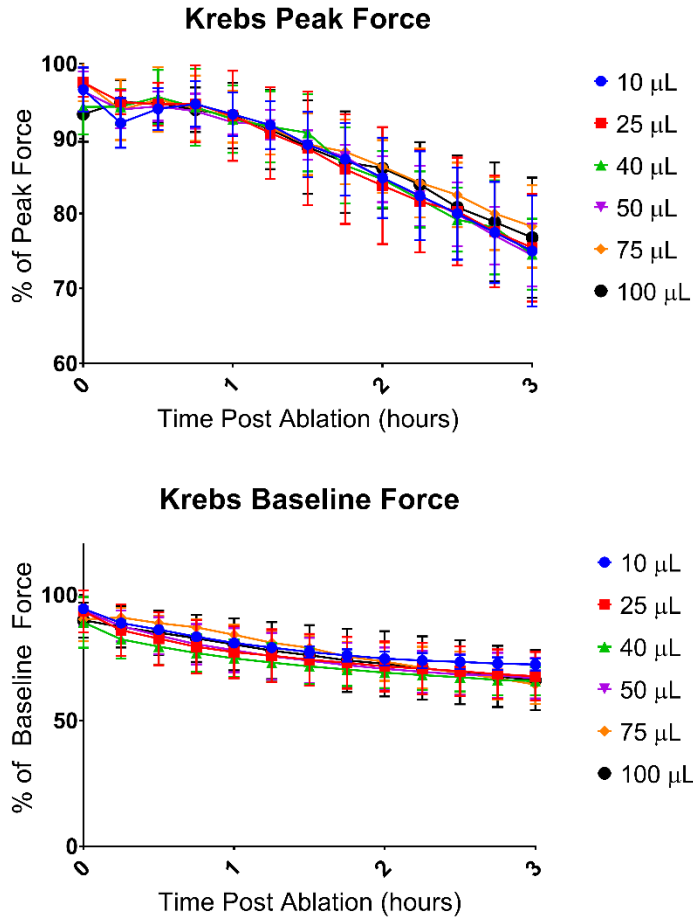
Fig. S8: Dose effects of percent change in peak force (top) and baseline force (bottom) of swine diaphragm muscle bundles post **injection of Krebs-Ringer solution**.

169
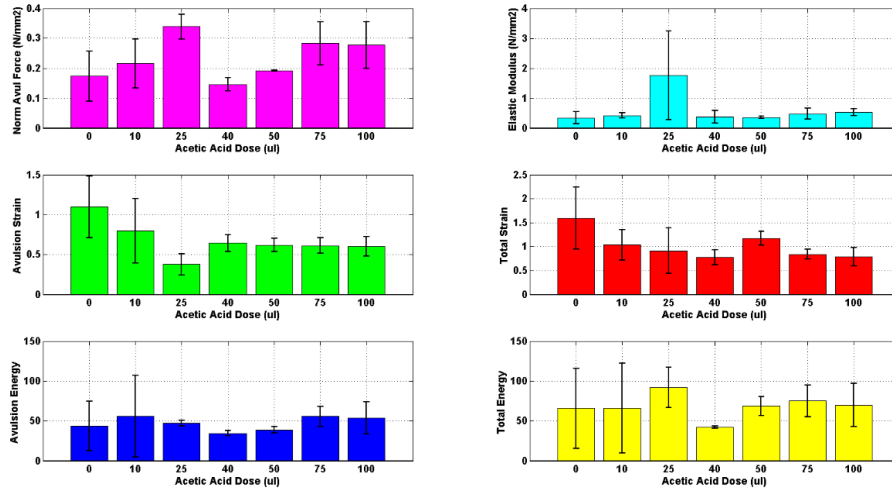
Fig. S9: Dose effects of **microwave ablation** (MWA) on biomechanical

properties of swine diaphragm muscle bundles compared to controls.
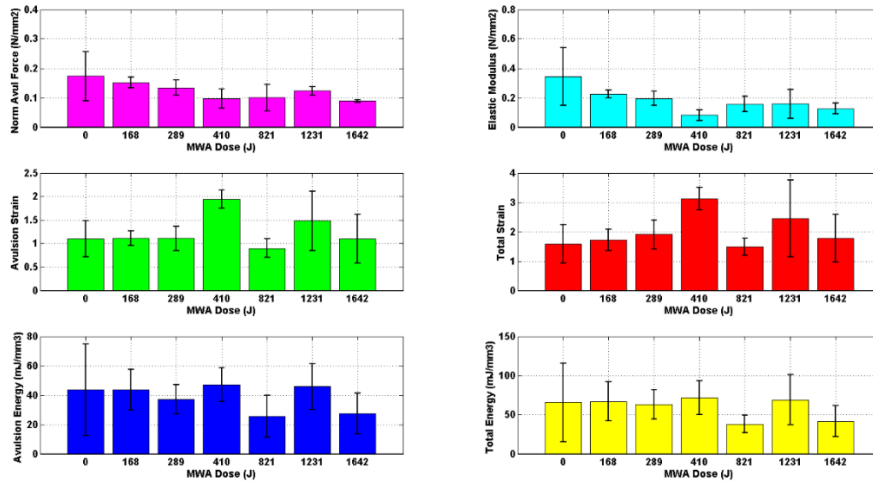
Fig. S10: Dose effects of **high-intensity focused ultrasound ablation** (HIFU)

ablation on biomechanical properties of swine diaphragm muscle bundles

compared to controls.

170
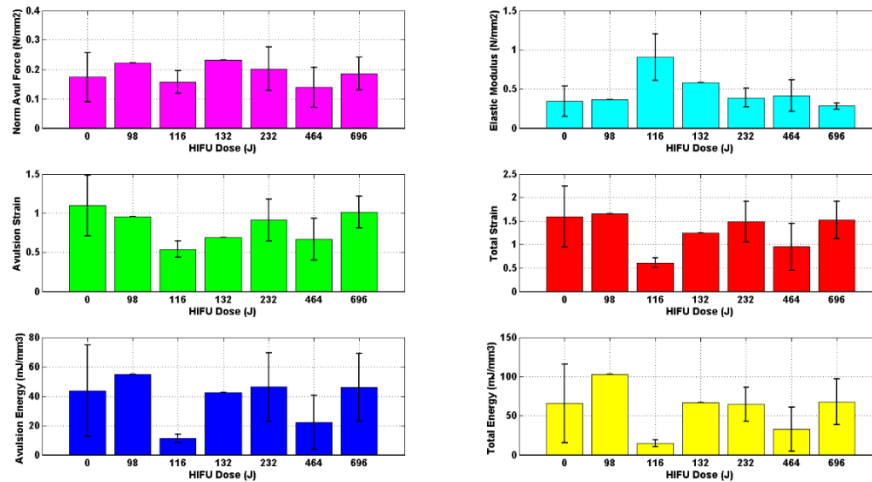
Fig. S11: Dose effects of **acetic acid ablation** on biomechanical properties of swine diaphragm muscle bundles compared to controls.

Fig. S12: Dose effects of **ethyl alcohol ablation** (EtOH) on biomechanical properties of swine diaphragm muscle bundles compared to controls.

Fig. S13: Dose effects of **sodium chloride ablation** on biomechanical properties

of swine diaphragm muscle bundles compared to controls.
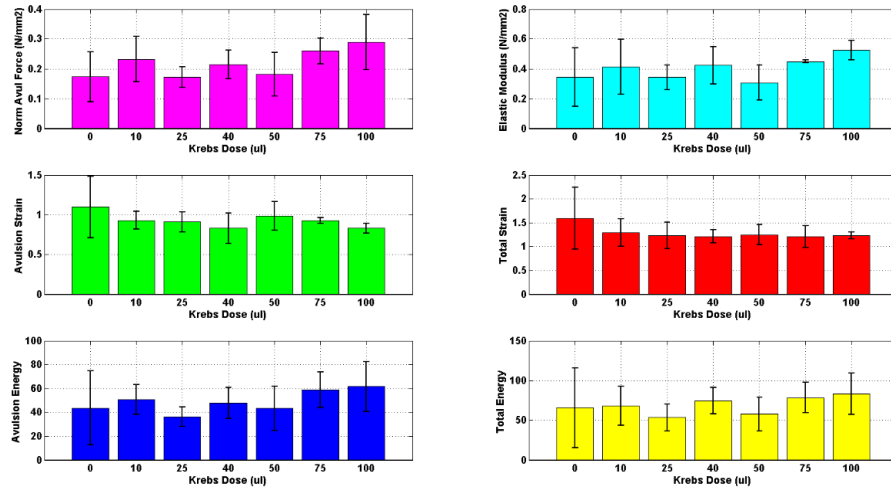
Fig. S14: Dose effects of **urea ablation** on biomechanical properties of swine

diaphragm muscle bundles compared to controls.
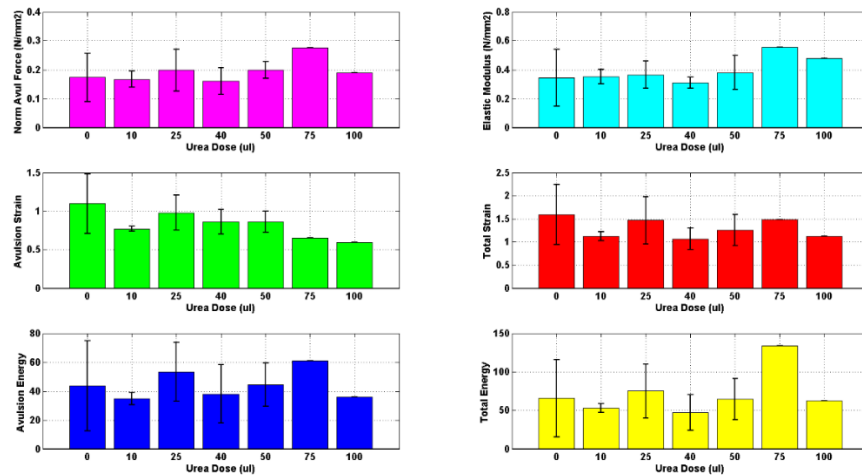
Fig. S15: Dose effects of **Krebs-Ringer injection** on biomechanical properties of swine diaphragm muscle bundles compared to controls.

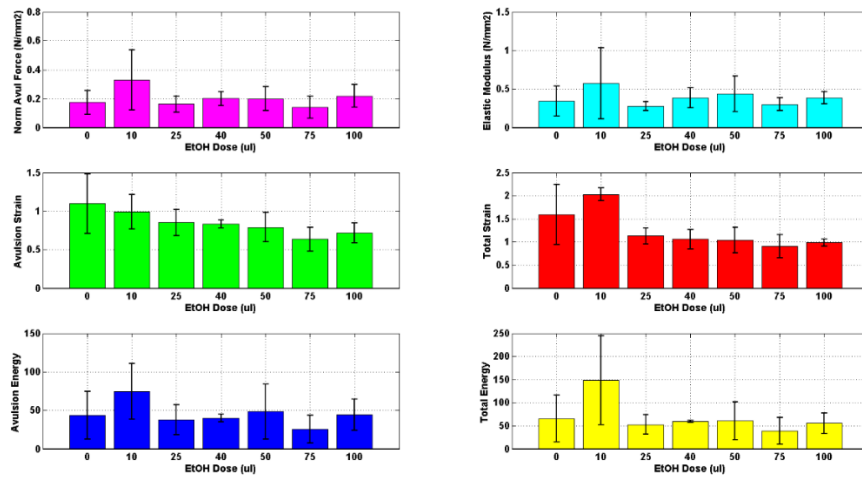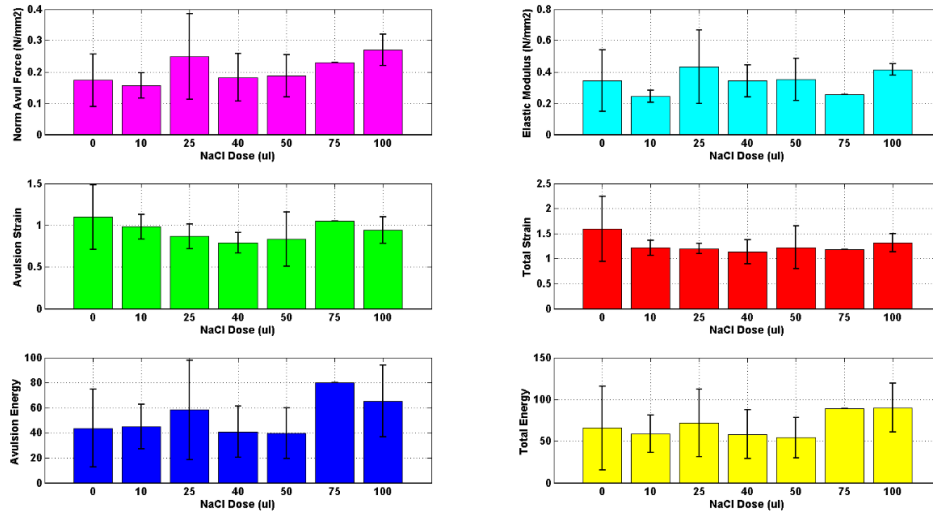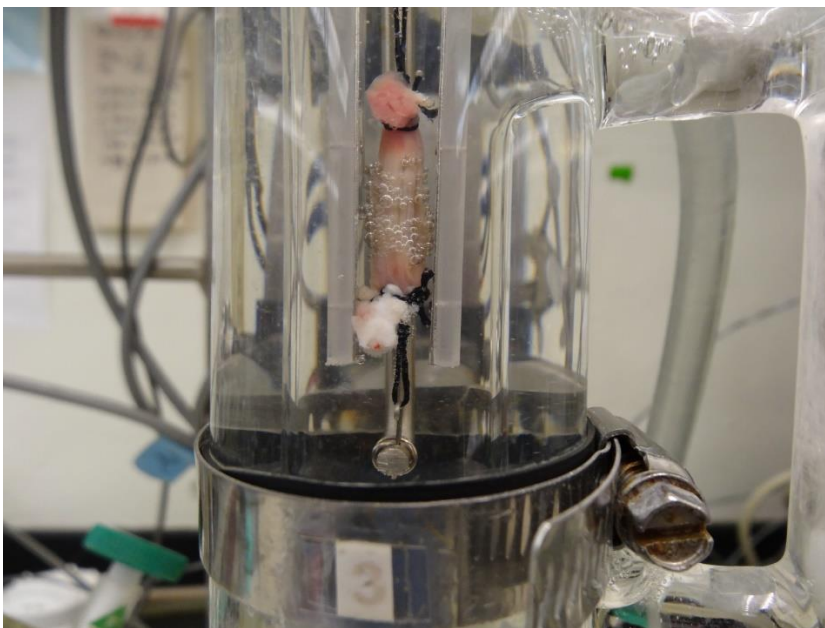**Fig. S16**: A swine diaphragm muscle ablated with 50 µl of acetic acid. Microbubbles on the ablated region of the muscle bundle can be seen that are caused by excessive dehydration, which further leads to tissue necrosis.

Table S1: Percent change in biomechanical properties of swine diaphragm

muscle bundles post ablation with different ablative modalities

	% Diff Avulsion Force	% Diff Elastic Modulus	% Diff Avulsion Strain	% Diff Total Strain	% Diff Avulsion Energy	% Diff Total Energy
RFA (n=10)	-2.3 p=0.8058	-8.4 p=0.5237	-15.0 p=0.0024	-20.9 p<0.05	-12.3 p=0.1884	-20.8 p=0.0440
CRA (n=9)	+6.3 p=0.4539	+90.0 p<0.05	-40.2 p<0.05	-48.7 p<0.05	-43.0 p<0.05	-51.8 p<0.05
MWA (n=24)	-37.9 p<0.05	-57.7 p<0.05	+11.8 p=0.1412	+19.4 p=0.0339	-21.4 p=0.1313	-21.6 p=0.1650
HIFU (n=13)	+2.1 p=0.8259	+24.8 p=0.0196	-24.8 p<0.05	-21.3 p=0.0120	-18.6 p=0.1895	-20.9 p=0.1732
Acetic Acid (n=20)	+30.9 p=0.0123	+32.4 p=0.0126	-45.4 p<0.05	-47.0 p<0.05	+2.0 p=0.9143	-6.5 p=0.7478
EtOH (n=14)	+13.2 p=0.2099	+16.5 p=0.1388	-33.8 p<0.05	-37.1 p<0.05	-4.5 p=0.7758	-11.6 p=0.5040
NaCl (n=17)	+16.7 p=0.1597	+8.7 p=0.4808	-22.5 p=0.0177	-29.1 p=0.0071	+10.1 p=0.5771	-5.1 p=0.7952
Urea (n=14)	+7.5 p=0.5360	+13.2 p=0.2995	-25.8 p=0.0084	-22.2 p=0.0462	+3.1 p=0.8655	-1.8 p=0.9289
Krebs Injected (n=14)	+18.2 p=0.1014	+16.2 p=0.1666	-22.0 p=0.0130	-28.0 p=0.0055	+0.3 p=0.9875	-8.2 p=0.6563
Study Controls (n=4)	+19.2 p=0.0857	+93.4 p<0.05	-32.3 p<0.05	-39.8 p<0.05	-23.4 p=0.1588	-31.7 p=0.0811

All values are in comparison to biomechanical control (n=187, non-ablated) muscle bundles. Each group represents the biomechanical controls averaged across all energies. A positive value indicates an increase and a negative value a decrease with respect to controls. Percent change in avulsion force, elastic modulus, strain, and energy are shown along with individual statistical significance (p<0.05). CRA=cryoablation, EtOH=ethyl alcohol ablation, HIFU=high-intensity focused ultrasound ablation; MWA=microwave ablation, RFA=radiofrequency ablation

Appendix C – Summary of Sample Sizes

Swine Diaphragm

	Voltage and Frequency			
	Muscle Baths		Pull Test	
	1.5 Hz	4 Hz	1.5 Hz	4 Hz
Control	136		135	
500	14	53	9	16
600	13	12	7	6
700	11	10	8	8
800	13	11	14	9
900	10	11	4	8
1000	10	9	8	7
1100	8	11	3	9

Number of pulses		
#	MB	Pull
0	136	135
10	23	13
20	27	13
30	30	21
40	33	16
50	36	32
60	33	28
70	53	16
80	3	0
90	2	0
100	2	0

Pulse Length		
us	MB	Pull
0	136	135
20	17	5
30	17	3
40	17	9
50	15	8
60	16	10
70	12	3
80	9	0
90	27	0
100	1	0

Human Diaphragm

	Muscle Baths		Pull Tests	
	1.5 Hz	4 Hz	1.5 Hz	4 Hz
Control		4		
500		2		
800		2		

Number of pulses		
	MB	Pull
Control	4	
10	2	
20	2	
30	2	
40	2	
50	2	
60	1	
70	2	

Human Vastus

	Muscle Baths		Pull Test	
	1.5 Hz	4 Hz	1.5 Hz	4 Hz
Control		13		4
500		9		7

Number of pulses		
	MB	Pull
0	13	
10	4	

600		3		1
700		8		2
800		3		1
900		2		1
1000		8		4

20	1	
30	3	
40	1	
50	4	
60	1	
70	9	

Swine Esophagus

	Muscle Baths		Pull Test	
	1.5 Hz	4 Hz	1.5 Hz	4 Hz
Control	56			
500	1	41		
600	4	7		
700	4	7		
800	5	7		
900	4	7		
1000	4	7		
1100	4	6		
1200	2	5		

Number of pulses		
	MB	Pull
Control	56	
10	11	
20	12	
30	15	
40	15	
50	15	
60	13	
70	41	
80	1	
90	1	
100	1	

Human Esophagus

	Muscle Baths		Pull Test	
	1.5 Hz	4 Hz	1.5 Hz	4 Hz
Control	48	48	26	26
500	12	31	7	7
600	13	13	6	6
700	12	11	5	7
800	13	12	8	7
900	13	12	8	6
1000	13	12	8	5
1100	3	8	0	4

Number of pulses		
	MB	Pull
10	2	
20	2	
30	3	
40	2	
50	3	
60	2	
70	15	
80	1	

Swine Cardiac

	Muscle Baths		Pull Test	
	1.5 Hz	4 Hz	1.5 Hz	4 Hz
Control	28	28		4
500	5	20		1
600	3	8		1
700	3	19		4
800	2	17		3
900	2	18		5
1000	2	18		4
1100	2	18		3
1200		12		5
1300		10		2

Human Cardiac

	Muscle Baths		Pull Test	
	1.5 Hz	4 Hz	1.5 Hz	4 Hz
Control		2		2
500		2		2
600		2		2
700		2		2
800		2		2
900		2		2
1000		2		2
1100		2		2